

Copyright
by
Heungbae Gil
1996

BRACING REQUIREMENTS FOR INELASTIC STEEL MEMBERS

by

HEUNGBAE GIL, B.S., M.S.

DISSERTATION

Presented to the Faculty of the Graduate School of
the University of Texas at Austin
in Partial Fulfillment
of the Requirements
for the Degree of

DOCTOR OF PHILOSOPHY

THE UNIVERSITY OF TEXAS AT AUSTIN

May 1996

Dedicated To My Mother

Acknowledgments

I would like to thank Dr. Joseph A. Yura, the supervisor of this dissertation. He showed me the true meaning of engineer and teacher. I will remember his attitude to students and structures throughout my life. I also liked to thank members of dissertation committee. I am grateful to Dr. Karl H. Frank who gave me the couple of opportunities to work with him. I extend my thanks to technical staffs at Ferguson Structural Engineering Laboratory.

I also need to mention help from the members of Korean graduate students in Civil Engineering and Korea University Alumni Association at UT. Kim, Keedong and Lee, Byung-Sik deserve a special recognition for their numerous *dinner* invitations and moral support. Because of them, I was able to eat home-made Korean foods. Special thanks to Kim, Youngeun *noona* who took care of me like a younger brother.

Finally, I thank to my family. I am especially grateful to my mother and the eldest brother for their supports and encouragement throughout the study, without which my education would have been impossible.

BRACING REQUIREMENTS FOR INELASTIC STEEL MEMBERS

Publication No. _____

Heungbae Gil, Ph. D.

The University of Texas at Austin, 1996

Supervisor: Joseph A. Yura

Braces which are used to prevent members from buckling are studied in this research. While bracing requirements for elastic members are well explained, those for inelastic members are not fully understood. This study is centered on the brace stiffness requirements of inelastic members. The study is divided into two parts. In Part I, inelastic column buckling tests were performed. In Part II, an inelastic buckling analysis program was developed.

In Part I, nine buckling tests of small scale inelastic columns were performed to determine bracing requirements for inelastic members. The columns had the elastic brace at the mid height. The tangent modulus of columns which governs the inelastic buckling loads was kept constant. Braced columns are modeled and analyzed by the finite element program, ABAQUS. It was found through experimental and analytical studies that the bracing requirements for inelastic columns depend on the buckling load and the braced length but not on the material state.

In Part II, the inelastic buckling analysis program, IBASP (Inelastic Buckling Analysis of Stiffened Plates), was developed to be used as the research tool in finding brace stiffness requirements for inelastic members. Singly and

doubly symmetric members can be analyzed. It can determine buckling loads and buckled shapes of elastic and inelastic members which failed by flexural, lateral-torsional and/or local buckling. Multilinear isotropic hardening rule was used to simulate the stress-strain relationship from material tests. IBASP was tested against theoretical solutions and experimental results. The results from IBASP show good agreement with those from experiments and theory.

Table of Contents

List of Tables	xii
List of Figures	xiii
Chapter 1. Introduction	1
1.1 General	1
1.2 Objective	2
1.3 Scope	2
Chapter 2. Literature Review and Background Information	4
2.1 Introduction	4
2.2 Inelastic Buckling Theory	4
2.3 Lateral Torsional Buckling	7
2.3.1 Elastic Lateral Torsional Buckling	7
2.3.2 Inelastic Lateral Torsional Buckling	9
2.4 Brace Stiffness Requirements	10
2.5 Brace Strength Requirements	18
PART I, Experimental Study	
Chapter 3. Inelastic Column Buckling Tests	22
3.1 Introduction	22
3.2 Test Program	23
3.2.1 Test Specimen	23

3.2.2 Test Setup	30
3.2.3 Test Results	36
3.3 Analytical Study	43
3.3.1 Backgrounds of Analytical Study.	43
3.3.2 Analysis Results	45
3.4 Brace Strength Requirements for Inelastic Columns	49
3.5 Summary.	50

PART II, Analytical Study

Chapter 4. Finite Element Method	52
4.1 Introduction	52
4.2 Literature Review and Theoretical Background	52
4.3 BASP	56
4.4 Elements for a New Program	59
4.4.1 Web Plate Element	59
4.4.2 Flange Beam Element	68
Chapter 5 Inelastic Finite Element Analysis Program	72
5.1 Introduction	72
5.2 Incremental Theory of Plasticity	73
5.2.1 Yield Surface	73
5.2.2 Flow Rule	75
5.2.3. Hardening Rule	79
5.2.4 Elasto-Plastic Stiffness Matrix	80
5.3 Deformation Theory of Plasticity	83

5.4 Plasticity of Beam Element	86
5.5 Inelastic Shear Modulus	87
5.5.1 Plasticity Theories	87
5.5.2 Literature Review	88
5.6 Solution Method for Non-Linear Problems	91
5.7 Eigenproblem Solution Routine	98
5.8 IBASP Program	101
5.8.1 IBASP Programming and Limit	101
5.8.2 Residual Stresses	101
Chapter 6. IBASP Calibration	103
6.1 Introduction	103
6.2 Inelastic Buckling Example	104
6.2.1 Cantilever Column	104
6.2.2 Simply Supported Beam with Constant Moment	107
6.3 Bansal's Tests	111
6.4 Elgaaly and Salkar's Tests	120
6.5 Ales and Yura's Tests	127
6.6 Parametric Study	131
6.7 Summary	134
Chapter 7. Summary, Conclusion and Future Research	135
7.1 Summary and Conclusion	135
7.2 Future Research	137
Appendix A. Consistent Constitutive Matrix and Elastic Predictor-Radial Return Algorithm for Plane Stress	138

Appendix B. Input Manual and A Example Input File for IBASP	141
Bibliography	148
Vita	157

List of Tables

3.1	Beam Length vs. Beam Stiffness	35
3.2	Column Buckling Test Results	37
3.3	Comparison of Experimental and Analytical Results	46
6.1	Material Properties of Tested Beams from Bansal (1971)	112
6.2	Cross-section Properties of Tested Beams from Bansal (1971)	112
6.3	Buckling Loads from Experiments and IBASP	119
6.4	Experimental and IBASP Results	123
B.1	Total and Plastic Strain	145

List of Figures

2.1	Stress and Strain Relationship	5
2.2	Load and Displacement of an Inelastic Column	6
2.3	Deflected Shape of a Fully Braced and an Unbraced Column Under Axial Load	11
2.4	Buckling Load vs. Brace Stiffness from Timoshenko and Gere (1961)	12
2.5	Winter's Fictitious Hinge Model for the Column with a Brace	14
2.6	Pincus' Model for the Inelastic Column with a Brace	15
2.7	Brace Stiffness and Brace Force Relationship from Winter's Model (1958)	19
2.8	Brace Stiffness and Brace Force Relationship from ANSYS (Helwig, 1994)	21
2.9	Brace Stiffness and Brace Displacement Relationship from ANSYS (Helwig, 1994)	21
3.1	Stress-Strain Relationships of Inelastic Materials	23
3.2	Cross-section of Test Columns	24
3.3	Material Characteristics from Tension Coupon Tests	26
3.4	Tangent Modulus of Composite Columns	27
3.5	Column and Cap	28
3.6	Buckling Machine and Brace Elements	29
3.7	Knife Edge and Cap	30
3.8	Schematic Plan View of Brace Elements	32
3.9	Schematic Elevation of Test Setup	32
3.10	Bracing Beam with Connection Attachments	34
3.11	Bracing Beam Details	34

3.12	Load vs. Displacements for S8N1 Tests	38
3.13	Load vs. Displacements for S10N1 Tests	38
3.14	Load vs. Displacements for S12N1 Tests	39
3.15	Load vs. Displacements for S14N1 Tests	39
3.16	Buckling Load vs. Brace Stiffness	41
3.17	Full Braced Column with Local Buckling	42
3.18	Full Braced Column with Anti-Symmetric Buckling	42
3.19	Initial Imperfection Shapes for Analytical Study	44
3.20	Buckling Loads vs. Stiffness from ABAQUS for 1st Mode	47
3.21	Buckling Loads vs. Stiffness from ABAQUS for 2nd Mode	47
3.22	Comparison of 1st and 2nd Mode Shapes Imperfection	48
3.23	Load vs. Displacement at Midheight for Inelastic Column	51
3.24	Load vs. Brace Strength Requirements for Inelastic Columns	51
4.1	BASP Input Model for I-Shaped Member	58
4.2	Nine-Node Isoparametric Elements	61
4.3	Cross-section of a Layered Beam	68
4.4	Degrees of Freedom for a Beam Element	69
5.1	Tresca and von Mises Yield Surface	73
5.2	Normality Rule	77
5.3	Kinematic Hardening	78
5.4	Isotropic Hardening	78
5.5	Effective Stress and Strain	84
5.6	Non-Linear Problem Solution Procedure	93
5.7	Assumed Residual Stresses Distribution	102
6.1	Cross-section Properties	104
6.2	Material Properties	105

6.3	Cantilever Column Model	106
6.4	Column Strength Curve	106
6.5	Simply Supported Beam Model under Constant Moment	108
6.6	Buckling Moments of Simply Supported Beam	109
6.7	Buckling Shapes of Simply Supported Beam and Cross-section Displacement	110
6.8	Bansal's Test Setup (Bansal, 1971)	113
6.9	Bansal's Test # 4	114
6.10	Bansal's Test # 6	115
6.11	Bansal's Test # 10	116
6.12	Bansal's Test # 15	117
6.13	Bansal's Test # 17	118
6.14	Stress-Strain Relationship for W16x31	121
6.15	Test Setup and Cross-section Dimension of W16x31 (Elgaaly and Salkar, 1991)	122
6.16	Results from the Beam with $N/d = 0.2$	124
6.17	Results from the Beam with $N/d = 0.4$	125
6.18	The Cross-section View of the Buckled Beam with $N/d = 0.2$	126
6.19	Cross-section Dimensions of S6x12.5	127
6.20	Test Setup and Moment Diagram for Ales and Yura's Test	128
6.21	Stress-Strain Diagram	128
6.22	Moment vs. Displacement of Simply Supported Beam	129
6.23	Buckled Shaped of Fully Braced Beam	130
6.24	Braced Beam under the Constant Moment	131
6.25	Buckling Moment vs. Lateral Brace Stiffness for a Simply Supported Beam	132

6.26	Buckling vs. Torsional Brace Stiffness for a Simply Supported Beam.	133
B.1	Material Data	145
B.2	A Cross-section Dimension	146
B.3	A Example Problem	146

CHAPTER 1:

Introduction

1.1 General

As the understanding and knowledge of structural members' behavior and material properties expand, more structural members are loaded to the inelastic range of the material to take full advantage of material strength. The main failure modes of inelastically loaded steel members are either yielding or buckling. Lateral torsional and local buckling can occur for the I-shaped steel members

The use of braces along the member length can substantially increase the lateral buckling capacity of a member. The brace stiffness and strength requirements to achieve specified increases in the buckling strength of the braced member have generally been developed for elastic structures. The requirements for elastic members can be easily determined by analytical methods or existing finite element programs.

The stability of inelastic members with braces is much more complex than for braced elastic members. As the brace stiffness is changed, the buckling strength of the member as well as the state of the material is altered. A very limited number of studies has been carried out to find the bracing requirements of inelastic members. Presently there are even conflicting requirements for inelastic members: one by Winter (1958) and another one by Pincus (1964) which will be discussed in detail later. The present study centers on brace requirements for inelastic members.

1.2 Objective

The purpose of this study is to determine the bracing requirements for inelastic steel members. The study is composed of two parts. In Part I, experimental studies are performed. In Part II, analytical studies are carried out.

In Part I, small scale column specimens were tested to resolve two conflicting bracing requirements for inelastic members. One suggested by Winter (1958) depends only on the buckling load while the other one by Pincus (1964) depends on the state of inelasticity. During the tests, the tangent modulus of columns was controlled.

In Part II, an inelastic buckling program which is computationally efficient was developed to find the buckling loads of unbraced and braced inelastic and elastic members. Until now, elastic buckling problem solvers, like BASP (Akay, Johnson, and Will, 1977), and inelastic buckling solvers with limited applications have been used. Commercially available finite element programs, like ABAQUS (1995) and ANSYS (1992), can solve elastic eigenvalue problems but fail to find inelastic instability loads. Flexural, lateral-torsional and local buckling capacities of inelastic members can be determined using the newly developed program, IBASP (Inelastic Buckling Analysis of Stiffened Plates). However, the members are limited to singly and doubly symmetric sections loaded in the plane of the web.

1.3 Scope

In the first part of the study, small columns with an ideal pin-pin support condition were tested in the inelastic range. An elastic brace which kept its elasticity throughout tests was located at the mid height of test columns. The main

variable was the stiffness of the brace. An experimental buckling load vs. brace stiffnesses relationship was developed for comparison with theory.

The capabilities of the program developed in the second part of the study are limited to calculation of elastic and inelastic out-of-plane buckling loads and buckled shapes. Distortional buckling capacities can also be calculated. However, the program can not determine post-buckling strength and the lateral displacement at the instant of and after the lateral instability. The program can be used to determine the brace stiffness requirements for elastic and inelastic members. However, the strength requirements of brace are not determined by the program. Braced members are modeled using lateral, rotational, and torsional braces. All braces are assumed to be elastic.

Before presenting the details of the experimental and theoretical studies which are found in Chapter 3 through 6, the general literature on bracing and background information are discussed in Chapter 2.

CHAPTER 2:

Literature Review and Background Information

2.1 Introduction

Braces are used to increase buckling strength of structural members. They need to have adequate strength and stiffness to prevent members from lower mode buckling. Brace requirements of elastic members are relatively well understood while those of inelastic members are not.

Previous work on buckling strength of braced and unbraced members is discussed in this chapter. Brace requirements are also discussed. First, inelastic buckling theories are reviewed. Then lateral torsional buckling strength of elastic and inelastic beams is studied. It is followed by a discussion of brace stiffness and strength requirements.

2.2 Inelastic Buckling Theory

The brief description of two inelastic buckling theories is given here. One is a tangent modulus buckling theory and the other one is a reduced modulus buckling theory. The difference between the two theories is whether elastic unloading is considered or not. The state of material at the incipient of inelastic buckling is specified as A in Figure 2.1. E and E_t designate the elastic and tangent modulus respectively

The tangent modulus theory predicts the buckling load by assuming that no elastic unloading has happened when the column starts to buckle. The column will

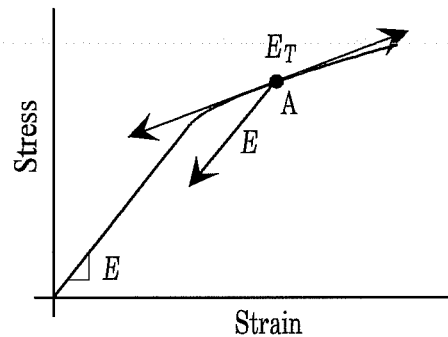


Figure 2.1 Stress and Strain Relationship

have the same tangent modulus E_T on both sides of Point A. If it is assumed that the left side of Point A follows the elastic modulus (E) and the right side of it follows the tangent modulus (E_T) as the column starts to bend, it will yield the reduced modulus buckling load. The reduced modulus for a rectangular cross-section is given by Johnston (1963) as

$$E_R = \frac{4EE_T}{(\sqrt{E} + \sqrt{E_T})^2} \quad (2.1)$$

where E_R is the reduced modulus. According to Equation 2.1, the reduced modulus is higher than the tangent modulus but lower than the elastic modulus. As a result, the reduced modulus theory yields buckling loads higher than the tangent modulus theory.

While the reduced modulus buckling theory appears more reasonable than the tangent modulus theory because it includes the elastic unloading effect, experimental buckling loads are closer to the tangent modulus buckling loads

(Johnston, 1983). The difference, called ‘column paradox’, was not explained until Shanley (1946) proved through carefully controlled experiments and analysis that the tangent modulus load is the lower bound of the buckling load. The reduced modulus buckling load is defined as the upper bound of the buckling load. von Karman (Johnston, 1983) redefined the tangent modulus load as follows;

“The tangent modulus load is the smallest value of the axial load at which bifurcation of the equilibrium positions can occur regardless of whether or not the transition to the bent position requires an increase of the axial load.”

Figure 2.2 demonstrates the behavior of the perfectly straight column without any initial imperfection. The column remains straight until the applied load reaches the tangent modulus load P_T . After reaching the tangent modulus load, the column starts to bend as the load is increased. As bending increases, a peak load, P_{max} , is reached. P_{max} is only a few percent higher than the tangent

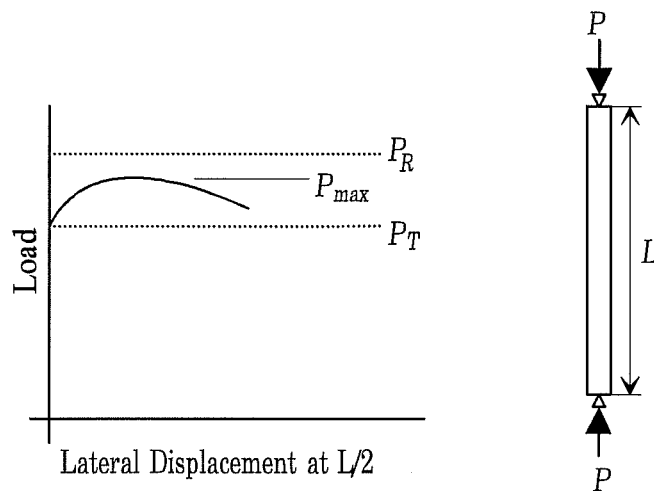


Figure 2.2 Load and Displacement of an Inelastic Column

modulus load.

The tangent modulus load generally accepted as the buckling capacity of the column is used in design practice. In this study, the tangent modulus is used to calculate member capacity.

2.3 Lateral Torsional Buckling

2.3.1 Elastic Lateral Torsional Buckling

The perfectly straight beam which is subjected to bending moments about the strong axis will deflect in the plane of applied moments until moments reach a certain critical value. When the buckling moment is reached, lateral torsional buckling is initiated by lateral deflection and twisting of the beam. Elastic lateral-torsional buckling strength of beams was solved mathematically by Timoshenko and Gere (1961) using differential equations. For a simply supported beam under constant moment, the lateral-torsional buckling moment M_{cr} is given by Timoshenko and Gere as:

$$M_{cr} = \frac{\pi}{l} \sqrt{EI_y (GJ + EC_w \frac{\pi^2}{l^2})} \quad (2.2)$$

where, l is the length of the beam,

I_y is the moment of inertia about a weak axis,

G is the elastic shear modulus,

J is the polar moment of inertia, and

C_w is the warping constant.

In Equation 2.2, GJ and EC_w are the torsional rigidity and warping rigidity of the beam respectively. The above equation is modified for beams under non-constant moments because buckling moments depend on moment gradients.

During 1950's and 1960's, differential equations were used to find lateral buckling loads of various beams. Buckling loads for single-span beams with different boundary and loading conditions were summarized by Clark and Hill (1960). Multi-span beam buckling problems were not given much attention until Hartmann (1967) found the buckling loads of two- and three-span continuous beams.

From early 1970's, the finite element method has been used to solve a wider range of buckling problems. Advantage of this approach is that it does not involve complex differential equations and it can treat a larger variety of loading cases and boundary conditions. Barsoum and Gallagher (1970) solved torsional and torsional-flexural instability of prismatic members using the finite element analysis. Powel and Klingner (1970) used the method to solve general beam buckling problems. Akay, Johnson, and Will (1977) further developed the finite element approach by considering cross-section distortion and local buckling. Their program, BASP (Buckling Analysis of Stiffened Plates), can deal with distortional buckling as well as flexural and lateral-torsional buckling but is limited to elastic buckling problems. BASP will be discussed in further detail in Chapter 3.

The finite element analysis was continuously employed in analytical studies by Trahair (1969), Nethercot and Trahair (1977), Hancock et al (1980), Bradford and Trahair (1981), Bradford (1985), Chin et al (1990). Theoretical solutions and the finite element analysis results for elastic lateral buckling problems were

reviewed by Nethercot (1983). Bradford (1992) summarized research efforts and solutions for distortional and lateral-torsional buckling of beams.

2.3.2 Inelastic Lateral Torsional Buckling

Buckling loads and moments for inelastic beams are calculated using the tangent modulus theory. It is assumed that, once beam fibers are yielded, the stiffness of fibers depends on the tangent modulus while no elastic unloading is considered.

Timoshenko and Gere (1961) assumed that the lateral flexural rigidity and the torsional rigidity of an inelastic beam diminish in the same proportion. The assumption leads to the inelastic shear modulus G_T as:

$$\frac{G_T}{G} = \frac{E_T}{E} \quad (2.3)$$

Then, the inelastic critical buckling moment for a simply-supported beam under a constant moment is expressed as follows;

$$M_{cr} = \frac{\pi}{l} \sqrt{E_T I_y (G_T J + E_T C_w \frac{\pi^2}{l^2})} \quad (2.4)$$

Equation 2.4 is basically the same as the elastic one, Equation 2.1, except for changes in modulus. When a moment is changing along the span under a concentrated load or a distributed load, Timoshenko and Gere (1961) recommend

that the inelastic modulus corresponding to maximum bending moment be applied over the whole span. This results in conservative estimates of the buckling load because the rigidity of less stressed sections is underestimated.

Galambos (1963) proposed a different solution for the inelastic lateral torsional buckling of simply supported beams under constant moments. He included the influence of residual stress upon inelastic buckling strength. It was assumed that resistance to buckling is furnished only by an elastic core of a cross-section. One thing different from Timoshenko's approach is an inelastic shear modulus. Using Neal (1950)'s experimental data which showed that the initial torsional stiffness is independent of the level of inelasticity, Galambos used the elastic shear modulus as the inelastic shear modulus ($G = G_T$). The inelastic shear modulus will be discussed in further detail in Chapter 5.

The finite element analysis was applied to inelastic buckling problems by Nethercot and Trahair (1976), El-Ghazaly et al (1984a, 1984b, and 1986), and Kitipornchai and Wong-Chong (1987). Analytical methods including the finite element method and solutions for inelastic lateral buckling problems were summarized by Trahair (1983).

2.4 Bracing Stiffness Requirements

A brace needs to satisfy stiffness and strength requirements (Winter, 1963). In this section, brace stiffness requirements are examined. When the stiffness of the brace is zero or small, the axially loaded member buckles in a symmetric shape as in Figure 2.3(b). As the stiffness of the brace is increased, the buckling load is increased. The stiff brace like the roller support in Figure 2.3(a) would force the axially loaded member to buckle in an anti-symmetric S-shape. The elastic

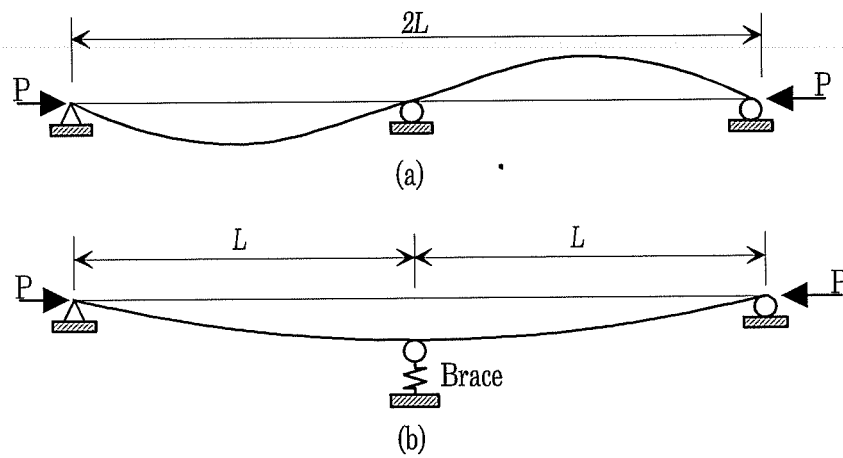


Figure 2.3 Deflected Shape of a Fully Braced and an Unbraced Column Under Axial Load

buckling strength of the fully braced member is four times higher than that of the unbraced one. However, the increase of brace stiffness after a certain critical stiffness, called *full brace*, would not increase the buckling strength of the axially loaded member. The full brace requirements are defined as the minimum required stiffness and strength which is comparable to an infinitely stiff support. Columns with multiple braces behave similar to columns with a single brace. When the column is braced by two stiff lateral braces at equal distance, the column buckles with two inflection points. The buckling load of the braced column is nine times larger than that of the column without braces.

Timoshenko and Gere (1961) using differential equations found brace stiffness requirements of axially loaded columns with lateral braces. The relationship between buckling load P_{cr} and brace stiffness β for the column with a brace is given as:

$$P_{cr} = \frac{\pi^2 EI}{4L^2} + \frac{3}{8}\beta L = P_e + \frac{3}{8}\beta L \quad (2.5)$$

where P_{cr} is the buckling load of the braced column,
 P_e is the buckling load of the unbraced column,
 L is the braced length of the column,
 β is the brace stiffness.

The relationship is plotted in Figure 2.4. It shows almost linear relationship between the brace stiffness and the buckling load up to full brace. The full brace stiffness is calculated as

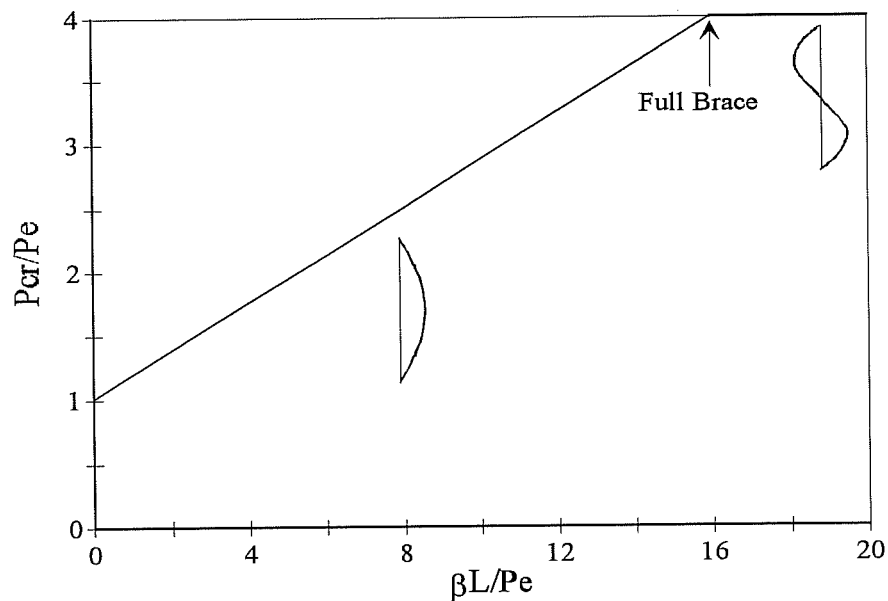


Figure 2.4 Buckling Load .vs. Brace Stiffness from Timoshenko and Gere (1961)

$$\beta = \frac{2\pi^2 EI}{L^3} = \frac{2P_{cr}}{L} \quad (2.6)$$

Winter (1958) gave a simple method to find the stiffness and strength requirements of a full brace. He introduced fictitious hinges with zero moment at brace points and assumed initial imperfection modes as in Figure 2.5. Then, moment equilibrium is taken at those hinges to find the most unfavorable mode which yields the highest brace stiffness. The brace stiffness from the most unfavorable mode constitutes the full bracing requirements of the column. For the column with a single brace, the required stiffness is;

$$\beta_{req} = \frac{2P_{cr}}{L} \left[1 + \frac{\Delta_o}{\Delta} \right] \quad (2.7)$$

where, β_{req} is the required brace stiffness for a full brace,

Δ_o is the initial imperfection amplitude,

Δ is the lateral displacement of the column at the brace.

For the *ideal* column without the initial imperfection ($\Delta_o=0$), the required full bracing stiffness is

$$\beta_{id} = \frac{2P_{cr}}{L} \quad (2.8)$$

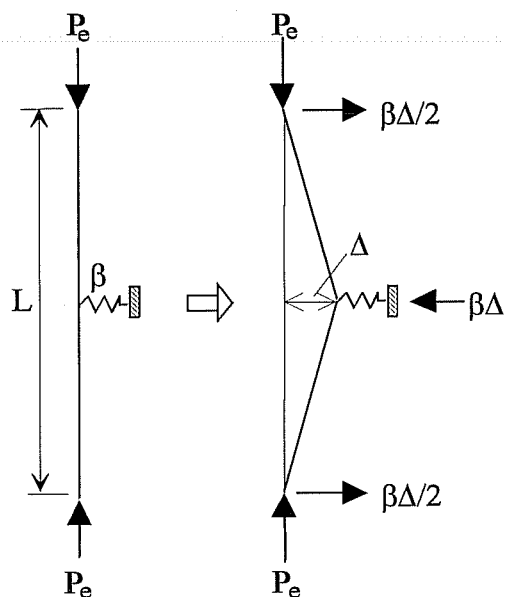


Figure 2.5 Winter's Fictitious Hinge Model for the Column with a Brace

which is the same brace stiffness suggested by Timoshenko, Equation 2.6, for full brace. Using Equation 2.8, the required brace stiffness for an initially imperfect column can be expressed as:

$$\beta_{req} = \beta_{id} \left[1 + \frac{\Delta_o}{\Delta} \right] \quad (2.9)$$

Pincus(1964) suggested the method which is similar to Winter's to determine inelastic column brace requirements. Rather than the fictitious hinge, Pincus introduced the rotational spring of stiffness α which represents the flexural stiffness of the column. The rotational spring is placed at the bracing point as

shown in Figure 2.6. When moment equilibrium is taken from the free body diagram of Figure 2.6,

$$M = 4\alpha\left(\frac{\Delta}{L}\right) = P\Delta - \left(\frac{\beta\Delta}{2}\right)\left(\frac{L}{2}\right) \quad (2.10)$$

The buckling capacity of the column with a brace is given from Equation 2.10 as:

$$P_{cr} = \frac{4\alpha}{L} + \frac{\beta L}{4} \quad (2.11)$$

where α is the rotational spring constant, $\alpha = \pi^2 EI / L^2$.

He reasoned that if the flexural stiffness α starts to decrease because E is reduced to E_T , then P would also be reduced. If the certain specified value of P in

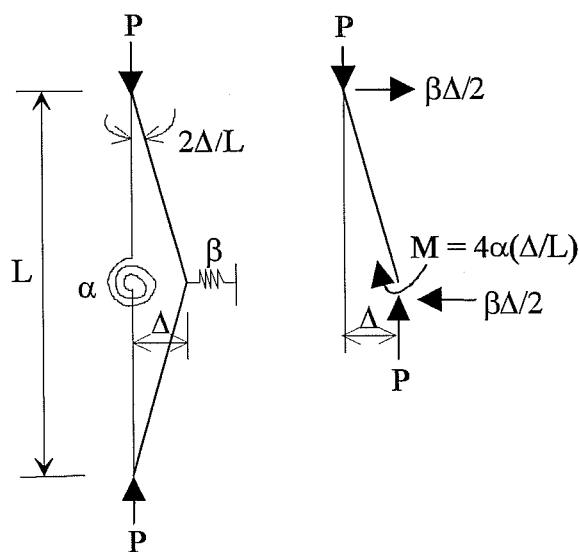


Figure 2.6 Pincus' Model for the Inelastic Column with a Brace

the inelastic range is desired, β has to be increased to compensate the decrease of α . It means that stiffer braces are required to brace inelastic members compared to elastic ones. Trahair and Nethercot (1984) adopted Pincus' approach for inelastic structures and recommended the use of stiffer braces for inelastic structures. However, Ales and Yura (1993) pointed out that the method proposed by Pincus fails to give the full brace requirements of elastic columns. The full bracing requirement of a simply supported elastic column by Winter (1963) and Timoshenko and Gere (1961) is given by Equation 2.8 as $\beta_{req} = 2P_{cr}/L$. Equation 2.11 by Pincus (1964) yields

$$\beta_{req} = \frac{3P_{cr}}{2L} \quad (2.12)$$

The comparison of two requirements indicates that Pincus recommendation does not provide full brace stiffness. In Part I of this study, braced inelastic column tests are carried out to examine Pincus suggestions. Winter's method for elastic structures are extended to inelastic structures and are experimentally reviewed.

Because of the lateral torsional buckling behavior of beams, bracing requirements of beams are more complex than those of columns. Four different types of braces, lateral, rotational, warping, and torsional, can be used individually or in combination to prevent lateral torsional buckling. The location of the braces within the cross-section influences the effectiveness of each.

Winter also proposed lateral bracing requirements of beams. He considered the compressed portion of a flange as an independent strut. The strut acts like a column and the same method that is used for braced columns is applied to find lateral brace requirements. Lay and Galambos (1966) proposed bracing

requirements of inelastic steel beams. They related the brace stiffness and spacing and concluded that relatively stiff braces are needed for closely braced members. Hartmann (1971) studied flexural-torsional buckling of partially yielded rectangular beams using differential equations. He investigated effects of bracing types and locations on buckling but did not provide specific stiffness requirements. Muton and Trahair (1973) suggested a closed form solution for elastic beams with lateral and rotational restraints. The elastic buckling program, BASP, by Akay, Johnson, and Will (1977) can be used to find brace stiffness requirements of elastic structures. Wakabayashi and Nakamura (1983) performed buckling tests of beams laterally braced by purlins. They reported that bracing effects of purlins on beam buckling strength is significant. Wong-Chung and Kitipornchai (1987) tested partially braced beams and studied influence of partial brace. It was concluded that a tension flange lateral brace has little effect on buckling capacity while lateral braces at shear center and compression flange are fully effective. Ales and Yura (1993) tested two inelastic braced beams to compare bracing requirements by Winter (1963) and Pincus (1964). The stiffness of the brace was slightly higher than the brace stiffness requirements by Winter. The beam buckled in S-shapes after reaching the tangent modulus lateral-torsional moment. It demonstrated that Winter's theory can be applied to inelastic members. In Part 2 of the study, the inelastic buckling program, IBASP, which is based on the tangent modulus buckling theory, is developed to find lateral-torsional buckling capacities of braced and unbraced members.

2.5 Brace Strength Requirements

As discussed earlier, a brace needs to satisfy both stiffness and strength requirements to act as full brace. Though brace stiffness requirements are the focus of the study, strength requirements warrant the same attention. The strength requirement is measured in terms of the force exerted on the brace by the members.

According to Winter (1963), the strength requirements can be calculated using the permissible displacement and the required stiffness of the brace. The strength requirement of the brace is expressed as:

$$F_{br} = \beta_{req} \Delta_p = \beta_{id} (\Delta_o + \Delta_p) \quad (2.13)$$

where F_{br} is the brace force,

Δ_p is the permissible displacement.

When the actual stiffness of the brace β_{act} is higher than the full brace stiffness β_{id} , the permissible displacement is

$$\Delta_p = \Delta_o \frac{\beta_{id}}{\beta_{act} - \beta_{id}} \quad (2.14)$$

and the required strength of the brace is

$$F_{br} = \beta_{act} \Delta_p = \Delta_o \frac{\beta_{id}}{1 - (\beta_{id} / \beta_{act})} \quad (2.15)$$

Equation 2.15 indicates that actual stiffness of the brace should be higher than the ideal stiffness to avoid a large brace force. The relationship between buckling loads and brace strength for different brace stiffnesses is plotted in Figure 2.7. The initial imperfection at the middle height of the column is assumed as $0.002L$. It shows that the stiffer brace would reduce the brace strength requirement. As an example, when the actual brace is two times stiffer than the full brace stiffness, the brace force is just 0.8% of the buckling load. According to Lay and Galambos (1966), 2% of the buckling load has been commonly used as the brace strength requirements in design practice.

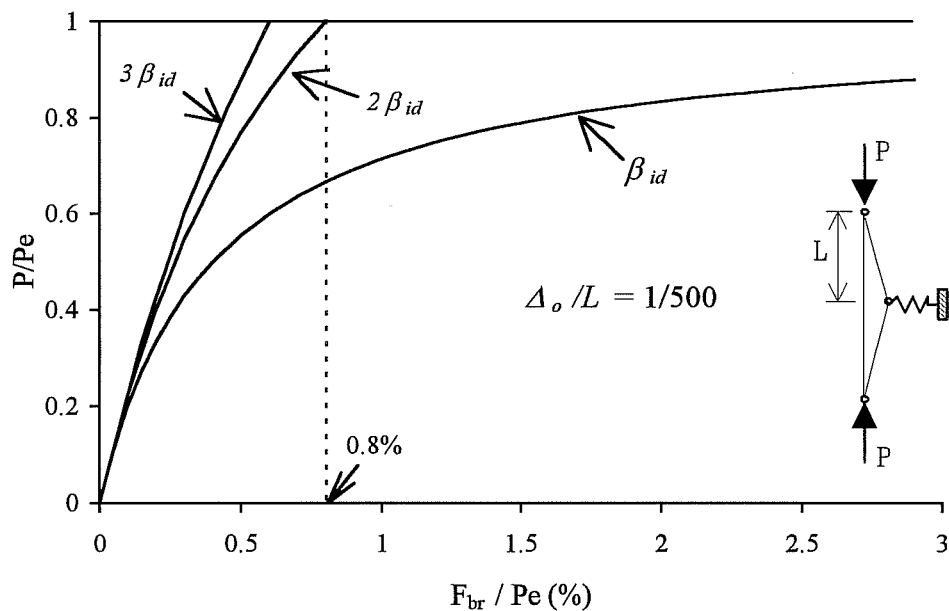


Figure 2.7 Brace Stiffness and Brace Force Relationship from Winter's Model (1958)

Helwig (1994) investigated the behavior of braced elastic columns using the finite element program, ANSYS. The ANSYS results (Figure 2.8) show that brace force is 1.05% of the buckling load when the brace stiffness is twice the ideal full brace stiffness. The total displacement is expected to be $2.32\Delta_o$ (Figure 2.9). Plaut (1993) also reported that the total displacement is $2.33\Delta_o$. According to Equation 2.14 by Winter, the expected total displacement is $2\Delta_o$. The difference between Winter's prediction and ANSYS results stems from the assumption of a fictitious hinge model. Winter's model has zero moment hinges at the bracing point while imperfect columns for ANSYS analysis have non-zero moment at the brace.

Nakamura (1988) claimed that Winter's model gives smaller bracing forces for H-shaped beams. Even so, he proposed 2% of the compression resultant force in the beam as a required lateral bracing force. Wang and Nethercot (1989 and 1990) performed analytical studies of braced W-shaped beams using finite element method program. They concluded that 1% of the axial force in the beam compression flange at failure would suffice as the lateral bracing force of the beam when the brace is stiff enough.

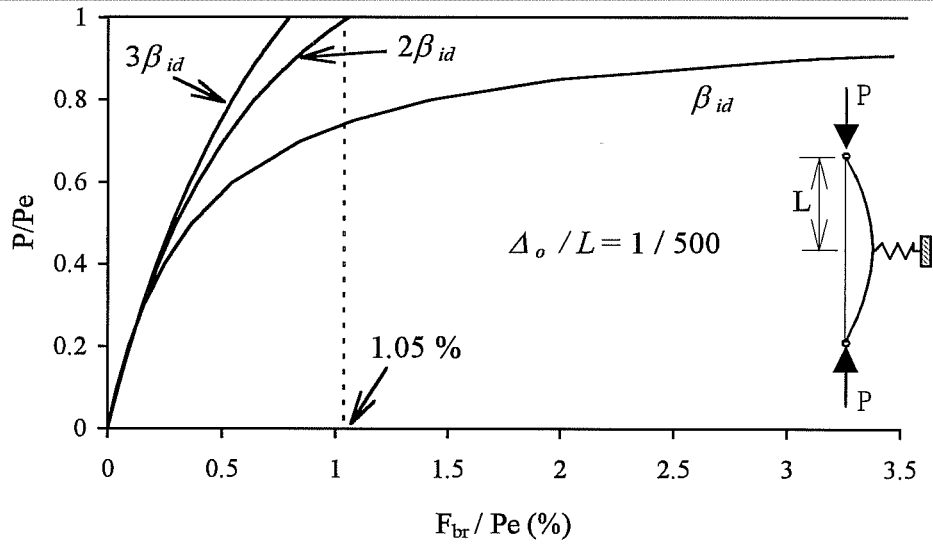


Figure 2.8 Brace Stiffness and Force Relationship from ANSYS (Helwig, 1994)

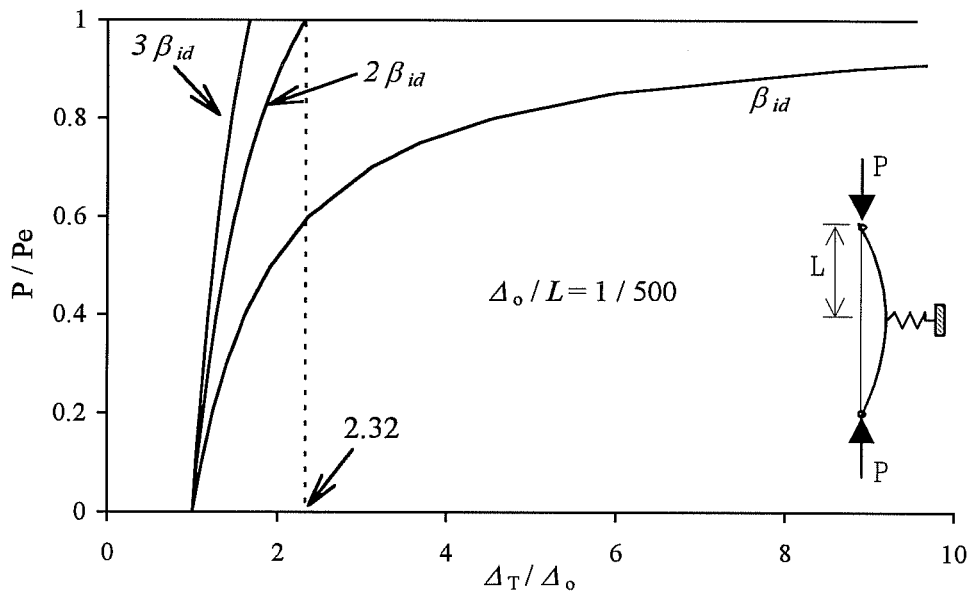


Figure 2.9 Brace Stiffness and Displacement Relationship from ANSYS

PART I: EXPERIMENTAL STUDY

CHAPTER 3:

Inelastic Column Buckling Tests

3.1 Introduction

There are two conflicting brace stiffness requirements for inelastic columns as discussed in Chapter 2: one by Winter (1958) and the other one by Pincus (1964). The full brace stiffness and strength requirements by Winter depend on the column load and the length of braced members. Winter's model which is independent of material state can be applied to inelastic as well as elastic structures. The requirements for inelastic members by Pincus depend on the state of material. Pincus qualitatively recommends that inelastic members need to have higher bracing stiffness than elastic structures. In this chapter, bracing requirements for inelastic members are determined by experimental and analytical studies.

Small scale inelastic column tests were carried out using a *composite column* composed of high strength and low strength steel. The columns tested had the elastic brace at the mid-height. Four different braces were used during tests.

A finite element method program, ABAQUS, was used in the analytical study to verify experimental results. Because the program cannot carry out inelastic buckling analysis, large displacement analysis was used to find the strength of inelastic columns with the elastic brace. Brace strength requirements of inelastic columns were also determined during the analytical study.

3.2 Test Program

3.2.1 Test Specimen

There are a number of ways to perform inelastic buckling tests. One is using a material like aluminum (Figure 3.1(a)) which has a nonlinear stress-strain relationship in the inelastic range. Inelastic buckling tests like one by Shanley (1946) have been carried out using aluminum alloy. Steel with residual stresses can also be used. Figure 3.1(b) illustrates the results of stub column tests showing that the stub column yields earlier than the tensile coupon due to residual stresses. The last one is using a linear strain hardening material as illustrated in Figure 3.1(c). The linear strain hardening material can be made by combining two materials with different yield strength but the same modulus. In general, aluminum alloy or steel with residual stresses were used in inelastic buckling tests. However, the buckling loads of the braced inelastic columns depend on both the tangent modulus and the brace stiffness. The tangent modulus of those two materials are constantly changed so that it is difficult to determine the correct tangent modulus

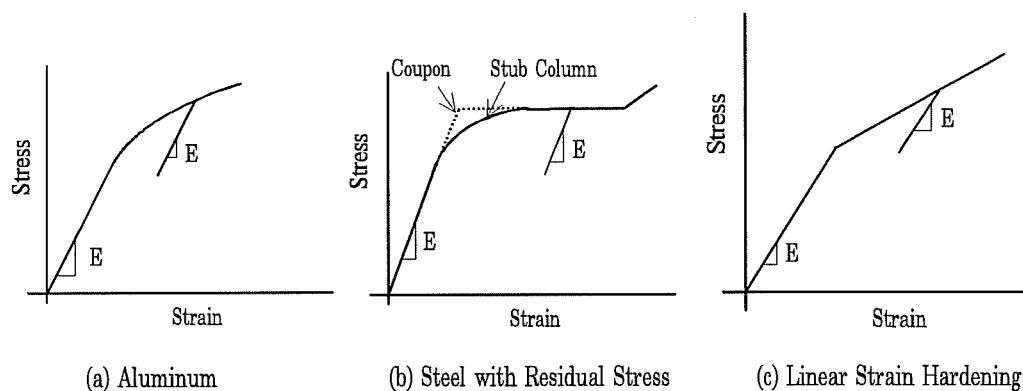


Figure 3.1 Stress-Strain Relationships of Inelastic Materials

at buckling and the brace requirements at the same time. If the linear strain hardening material is used, the brace requirements of the inelastic columns become the only variable that needs to be determined. In this study, the last approach with the constant tangent modulus is employed to measure the effects of braces.

The cross-section of a composite column composed of high strength and low strength steel bars is shown in Figure 3.2. A core material is high strength steel and the outside material is low strength steel. The buckling will occur about X-X axis in Figure 3.2. If the composite column buckles above the stress at which lower strength steel bars yield, low strength steel bars would have no influence on the buckling strength of the composite column because the tangent modulus of the low strength steel bars are zero. The buckling load is solely governed by a high strength core steel bar which still remains at the elastic state. Buckling loads of the elastic core column and the inelastic composite column are equal and expressed as follows:

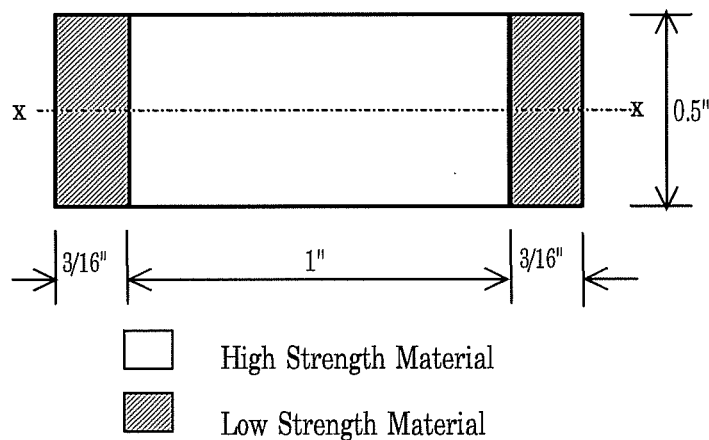


Figure 3.2 Cross-section of Test Columns

$$P_{cr} = \frac{\pi^2 E I_{CORE}}{L^2} = \frac{\pi^2 E_T I_{GROSS}}{L^2} \quad (3.1)$$

where, I_{CORE} is the moment of inertia of the elastic core steel bar;

I_{GROSS} is the moment of inertia of the composite column.

Equation 3.1 leads to the tangent modulus of the composite column which is equal to the elastic modulus of the core steel bar times the ratio of moment of inertia's. Equation (3.2) and (3.3) are used to find the tangent modulus of the composite column.

$$E_T \times I_{GROSS} = E \times I_{CORE} \quad (3.2)$$

$$E_T = (I_{CORE} / I_{GROSS}) \times E \quad (3.3)$$

High strength steel bars need to have high proportional limit as well as high yield strength because the elastic modulus of steel is reduced after it passes the proportional limit. Because high strength steels do not necessarily have high proportional limit, a few high strength steel bars were tried before choosing one. Bigger difference between the proportional limit of high strength steel and the yield strength of lower strength steel was preferred for experiments. The proportional limit of high strength steel was targeted at least 60 ksi while the yield strength of low strength steel was expected to be less than 40 ksi.

For selected steel bars, static tensile coupon tests were performed according to ASTM Standard E8-93a. After a series of materials tests, AISI 1018 (UNS G 10180) cold finished carbon steel bars which conformed to ASTM A-108 Specification were chosen as high strength steel with the specified yield strength of

70 ksi. AISI 1008 (UNS G 10080) hot rolled carbon steel bars which conformed to ASTM A569 Specification were selected as the lower strength steel. The bars had a specified yield strength of 40.0 ksi. The nominal dimension of the AISI 1018 steel bar was 1"x1/2" and that of the AISI 1008 bar was 3/16"x1/2". The difference between the actual and nominal dimension of the bars was less than 1/100" so that the nominal dimension was used in analytical studies.

Three coupon tests were performed for each strength and the averaged results are plotted in Figure 3.3. Lower strength steel bars had a static yield strength of 38.8 ksi. After yielding was initiated, bars had a yield plateau with almost zero modulus. Even though AISI 1018 steel bars yielded at a stress above 80 ksi, their proportional limit was less than 70 ksi. The difference between the proportional limit of high strength bars and the yield strength of low strength bars

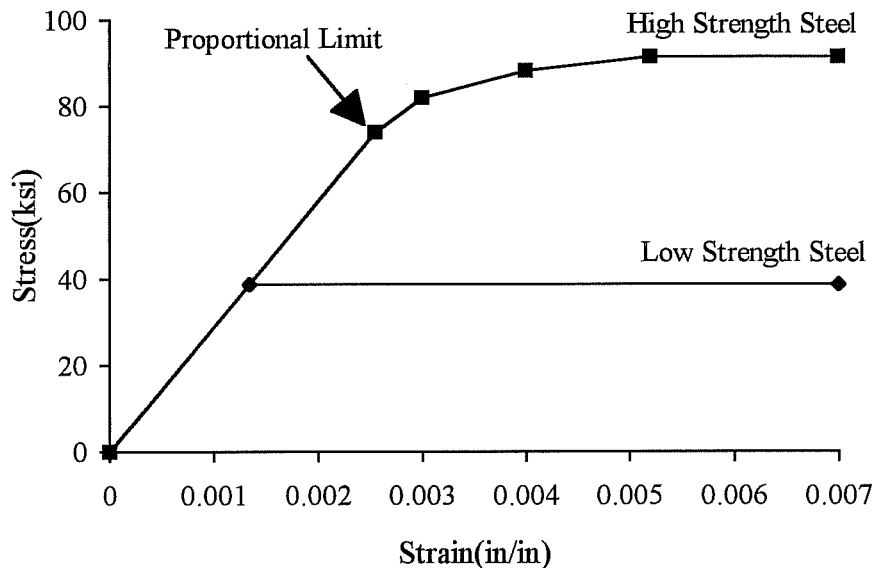


Figure 3.3 Material Characteristics from Tension Coupon Tests

was about 28 ksi. The elastic modulus of both steel bars was equal to 29000 ksi. The modulus of the composite column was reduced to the tangent modulus after low strength steel bars yielded at 38.8 ksi as shown in Figure 3.4. The tangent modulus of the composite column using Equation 3.3 was 21000 ksi.

The stress of the composite column at which the fully braced column would buckle was targeted at about 50 ksi. Various lengths of the column were examined to find that level of stress. It was determined that a 9.5" column length was the appropriate braced half column length which resulted in the expected buckling load of 33.0 kips and a corresponding stress of 48.0 ksi. For the braced column tests, that length should be doubled so a 19" long column was targeted. The length of the testing column included 1" of a *cap* height as shown in Figure 3.5. Caps which are made of hardened steel were placed at the top and the bottom

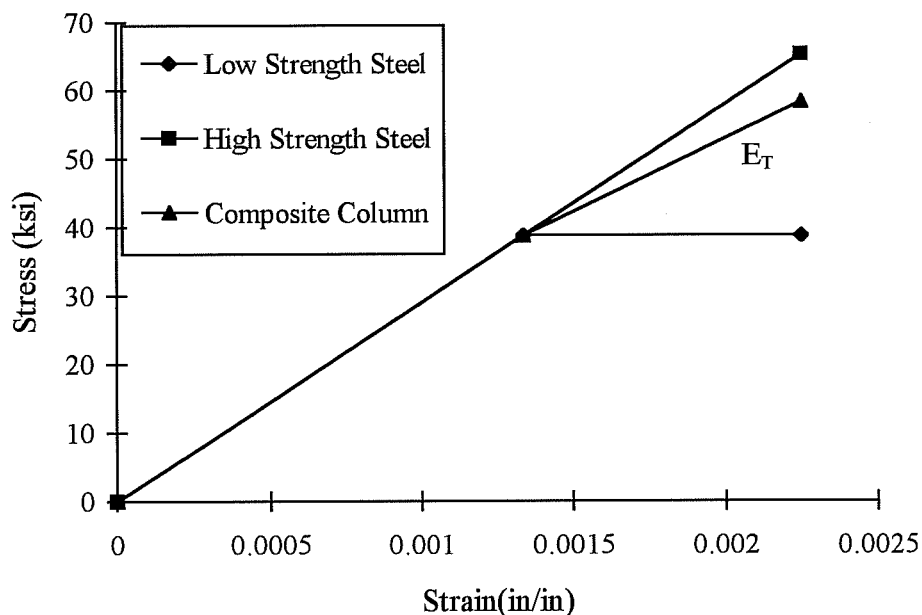


Figure 3.4 Tangent Modulus of Composite Column

of the column and were used for uniform distribution of a load. They also prevented localized yielding under the concentrated line load from the testing machine. It was assumed that the caps had minimal influence on the overall behavior and buckling strength of the column because most of lateral deflection occurred away from the ends.

The steel bars were made into composite columns using epoxy. The first step to make composite columns was sand-blasting of contact surfaces of the steel bars. Surfaces of cold drawn steel bars were so smooth that epoxy could not be applied effectively. The sand blast cleaned and roughened the surfaces. Then, the sand blasted surfaces were cleaned with acetone to remove dirt. After that, a special type of epoxy, called JB Welds, was applied. JB Welds proved to be strong enough to hold the composite column together during buckling.

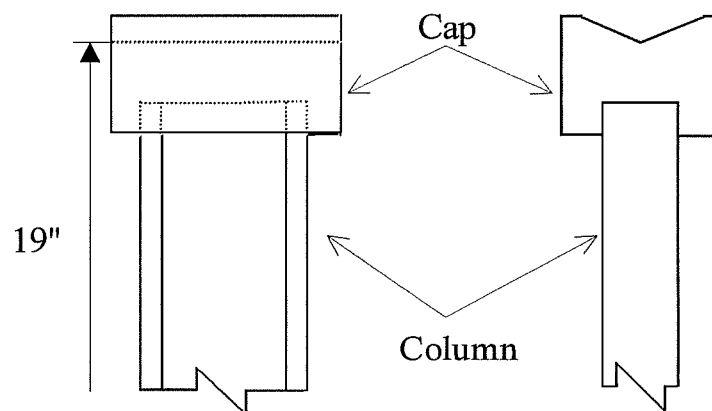


Figure 3.5 Column and Cap

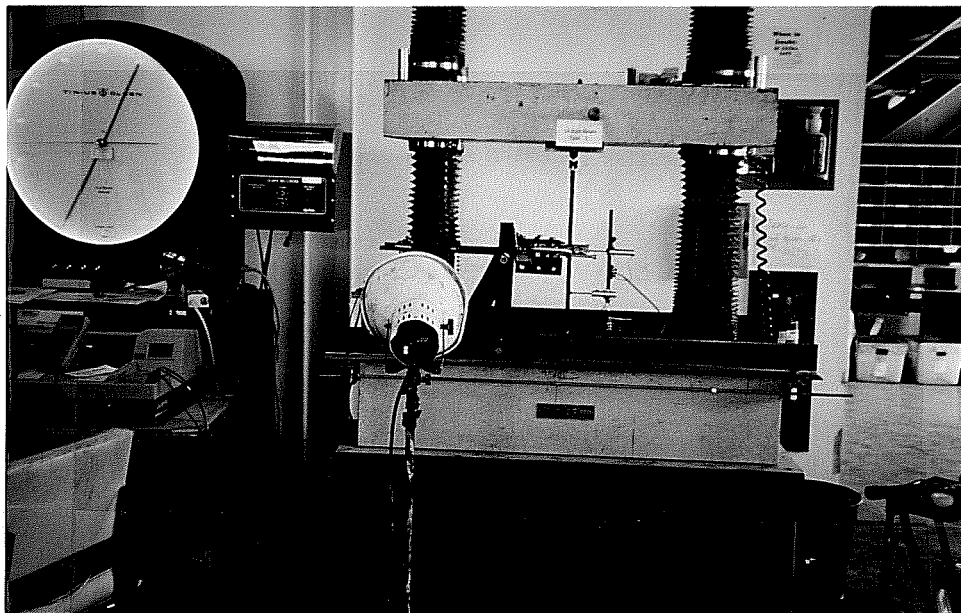


Figure 3.6 Testing Machine and Brace Elements

3.2.2 Test Setup

Tests were performed using a Tinius-Olson Universal Testing Machine with the capacity of 120 Kips. The Testing Machine which is shown in Figure 3.6 can provide electrical output as well as analog output. The machine and its output were first calibrated using a load cell. Linear potentiometers were used to measure displacements at a middle and a quarter height of testing columns. The outputs from the load cell and potentiometers were collected using a HP Plotter which can convert analog input into digital data for later use. XY Plotter was also used to observe the behavior of the columns during tests.

The load from the Testing Machine was transferred to the column by a knife edge acting on a cap. Figure 3.7 illustrates the transfer of load between the knife edge and the cap at the top of the column. The same load transfer fixture was installed at the bottom of the column. End conditions simulate the ideal pin-pin support

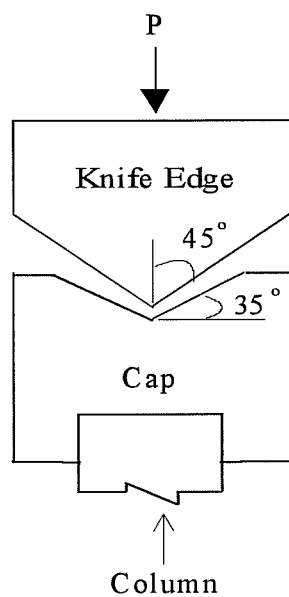


Figure 3.7 Knife Edge and Cap

that results in the effective length factor of 1.0 in a column buckling equation. The angle difference between the knife edge and the cap accommodated the rotation of the column at each end as it buckled. Oil hardening process was used to harden caps and edges after they were machined.

All brace elements shown were sitting on the top of the Testing Machine floor. The main brace elements are composed of an *Angle A and B* and a *bracing beam* as illustrated in Figure 3.8 and 3.9. The bracing beam was placed on the top of the Angle B. Knife edges that were bolted to the Angle B acted as pin supports to the bracing beam. Knife edges were placed on both sides of the beam to restrain lateral displacements which can happen in either direction. The Angle Bs were attached to the Angle A using bolts. The Angle A had rows of bolt holes as shown in Figure 3.8. The simply supported length of the bracing beam can be changed by anchoring the Angles Bs to the Angle A at different locations. The length can be changed from 8" to 14". The brace stiffness changed as the supported length of the bracing beam was altered. Reactions from the bracing beam were carried by the Angle B and the Angle A to the Testing Machine column and floor.

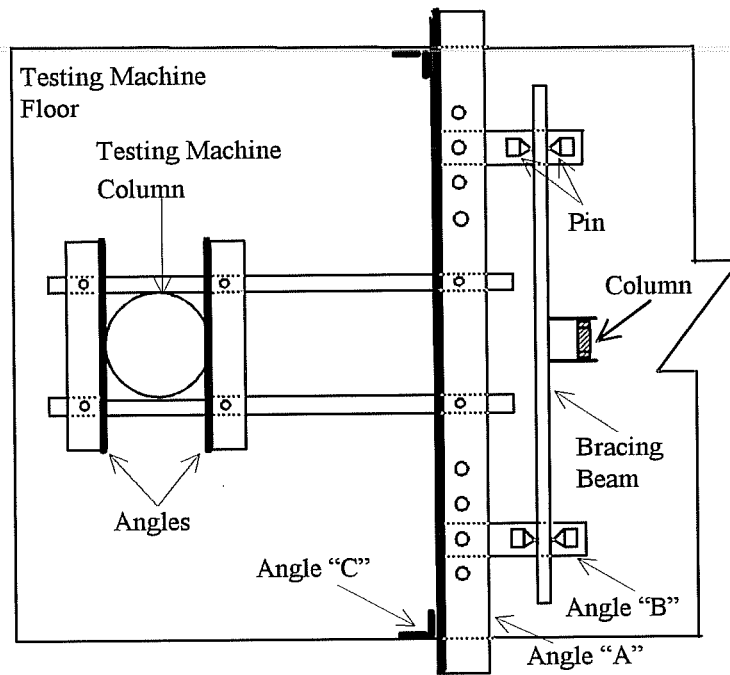


Figure 3.8 Schematic Plan View of Brace Elements

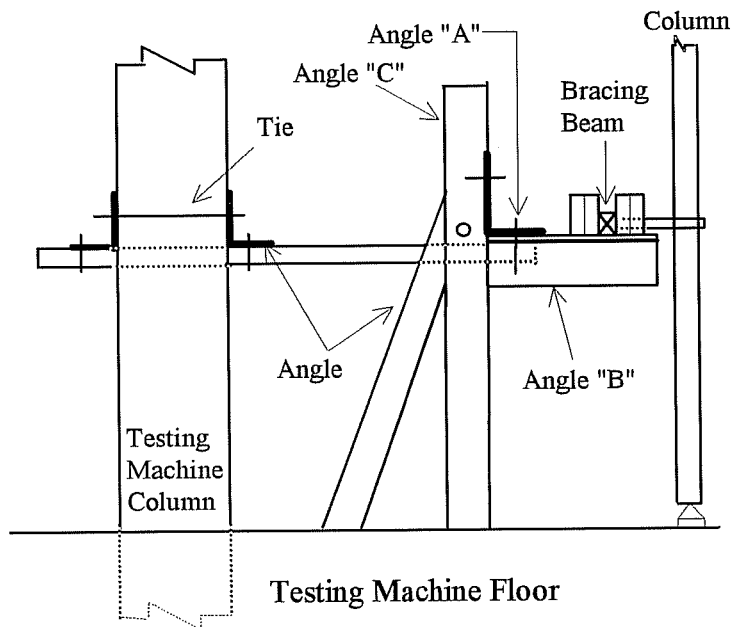


Figure 3.9 Schematic Elevation of Test Setup

Details of the bracing beam are illustrated in Figure 3.10 and Figure 3.11. The bracing beam is the one of main brace elements as discussed previously. It was placed on the top of the Angles B using bolts. The bracing beam was made of the high strength steel bar with the yield strength of over 100.0 ksi. During brace stiffness calibration and column buckling tests, the lateral deflection of the beam was limited to keep the beam in the elastic range throughout tests. The cross-sectional dimension of the beam was 1/2"x1/2" square. The length of the beam was 16".

The bracing beam had the *arm* on the side which contacted with the column. The columns were placed between two rollers of the arm as shown in Figure 3.11. Rollers acted as pin supports on each side of the columns. They allowed lateral displacements and frictionless rotations. Lateral displacements of the column happened in an East-West direction in Figure 3. 11. In Figure 3.11, the left roller was fixed in position while the right one could be moved depending on the thickness of columns. The circular rod was able to be shifted by making the diameter of holes in the rectangular steel bars larger than that of the circular rod. The movable circular rod had threads and nuts at both ends. After pushing the roller against the column, the movable roller was fixed by tightening the nuts against rectangular steel bars.

The stiffness of the bracing beam was measured before column buckling tests. A small hydraulic ram and linear potentiometers were used to measure the stiffness of the bracing beam. The bracing beam tests were performed after complete installation of all bracing elements. The torque of bolts was kept at the same level using a torque wrench for the consistency of tests. Loads were applied to both east and west direction because testing columns could move in either direction during buckling tests.

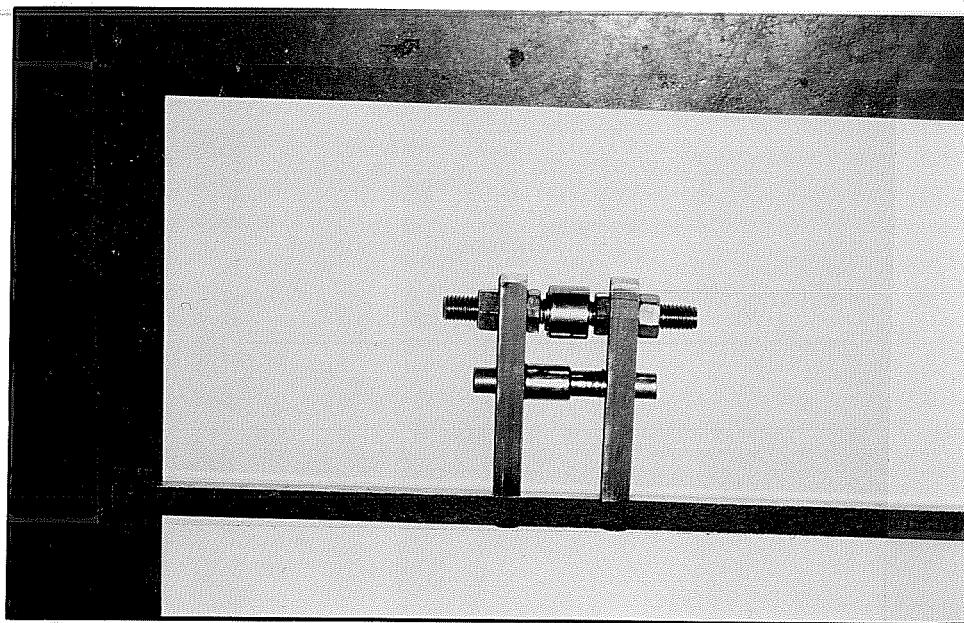


Figure 3.10 Bracing Beam with Connection Attachments

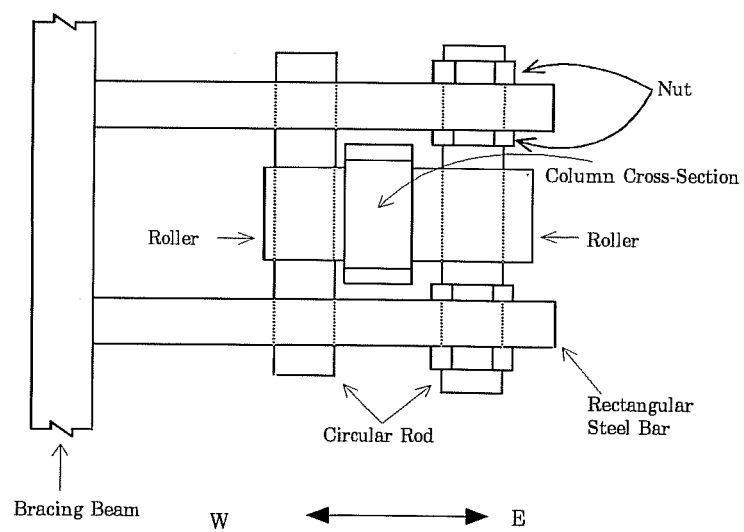


Figure 3.11 Bracing Beam Details

Table 3.1 Beam Length vs. Beam Stiffness

Beam Length (inch)	Beam Stiffness (kips/inch)
8.0	20.9
10.0	11.0
12.0	6.4
14.0	4.1

After a series of tests, a linear regression analysis was used to establish the stiffness. The simply supported bracing beam length and stiffness are shown in the Table 3.1. The stiffness given in Table 3.1 was valid for either direction. The ideal full brace stiffness β_{id} according to Winter is

$$\beta_{id} = \frac{2 \times P_{cr}}{L} = \frac{2 \times 33}{9.5} = 6.95 \text{ (kips / inch)} \quad (3.4)$$

where P_{cr} is the tangent modulus buckling load. Comparison showed that two bracing beams had stiffness higher than the ideal stiffness from Equation 3.4.

Static loading procedure was applied during tests. In the elastic region, loads were applied slowly but continuously. In the inelastic region, the testing machine was stopped for 3 minutes to allow unloading after each increment of 2.0 kips. During tensile coupon tests, the machine was also stopped for 3 minutes to get static material characteristics. After 3 minutes, a load was read and recorded. Then, the increment of 2.0 kips was applied again. The process was continued until the column buckled.

If the brace stiffness was higher than the ideal full brace stiffness, sudden instability, buckling, was expected. The Testing Machine automatically reduced load if buckling was initiated. No obvious buckling was anticipated if the stiffness was less than the full brace stiffness. When the stiffness was less than the full brace stiffness, the machine was stopped after the certain amount (0.25 inch) of the lateral displacement of the bracing beam. As discussed earlier, the magnitude of the allowable displacement was determined to keep the bracing beam in the elastic state. Excessive deflection would lead to plastic deformation and change the stiffness of the bracing beam. Two or three buckling tests were carried out for each brace stiffness. Along with those tests, the one-half column whose length was 9.5" was also tested to compare with fully braced columns. Ideally, the buckling load of a one-half length column and that of the fully braced column should be identical.

3.2 3 Test Results

Test results are presented in Table 3.2. The last column of the Table 3.2 describes the buckling shape. The buckling load from the one-half length column shown at the last row of the table is close to those from the columns with stiff braces. A typical load versus displacement relationship for each stiffness is given in Figure 3.12 through 3.15. Displacements in the figures were measured from the one-quarter height of columns. When the brace stiffness was higher than the ideal stiffness, rapid drop of load after buckling was observed as illustrated in Figure 3.12 and 3.13.

Table 3.2 Column Buckling Test Results

Test Name	Brace Stiffness(kips/inch)	Buckling Load(kips)	Buckling Shape
S8IN1	21.0	35.7	Anti-Symmetric
S8IN2	21.0	36.5	Local
S10IN1	11.0	34.0	Local
S10IN2	11.0	33.5	Local
S12IN1	6.4	27.7	Symmetric
S12IN2	6.4	30.4	Symmetric
S12IN3	6.4	30.8	Symmetric
S14IN1	4.1	23.7	Symmetric
S14IN2	4.1	23.7	Symmetric
One-Half Column		34.5	Symmetric

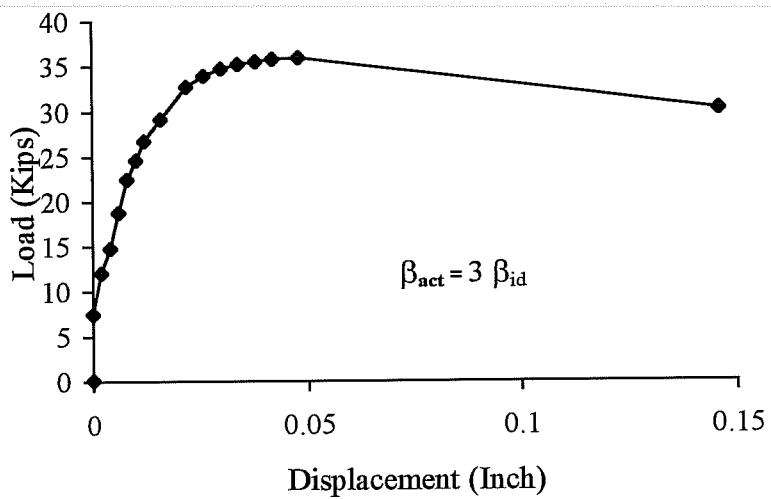


Figure 3.12 Load vs. Displacement for S8IN1 Tests

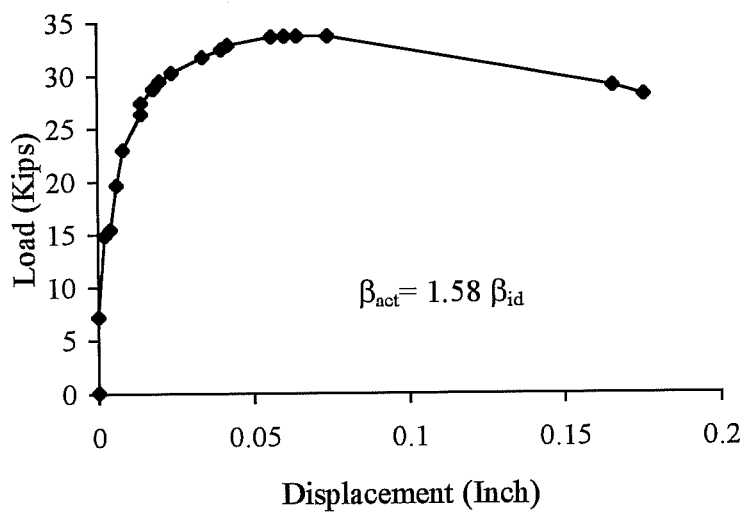


Figure 3.13 Load vs. Displacement for S10IN1 Tests

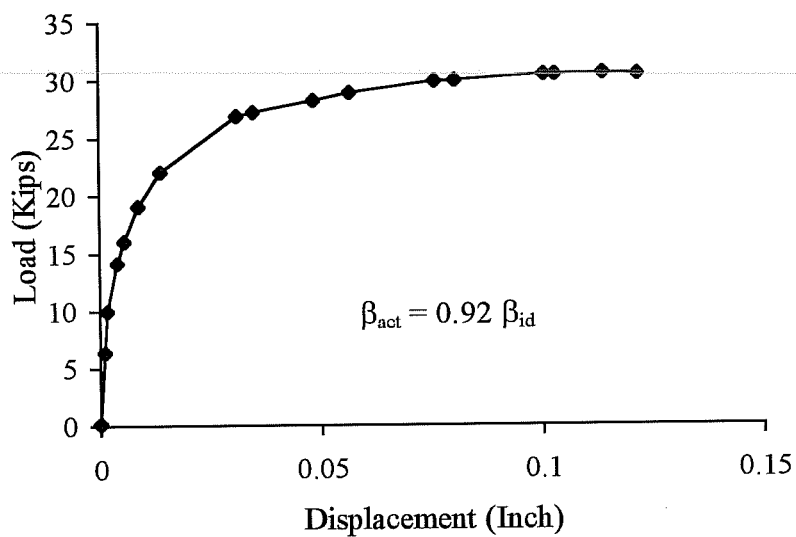


Figure 3.14 Load vs. Displacement S12IN2 Tests

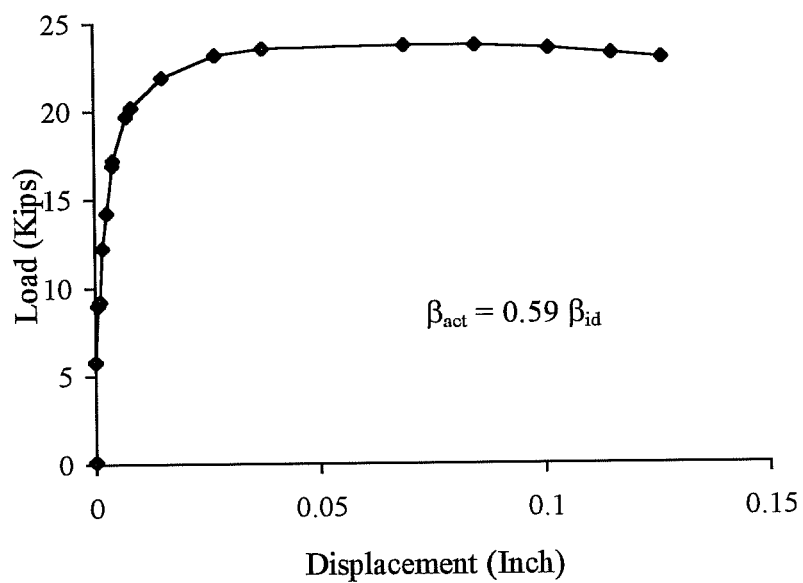


Figure 3.15 Load vs. Displacement for S14IN1 Tests

When the brace stiffness was lower than the ideal stiffness, the load was gradually reduced after reaching the maximum load as shown in Figure 3.14 and 3.15. The maximum loads were taken as the buckling capacities of the columns. The columns deflected in a first mode shape.

Main purpose of experimental work was to find the relationship between the inelastic column buckling loads and the brace stiffness. The relationship is illustrated in Figure 3.16. Braced column buckling loads along with the buckling load from the one-half column and the theoretical tangent modulus buckling load are plotted in Figure 3.16. β_{id} is the ideal bracing stiffness which was calculated in Equation 3.4. Most of buckling loads were above the yield loading of columns (26.7 kips).

A few observations were made out of test results. The tangent modulus theory proves to be the lower bound theory. All inelastic buckling loads from the fully braced columns and the one-half column were higher than the tangent modulus load. However, they were still lower than the reduced modulus buckling load (38.2 kips). The buckling loads were increased as the brace stiffness was raised. That happened even after the brace stiffness was above the ideal stiffness, β_{id} . Theoretically, the increment of brace stiffness should not affect the buckling load once the ideal stiffness is reached. When the 8" bracing beam was used ($\beta_{act} = 3\beta_{id}$), buckling loads were higher than the one-half column buckling load. Buckled shapes of fully braced inelastic columns were not anti-symmetrical in three out of four tests. Only a half of the column was buckled while the other half remained almost straight. A typical buckled column is shown in Figure 3.17 where buckling occurred at the bottom half of the column.

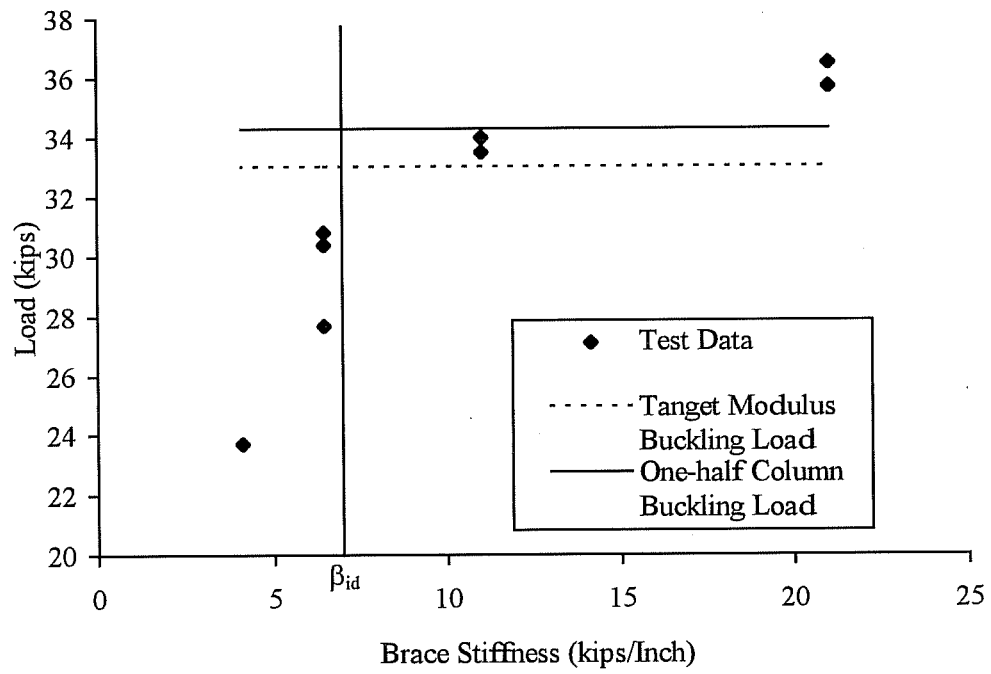


Figure 3.16 Buckling Load vs. Brace Stiffness

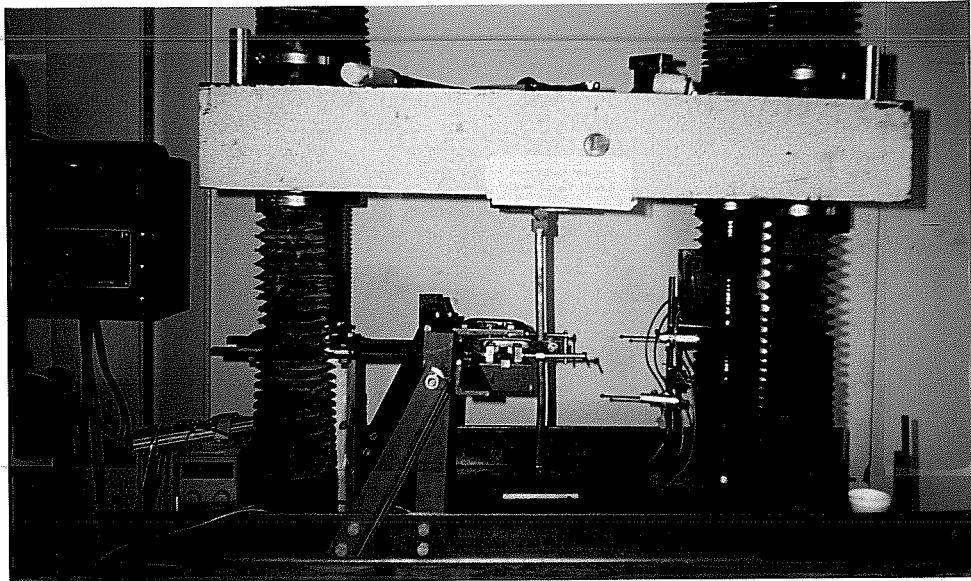


Figure 3.17 Full Braced Column with Local Buckling

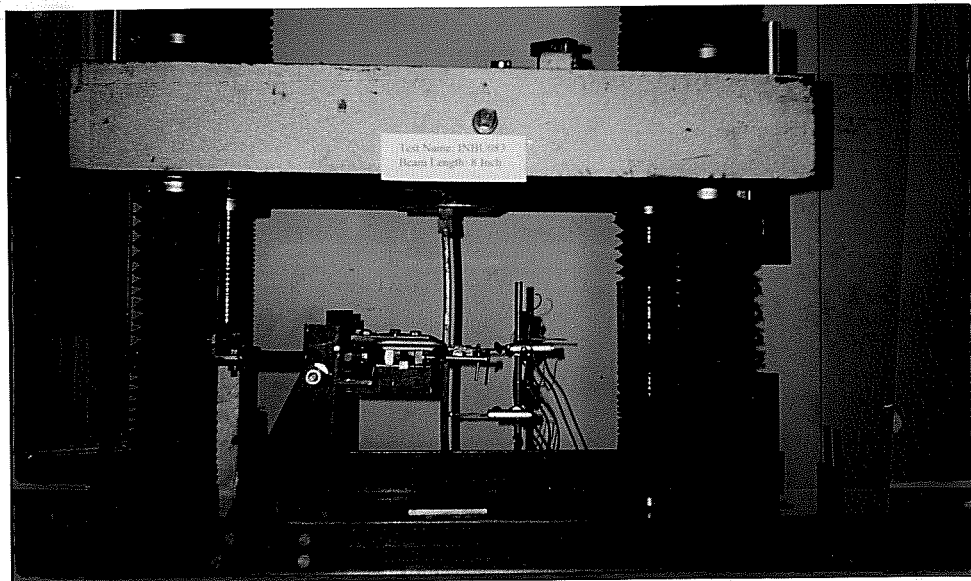


Figure 3.18 Full Braced Column with Anti-Symmetric Buckling

One of possible causes of high buckling loads and localized buckling would be brace fixtures. Rollers substituted theoretical pin supports which had to rotate freely without vertical movement at the center of the column as the column buckled in the anti-symmetrical 2nd mode shape. In reality, there must be some amount of frictional forces and vertical movements. Non-uniform distribution of material characteristics would also contribute to localized buckling.

3.3 Analytical Study

3.3.1 Backgrounds of Analytical Study

A finite element program package, ABAQUS, was used to analyze inelastic columns. ABAQUS outputs were compared with experimental results. ABAQUS (ABAQUS Manual, 1993) can solve the problem of nonlinear geometry and material non-linearity. It can also perform linear elastic buckling analysis but cannot do inelastic bifurcation or buckling analysis (ABAQUS Manual, 1993). In this study, nonlinear large displacement analysis was employed to find the strength of the braced inelastic columns. Maximum load from large displacement analysis was taken as the strength of the columns.

The column was modeled using an eight-node layered shell element. Linear spring elements were utilized to model the elastic braces. Tensile coupon test results of the low and high strength steel bars were given as material characteristics.

Large displacement analysis is known to be sensitive to the initial imperfection of structures. Both the magnitude and shape of initial imperfection affect the strength of inelastic columns. The magnitudes of initial imperfections of the tested columns were measured using filler gauges before tests and used as

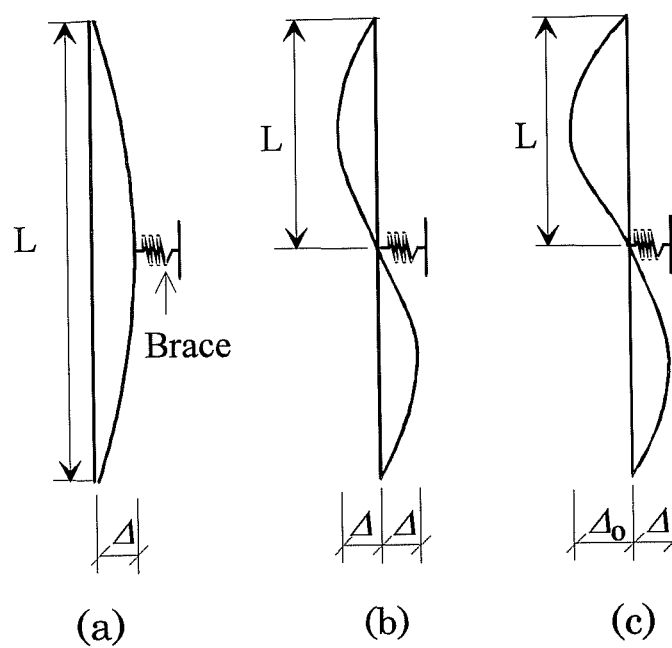


Figure 3.19 Initial Imperfection Shapes for Analytical Study

ABAQUS inputs. The measured initial imperfection ratio defined as the ratio of the maximum initial imperfection magnitude over the unbraced column length was close to 1/1000. Three types of imperfection shapes which are illustrated in Figure 3.19 were employed in analysis. In all three cases, the initial imperfection magnitude Δ was given as follows:

$$\frac{\Delta}{L} = \frac{1}{1000} \quad (3.5)$$

in which L is the column length as shown in Figure 3.19. The first one (Figure 3.19 (a)) represents a symmetric first mode shape. The second one (Figure 3.19 (b)) is an anti-symmetric second mode shape. The last one (Figure 3.19 (c)) is the non-symmetric second mode shape where the imperfection of one half is bigger than that of the other half. The ratio of Δ/Δ_o was varied during analysis to match the behavior of columns during experiments. It was observed during tests that buckled shapes of full braced columns were close to the non-symmetric shape. The columns were simply supported at each end and brace was located at the mid-height of columns.

3.3.2 Analysis Results

The results from the analysis were shown in Figure 3.20 and Figure 3.21. In Table 3.3, the experimental and analytical results were compared. Figure 3.20 and Table 3.3 showed that the maximum strength of braced columns with the symmetric 1st mode shape imperfection kept increasing with the increment of the brace stiffness. The strength of the column continued to increase even after it

Table 3.3 Comparison of Experimental and Analytical Results

Brace Stiffness (kips/in)	Experimental Results	ABAQUS Results 1st Mode Shape	ABAQUS Results 2nd Mode Shape
4.1	23.7	23.7	25.1
6.4	29.2	29.9	30.5
11.0	33.8	37.8	30.7
21.0	36.1	42.1	30.7

passed the tangent modulus buckling load. It occurred because ABAQUS does not perform the inelastic bifurcation analysis and it also does not determine an inelastic instability load. Figure 3.21 showed that the loads from the 2nd mode shape imperfections (Figure 3.19 (b) & (c)) were smaller than the tangent modulus buckling load. The column with the anti-symmetric 2nd mode shape imperfection (Table 3.3 & Figure 3.19 (b)) yielded the constant load once the brace stiffness reached a certain value. When the column with the initial imperfection shape of Figure 3.19 (c) was used, very slight increase in the loads was observed with the increment of the brace stiffness. The non-symmetric 2nd mode shape column gave the higher buckling load than the anti-symmetric one under the same brace stiffness.

The ideal full brace stiffness was determined using the ABAQUS results. When the brace stiffness is lower than the ideal brace stiffness, the columns with the anti-symmetric 2nd mode shape imperfection would yield higher maximum load than the symmetric 1st mode shape columns. The opposite phenomenon would occur if the brace is stiffer than the ideal brace. The buckling loads of the

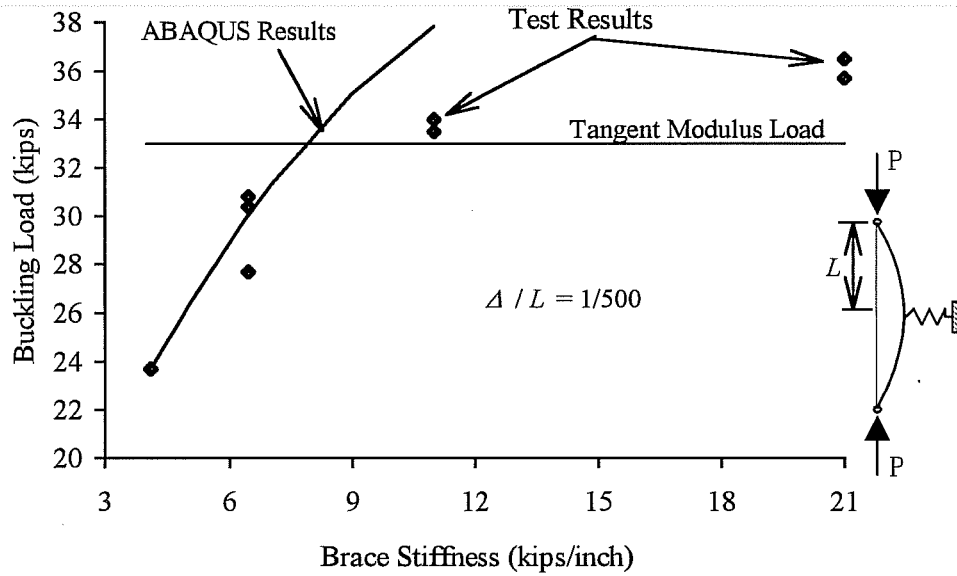


Figure 3.20 Buckling Loads vs. Stiffness from ABAQUS for 1st Mode

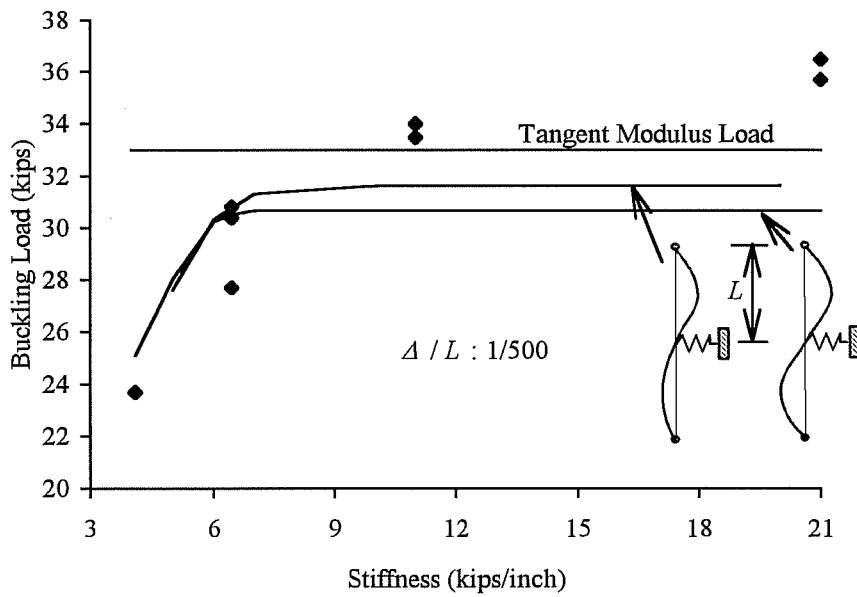


Figure 3.21 Buckling Loads vs. Stiffness from ABAQUS for 2nd Mode

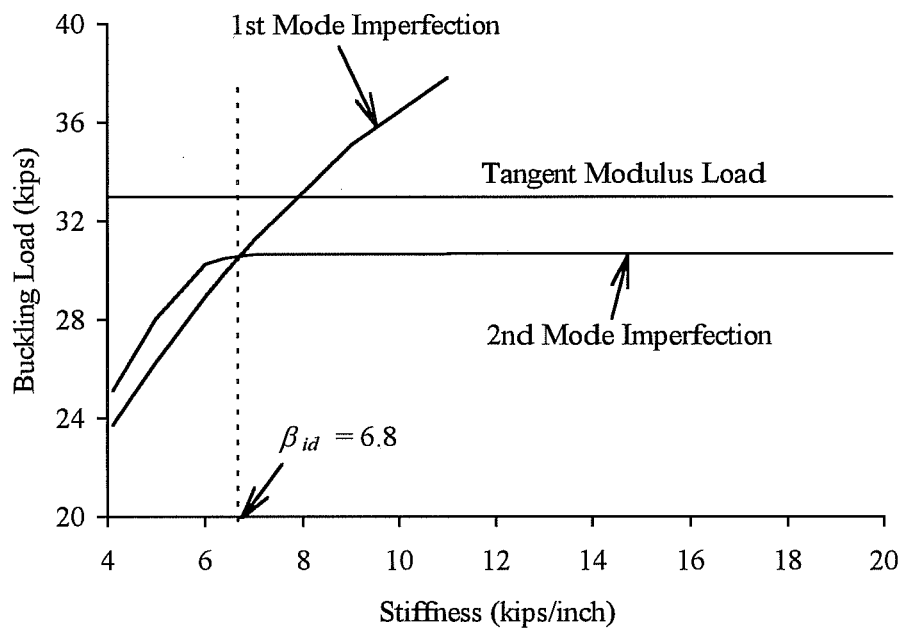


Figure 3.22 Comparison of 1st and 2nd Mode Shapes Imperfections

braced column is chosen as the lower of two loads. As shown in Figure 3.22, the ideal stiffness β_{id} from the analysis was determined as 6.8 kips/in which is close to the one by Winter (Equation 3.4). If the brace stiffness was lower than the ideal stiffness β_{id} , experimental and analytical buckling loads were very close as shown in Figure 3.20 and Table 3.3. When the column was fully braced ($\beta > \beta_{id}$), analytical buckling loads were lower than the tangent modulus load (Figure 3.21).

3.4 Brace Strength Requirements for Inelastic Columns

As discussed in Chapter 2, the finite element method program, ANSYS (1992), was used by Helwig (1994) to find the brace strength requirements and displacements of elastic columns. ANSYS results showed that Winter's (1958) model unconservatively predicted the brace force and displacement at the midheight of the column. When the brace stiffness was twice stiffer than the ideal stiffness, the total displacement was reported as $2.32 \Delta_o$ where Δ_o represents the magnitude of initial imperfection. The brace force was also reported as 1.05% of the buckling load. Winter's model suggested that the total displacement is $2 \Delta_o$ and the brace force is 0.8% of the buckling load.

The finite element program, ABAQUS (1995), was utilized in the analysis of braced inelastic columns as discussed in the previous section. Details of inelastic analysis process were also described. The magnitude of initial imperfection was kept as $\Delta_o = 0.002L$ where L is the braced length of the column. The shape of initial imperfection was a symmetric half sine curve.

The ABAQUS results are plotted in Figure 3.23 and 3.24. P_{cr} in the figures represents the tangent modulus buckling load of a fully braced column. The

loads above the P_{cr} in Figure 3.23 and 3.24 are dotted to show that they are invalid because the tangent modulus buckling load is the true buckling capacity of inelastic columns. Figure 3.23 shows the relationship between the buckling load and displacement at the midheight of the braced column. When the brace stiffness is twice the ideal full brace stiffness by Winter, the total displacement at the tangent modulus buckling load is $2.35 \Delta_o$ which is close to that of the elastic columns ($2.32 \Delta_o$). Figure 3.24 displays the relationship between the buckling load and the brace force. The brace force at the tangent modulus buckling load is 1.05% of the P_{cr} when the brace is twice stiffer than the ideal full brace. The brace force is the same as the one for the elastic columns. It is concluded that the brace strength requirements for elastic members can be applied to inelastic members.

3.5 Summary

Brace stiffness and strength requirements for inelastic columns were determined by experimental and analytical works. It was shown that Winter's fictitious hinge model can be applied to inelastic structures as well as elastic structures. His simplified bracing formula which depends on buckling load and column length can be utilized in the design of inelastic members. Pincus' conjecture that inelastic members need stiffer brace than elastic ones was demonstrated to be incorrect.

Brace strength requirements for inelastic members were also determined from ABAQUS results. No difference between elastic and inelastic brace strength requirements were observed.

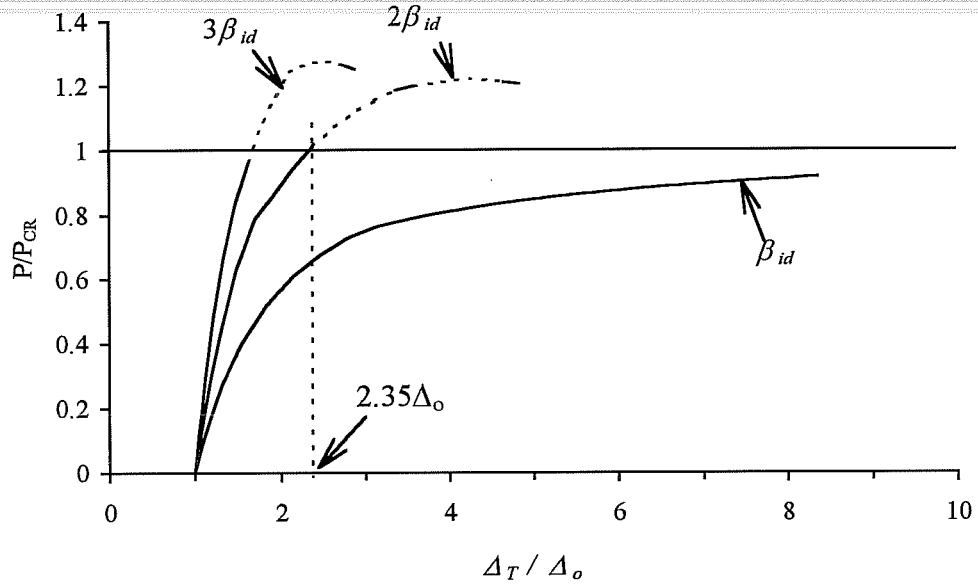


Figure 3.23 Load vs. Displacement at Midheight for Inelastic Column

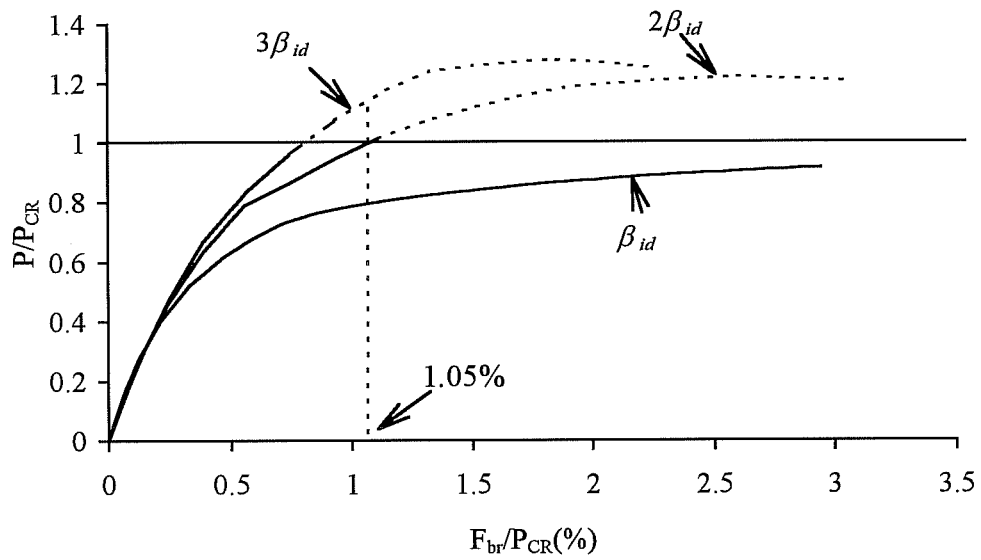


Figure 3.24 Load vs. Brace Strength Requirements for Inelastic Column

PART II: ANALYTICAL STUDY

CHAPTER 4

FINITE ELEMENT METHOD

4.1 Introduction

The finite element method which is widely used in structural analysis is employed to solve the buckling problem. Theoretical background of finite element analysis and the application of the finite element method to buckling problems are discussed in Chapter 4. The existing elastic buckling analysis program, BASP, which utilizes the finite element method to find buckling loads of stiffened members is also reviewed. The isoparametric plate element and layered beam element which are used in the development of an inelastic buckling program in Chapter 5 are discussed. The elastic stiffness matrices and geometric stiffness matrices of those two elements are formulated.

4.2 Literature Review and Theoretical Background

The finite element method, which was derived using the principle of stationary potential energy, can be effectively employed to solve general buckling problems. Kapur and Harts (1966) solved the problem of plate stability using the method. Barsoum and Gallagher (1970) solved torsional and flexural-torsional buckling of one-dimensional prismatic members. Powel and Klingner (1970) employed the finite element method to solve elastic lateral torsional buckling of

steel beams. Local and distortional buckling was not considered in their model. Akay, Johnson, and Will (1977) developed the two-dimensional elastic buckling analysis program, BASP. BASP which stands for Buckling Analysis of Stiffened Plates can find lateral torsional, local, and distortional buckling loads of structural members. Further details of BASP are given in the next section. The application of finite element method for inelastic buckling will be described in Chapter 5.

Buckling can be described in terms of potential energies. Cook et al. (1989) stated that buckling occurs when a structure converts membrane strain energy into strain energy of bending with no change in externally applied load. The principle of stationary potential energy is used to derive the buckling equation. The total potential energy, Π_p , is expressed as:

$$\Pi_p = U - V \quad (4.1)$$

where U is the strain energy stored in the element and V is the external work done by applied forces. The strain energy is given by

$$U = \frac{1}{2} \int_v \{\sigma\}^T \{\varepsilon\} dv \quad (4.2.a)$$

$$= \frac{1}{2} \int_v \{\varepsilon\}^T [E] \{\varepsilon\} dv \quad (4.2.b)$$

where $\{\sigma\}$ and $\{\varepsilon\}$ are the stress and strain tensor respectively, and the matrix $[E]$ represents the material properties. The strain tensor is composed of linear and nonlinear components. The strain components are expressed as follows;

$$\{\varepsilon\}^T = \{\varepsilon_L\}^T + \{\varepsilon_{NL}\}^T \quad (4.3)$$

in which $\{\varepsilon_L\}$ represents the linear strain and $\{\varepsilon_{NL}\}$ represents the nonlinear strain. The general expression for the strain-displacement relationship is

$$\varepsilon_{ij} = \varepsilon_{Lij} + \varepsilon_{NLij} \quad (4.4)$$

where

$$\varepsilon_{Lij} = \frac{1}{2}(u_{i,j} + u_{j,i}) \quad (4.5.a)$$

$$\varepsilon_{NLij} = \frac{1}{2}(u_{k,i}u_{k,j}) \quad (4.5.b)$$

Equations 4.5.a and 4.5.b indicate that the linear and nonlinear strains are linear and quadratic functions of displacements. When Equation 4.3 is substituted into Equation 4.2, the strain energy becomes

$$U = \int_v \left(\{\varepsilon_L\}^T [E] \{\varepsilon_L\} + 2\{\varepsilon_{NL}\}^T [E] \{\varepsilon_L\} + \{\varepsilon_{NL}\}^T [E] \{\varepsilon_{NL}\} \right) dv \quad (4.6)$$

According to Akay(1974), the critical equilibrium configuration or the equilibrium at which the structure ceases to be stable is characterized by the second variation of the potential energy changing the sign from positive to negative. When the second variation of the potential energy is equal to zero, the critical equilibrium is obtained. It also yields buckling equations and is expressed as follows

$$\delta^2 \Pi_p = 0 \quad (4.7)$$

The second order differentiation of Equation 4.6 with respect to displacements yields the following

$$\frac{\partial^2 U}{\partial D^2} = \{0\} = ([K] + [K_G])\{\partial D\} \quad (4.8)$$

where $[K]$ is the conventional stiffness matrix, $[K_G]$ is the geometric stiffness matrix, and $\{\partial D\}$ is the infinitesimal displacement vector. The geometric stiffness matrix $[K_G]$ is the function of membrane stress components that are present in the element prior to buckling. In deriving of Equation 4.8, the last term in Equation 4.6 which is the quadratic function of displacements is discarded by assuming small displacements. Deletion of the quadratic term will lead to a linear buckling problem.

The nontrivial solution, $\{\partial D\} \neq \{0\}$, of the Equation 4.8 exists only if the determinant of the coefficient matrix of $\{\partial D\}$ is zero. In other words, the nontrivial solution is given by

$$|[K] + [K_G]| = 0 \quad (4.9)$$

If the reference level of load $\{f\}_{ref}$ is multiplied by the scalar multiplier λ_{cr} , the geometric stiffness becomes

$$[K_G] = \lambda_{cr} [K_G]_{ref} \quad (4.10)$$

The multiplication by λ_{cr} changes the intensity of stress state in the element but does not alter the distribution of stress. Substitution of Equation 4.10 into Equation 4.8. gives

$$\left([K] + \lambda_{cr} [K_G]_{ref} \right) \{ \partial D \} = \{ 0 \} \quad (4.11)$$

Equation 4.11 is characterized as the standard eigenvalue problem whose eigenvalues are buckling load multipliers. In buckling problems, the lowest eigenvalue λ_{cr} is usually of the greater interest. The buckling load is given by

$$\{ f \} = \lambda_{cr} \{ f \}_{ref} \quad (4.12)$$

This load is the bifurcation buckling load but may not be the true collapse load of a member. The collapse load can be quite different from the buckling load because of yielding and postbuckling strength. The eigenvector $\{ \partial D \}$ associated with the λ_{cr} is defined as the buckling mode shape.

4.3 BASP

The linear elastic buckling program, BASP, developed by Akay (1974) is described in detail because the inelastic buckling program developed herein is based on the BASP approach. The program is restricted to the determination of

out-of-plane buckling loads. The plane refers to the plane of web. As stated earlier, BASP can find the elastic distortional and local as well as lateral torsional buckling strength of mono symmetric and double symmetric structures. The program can also be used to study the behavior of braced members.

The computational process used in BASP is composed of three parts. First, in-plane stress analysis of a member is performed to find the membrane stress distribution under a reference load. It is followed by out-of-plane stiffness analysis. In the second part, conventional and geometric stiffness matrices are assembled. Last, the standard eigenvalue problem is solved to determine the buckling load and mode shape. An inverse iteration method is used to solve the eigenvalue problem.

The flange of a member is modeled using one-dimensional elements and the web is modeled using two-dimensional elements. The BASP input model of the I-shaped member is shown in Figure 4.1. Vertical and horizontal stiffeners are also modeled using one-dimensional elements. Akay, Johnson, and Will (1977) observed that modeling of flanges and stiffeners as one-dimensional elements resulted in a substantial reduction in computation time and no significant loss in accuracy. Braces are modeled using elastic axial and rotational spring elements.

During the in-plane stress analysis step, quadrilateral plane stress elements are used as two-dimensional web elements. Each node has two displacement degrees of freedom. Flanges and stiffeners are idealized using one-dimensional truss elements which have only axial stiffness.

Quadrilateral plate bending elements by Clough and Felippa (1968) are used as web plate elements in the out-of-plane analysis step. The element has four nodes, and each node has three degrees of freedom. Flanges are modeled using

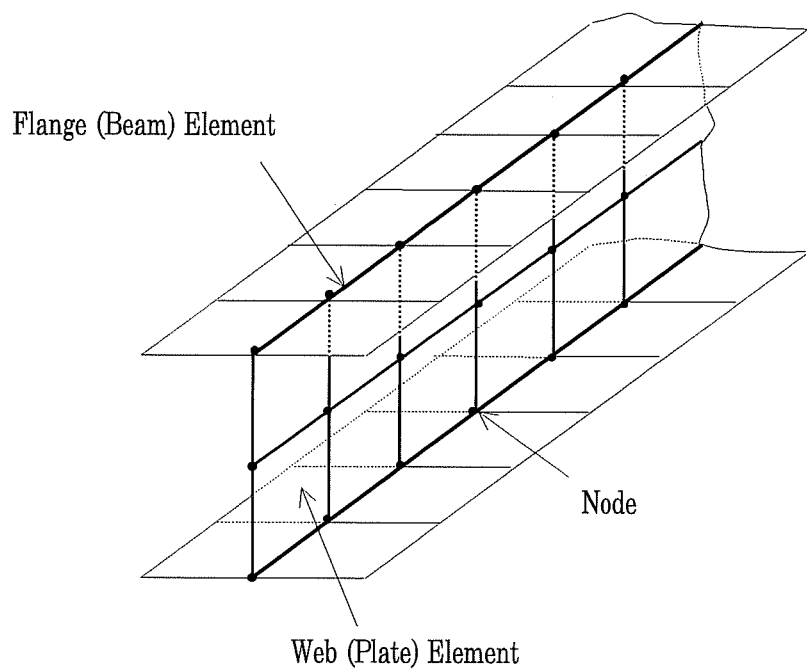


Figure 4.1 BASP Input Model of I-Shaped Member

beam elements with three degrees of freedom: two bending degrees of freedom and one torsional degree of freedom.

The geometric stiffness matrix is constructed by using the membrane stress from in-plane stress analysis and by prescribing out-of-plane displacement shape functions (Akay, 1974). Shape functions for the geometric stiffness matrix can be the same as those for the plate bending element. In BASP, however, the geometric stiffness matrix is derived using displacement shape functions simpler than those for the plate bending stiffness matrix. This resulted in reduced computation time with little loss in accuracy.

4.4 Elements for a New Program

The quadrilateral element used in the elastic buckling program, BASP, does not have the capacity to deal with inelasticity (Johnson, 1995). In the newly developed program, an isoparametric element which can accommodate inelastic deformation is used as discussed later. The web of a member is modeled using the isoparametric plane stress element for in-plane stress analysis and degenerated isoparametric plate element for out-of-plane behavior. For the new program, flanges and stiffeners of the member are modeled using the layered beam element by Owen and Hinton (1980). The layered beam element discussed later can account for the spread of inelasticity through the depth of the beam.

4.4.1 Web Plate Element

In the new inelastic buckling analysis program, the isoparametric elements like the nine-node element shown in Figure 4.2 are used to model the web of a

member. Each node of the element has five degrees of freedom. Two degrees of freedom are for the plane stress elements and remaining three are for plate elements.

A natural coordinate system, ξ and η shown in Figure 4.2, is used in the formulation of an isoparametric element. Displacements at any point in the isoparametric element are interpolated from nodal displacements using shape functions. Coordinates of the point are also interpolated from nodal coordinates using the same shape functions. The interpolation of displacements is expressed as follows

$$u = \sum N_i(\xi, \eta)u_i. \quad (4.13)$$

Although shape functions N_i are defined in terms of natural coordinates ξ and η , they are differentiated in terms of the global coordinates x and y to obtain strain and stiffness matrices.

In-plane stress analysis is performed first to find membrane stresses and the state of material. They are used in the formulation of the out-of-plane stiffness matrix and geometric stiffness matrix. In-plane displacements u and v are interpolated from nodal displacements u_i and v_i of Figure 4.2. Displacements are expressed as

$$\begin{Bmatrix} u \\ v \end{Bmatrix} = \sum_{i=1}^N \begin{bmatrix} N_i & 0 \\ 0 & N_i \end{bmatrix} \begin{Bmatrix} u_i \\ v_i \end{Bmatrix} = [N] \{d_i\} \quad (4.14)$$

where $\{d_i\}$ is the in-plane nodal displacement vector.

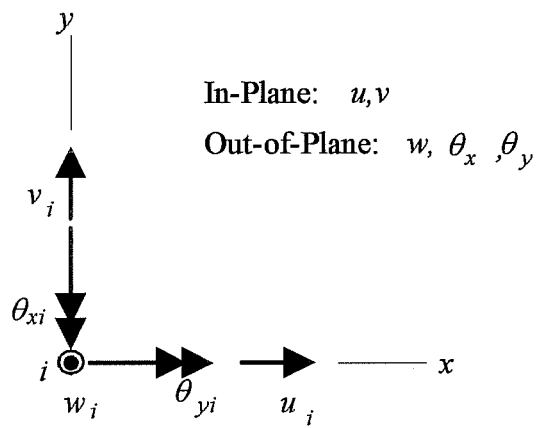
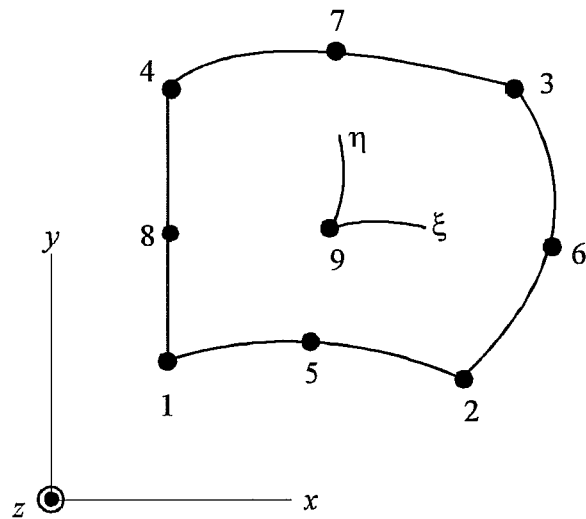


Figure 4.2 Nine-Node Isoparametric Plate Elements

Membrane strains $\{\varepsilon\}$ are obtained by differentiating displacements with respect to the global coordinates x and y and are given by:

$$\{\varepsilon\} = [\partial][N]\{d_i\} = [B]\{d_i\} \quad \text{where } [\partial] = \begin{bmatrix} \partial/\partial x & 0 & \cdot & \cdot \\ 0 & \partial/\partial y & \cdot & \cdot \\ \partial/\partial y & \partial/\partial x & \cdot & \cdot \end{bmatrix} \quad (4.15)$$

where the strain vector, $\{\varepsilon\}$, is composed of three in-plane strain components,

$$\{\varepsilon\} = \begin{bmatrix} \varepsilon_x & \varepsilon_y & \gamma_{xy} \end{bmatrix}^T.$$

The membrane stress-strain relationship follows Hook's law which is defined as:

$$\{\sigma\} = [E]\{\varepsilon\} \quad (4.16)$$

where $\{\sigma\}$ is the in-plane stress vector, $\{\sigma\} = \begin{bmatrix} \sigma_x & \sigma_y & \tau_{xy} \end{bmatrix}^T$, and $[E]$ is the material property matrix. The elastic material property matrix is given by

$$[E] = \frac{E}{1-\nu^2} \begin{bmatrix} 1 & \nu & 0 \\ \nu & 1 & 0 \\ 0 & 0 & \frac{1-\nu}{2} \end{bmatrix}, \quad (4.17)$$

In the matrix $[E]$, E and ν represent Young's elastic modulus and Poisson's ratio, respectively. Then, the plane stress element stiffness matrix from Cook (1983) is defined as follows;

$$[K] = \iint [B]^T [E] [B] t \, dx \, dy. \quad (4.18)$$

According to the survey by Harbok and Hurry (1984), there are almost 100 different types of plate elements available. Plate elements are derived from either Kirchhoff plate theory or Mindlin plate theory. Kirchhoff plate theory assumes that a line that is straight and normal to the midsurface before loading remains straight and normal to the midsurface after loading. Thus, the theory neglects transverse shear deformation. It is generally applied to a thin plate. Mindlin plate theory allows transverse shear deformations so that a line that is straight and normal to the midsurface before loading is assumed to remain straight but not normal to the midsurface. Mindlin theory is applicable to thick plates as well as thin plates. When thin plates are analyzed, Mindlin plate theory may yield less accurate results than Kirchhoff plate theory because of non zero shear stiffness.

The eight-node and nine-node degenerated isoparametric shell element which is developed by Ahmad et al. (1970) are used in this study. The element is based on Mindlin plate theory. The advantage of the isoparametric plate element is that the shape functions from plane stress elements can be used again for plate bending element. Each node of the plate element has three out-of-plane independent degrees of freedom: one translation, w , and two rotations, θ_x and θ_y . The nine-node element and the three degrees of freedom at node i are shown in Figure 4.2.

The moment-curvature and the transverse shear force-strain relationships of Mindlin plate theory (Cook et al., 1989) are given by:

$$\begin{Bmatrix} M_x \\ M_y \\ M_{xy} \\ Q_y \\ Q_x \end{Bmatrix} = - \underbrace{\begin{bmatrix} D & \nu D & 0 & 0 & 0 \\ \nu D & D & 0 & 0 & 0 \\ 0 & 0 & (1-\nu)D/2 & 0 & 0 \\ 0 & 0 & 0 & G_{yz}t & 0 \\ 0 & 0 & 0 & 0 & G_{zx}t \end{bmatrix}}_{[D_M]} \underbrace{\begin{Bmatrix} \theta_{x,x} \\ \theta_{y,y} \\ \theta_{x,y} + \theta_{y,x} \\ \theta_y - w_{,y} \\ \theta_x - w_{,x} \end{Bmatrix}}_{\{\kappa\}} \quad (4.19)$$

where M represents bending moments, Q denotes transverse shear forces, ν is Poisson's ratio, t is the thickness of the plate, G_{yz} and G_{zx} are transverse shear moduli, and D is called the 'flexural rigidity' and defined as

$$D = \frac{Et^3}{12(1-\nu^2)} \quad (4.20)$$

The shear stiffness terms $G_{yz}t$ and $G_{zx}t$ in Equation 4.19 may be divided by 1.2 to account for parabolic distributions of shear stresses τ_{yz} and τ_{zx} .

Displacements (w , θ_x , and θ_y) are interpolated from the out-of-plane nodal displacements $\{d_o\}$ using shape functions N_i . The relationship is expressed as follows:

$$\begin{Bmatrix} w \\ \theta_x \\ \theta_y \end{Bmatrix} = \sum_{i=1}^N \begin{bmatrix} N_i & 0 & 0 \\ 0 & N_i & 0 \\ 0 & 0 & N_i \end{bmatrix} \begin{Bmatrix} w_i \\ \theta_{xi} \\ \theta_{yi} \end{Bmatrix} \quad \text{or} \quad \{u\} = [N]\{d_o\} \quad (4.21)$$

where N is the number of nodes in the element. Curvatures $\{\kappa\}$ are derived from displacements and given by

$$\{\kappa\} = \begin{Bmatrix} \theta_{x,x} \\ \theta_{y,y} \\ \theta_{x,y} + \theta_{y,x} \\ \theta_y - w_{,y} \\ \theta_x - w_{,x} \end{Bmatrix} = [\partial]\{u\} \quad \text{where} \quad [\partial] = \begin{bmatrix} 0 & \partial/\partial x & 0 \\ 0 & 0 & \partial/\partial y \\ 0 & \partial/\partial y & \partial/\partial x \\ -\partial/\partial y & 0 & 1 \\ -\partial/\partial x & 0 & 1 \end{bmatrix} \quad (4.22)$$

When $\{u\}$ is replaced by $[N]\{d_o\}$ from Equation 4.21, curvatures become

$$\{\kappa\} = [\partial][N]\{d_o\} = [B]\{d_o\} \quad (4.23)$$

Then, the plate bending stiffness matrix becomes

$$[K] = \int_A [B]^T [D_M] [B] dA \quad (4.24)$$

The plate element stiffness matrix $[K]$ can be divided into two matrices: a bending stiffness matrix $[K_b]$ and a transverse shear stiffness matrix $[K_s]$. The two matrices are defined as follows:

$$[K] = \underbrace{\int_A [B_b]^T [D_M] [B_b] dA}_{[K_b]} + \underbrace{\int_A [B_s]^T [D_M] [B_s] dA}_{[K_s]} \quad (4.25)$$

The matrix $[B_b]$ of Equation 4.25 is associated with curvatures and is obtained by replacing the fourth and fifth row of $[B]$ with zeros. The matrix $[B_s]$ is associated with transverse shear strains and is obtained by placing zeros at the first, second, and third row of $[B]$.

A numerical integration technique is used to obtain the stiffness matrices because of its convenience and easy implementation. In this study, the Gauss quadrature rule is employed for numerical integration. For eight-node and nine-node isoparametric elements, a 3x3 (nine) mesh of Gauss points is needed for full numerical integration. Full integration works satisfactorily with thick shells and plates. However, it is reported (Cook et al., 1989) that fully integrated isoparametric elements for thin plates suffer from excessive shear rigidity. The phenomenon is called 'locking'. Zienkiewicz, Taylor, and Too (1971) proposed a reduced integration technique to avoid shear locking problems. The reduced integration scheme utilizes a 2x2 (four) mesh of Gauss points to form the bending and shear stiffness matrix. Pugh, Hinton, and Zienkiewicz (1978) further demonstrated the effectiveness of reduced integration techniques for thick and thin isoparametric plate elements. In this study, both full and reduced numerical integration are tried.

The geometric stiffness matrix of the plate element $[K_G]$ is formed using membrane stresses from the prior in-plane stress analysis. Membrane forces which are a summation of membrane stresses through the thickness are defined as

$$N_x = \int_{-t/2}^{t/2} \sigma_x dz \quad N_y = \int_{-t/2}^{t/2} \sigma_y dz \quad N_{xy} = \int_{-t/2}^{t/2} \tau_{xy} dz \quad (4.26)$$

The geometric stiffness is derived from the stationary potential energy and given by

$$[K_G] = \iint [G]^T \begin{bmatrix} N_x & N_{xy} \\ N_{xy} & N_y \end{bmatrix} [G] dx dy \quad (4.27)$$

where the matrix $[G]$ is obtained from a small rotation-displacement relationship and defined by

$$\begin{Bmatrix} w_{,x} \\ w_{,y} \end{Bmatrix} = [G] \{d_o\} \text{ from } w = [N] \{d_o\} \quad (4.28)$$

In the derivation of the geometric matrix, the out-of-plane displacement, w , and membrane forces, N_x , N_y , and N_{xy} , are assumed to be independent of each other.

The geometric stiffness matrix of isoparametric plate elements is also formed using the numerical integration technique. When the in-plane analysis is completed, membrane stresses at Gauss points are saved. Those stresses are utilized in the formation of the geometric stiffness matrix.

4.4.2 Flange Beam Element

The layered beam element by Owen and Hinton (1980) is used to model flanges and stiffeners in the new program. As shown in Figure 4.3, the beam is subdivided into N layers. The layered beam can follow the spread of inelasticity through the depth of the beam by assessing the state of the material at each layer during in-plane and out-of-plane analysis.

The axial stiffness (EA), bending stiffness (EI), and torsional stiffness (GJ) of the layered beam is calculated as:

$$EA = \sum_{l=1}^N E_l b_l t_f \quad (4.29)$$

$$EI = \sum_{l=1}^N (E_l b_l t_f z_l^2 + E_l t_f b_l^3 / 12) \quad (4.30)$$

$$GJ = \sum_{l=1}^N G_l b_l t_f^3 / 3 \quad (4.31)$$

where E_l is the Young's modulus of the layer, G_l is the shear modulus of the

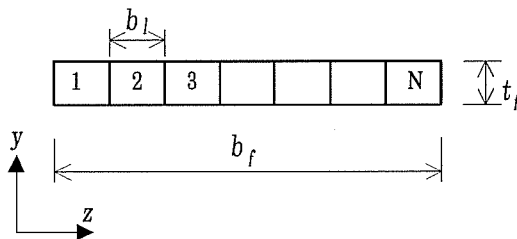


Figure 4.3 Cross-section of a Layered Beam

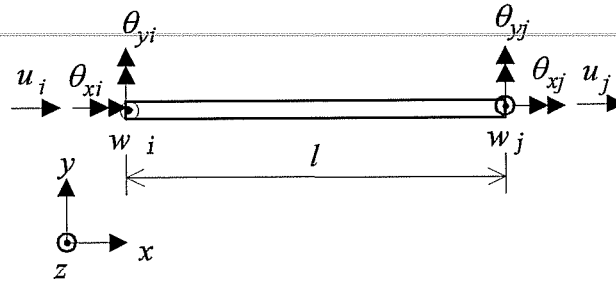


Figure 4.4 Degree of Freedom for a Beam Element

layer, b_l is the width of the layer, t_f is the thickness of the beam element, and the z -coordinate at the middle of the layer.

Four nodal degrees of freedom per node for the layered beam element are shown in Figure 4.4. During in-plane stress analysis, only the axial degree of freedom u is utilized. The rest of the degrees of freedom at each node, an out-of-plane displacement (w) and two rotations (θ_x and θ_y), are used in out-of-plane analysis:

The stiffness matrix of a truss element from Cook et al. (1989) is adopted to idealize the in-plane stiffness of the beam element. The stiffness matrix of the truss element is defined as follows:

$$\left[K_I^b \right] = \frac{EA}{l} \begin{bmatrix} 1 & -1 \\ -1 & 1 \end{bmatrix} \quad (4.32)$$

where l is the length of the element and EA of Equation 4.29 is used as the axial stiffness for the layered beam element.

The bending and torsional stiffness matrices of the beam elements are needed for the out-of-plane buckling analysis. The degrees of freedom w and θ_y in Figure 4.4 are related to the flexural behavior of the beam element in the x - z plane and the degree of freedom θ_x represents the torsion of the beam element. The flexural stiffness matrix, $[K_f^b]$, and the torsional stiffness matrix, $[K_T^b]$, for the beam element (Cook et al., 1989) are given by:

$$[K_f^b] = \begin{bmatrix} \frac{12EI}{l^3} & \frac{6EI}{l^2} & -\frac{12EI}{l^3} & \frac{6EI}{l^2} \\ & \frac{4EI}{l} & -\frac{6EI}{l^2} & \frac{2EI}{l} \\ sym. & & \frac{12EI}{l^3} & -\frac{6EI}{l^2} \\ & & & \frac{4EI}{l} \end{bmatrix} \quad [K_T^b] = \begin{bmatrix} \frac{GJ}{l} & -\frac{GJ}{l} \\ -\frac{GJ}{l} & \frac{GJ}{l} \end{bmatrix} \quad (4.33)$$

where EI is the bending rigidity about y axis and GJ is the torsional rigidity about the x axis. The bending and torsional stiffness given in Equation 4.30 and 4.31 are used for the layered beam element.

The geometric stiffness of the beam element depends only on the axial load and the length of the element. The geometric stiffness matrix for the beam element, $[K_G^b]$, from Cook et al. (1989) is given as follows:

$$[K_G^b] = \frac{P}{l} \begin{bmatrix} 1 & -1 \\ -1 & 1 \end{bmatrix} \quad (4.34)$$

where P represents the axial load. The axial load of the layered beam is obtained using $P = \sum_{l=1}^N \sigma_l b_l t_f$. Degrees of freedom associated with $[K_G^b]$ are out-of-plane displacements, w_i and w_j .

The geometric torsional stiffness matrix of a beam element by Johnson (1972) is defined as

$$[K_G^T] = \frac{GT}{l} \begin{bmatrix} 1 & -1 \\ -1 & 1 \end{bmatrix} \quad (4.35)$$

where l is the length of the flange. GT is the geometric torsional stiffness defined as follows:

$$GT = \int_A \sigma_x y^2 dA = t_f \int_{-b_f/2}^{b_f/2} \sigma_x y^2 dy \quad (4.36)$$

where σ_x is the axial stress, and b_f is the depth of the beam. In the layered beam approach, the geometric torsional stiffness is obtained by adding the stiffness from the each layer.

CHAPTER 5:

Inelastic Finite Element Analysis Program

5.1 Introduction

The inelastic buckling analysis program developed herein is named IBASP. When applied stress or stresses exceed the yield strength of a material, plasticity theories are used to describe the behavior of the material and form stiffness matrices for finite element analysis. In this chapter, plasticity theories are reviewed first. Because of material inelasticity, non-linear analysis methods are required. Iteration methods for material non-linearity problems are also reviewed. The routine which is required to determine the inelastic state of the material during iterations is discussed. Later, eigenproblem solution techniques are discussed to determine buckling loads because the buckling equation is considered as a standard eigenproblem. At the end, the limits of IBASP and a residual stress option are discussed.

Two plasticity theories are employed in this study. An incremental plasticity theory relates the increment of plastic strain to the increment of stresses. The theory depends on stress history. In a deformation plasticity theory, total plastic strain is simply related to total stress. Thus, the deformation theory is independent of stress history. It is reported by Stowel (1948) and Lubliner (1990) that, while the incremental theory is more logical, results from plate buckling tests show that the deformation theory works better. Predicted plate buckling loads by the incremental theory tend to be higher than experimental buckling loads. Results from the two theories will be compared with results from stiffened plate buckling tests and one theory will be selected in Chapter 6.

5.2 Incremental Theory of Plasticity

The three components of the incremental theory of plasticity, which are a yield surface, a flow rule, and a hardening rule, are reviewed.

5.2.1 Yield Surface

The yield condition for a material defines the limit of purely elastic behavior under any combination of stresses. According to Owen and Hinton (1980), two yield criteria are generally used for metals: the Tresca yield criterion and the von Mises yield criterion. In Figure 5.1, both criteria are plotted in a two-dimensional principal stress plane $\sigma_1 \sigma_2$. The yield surface is defined as the shape of the yield function in the stress plane.

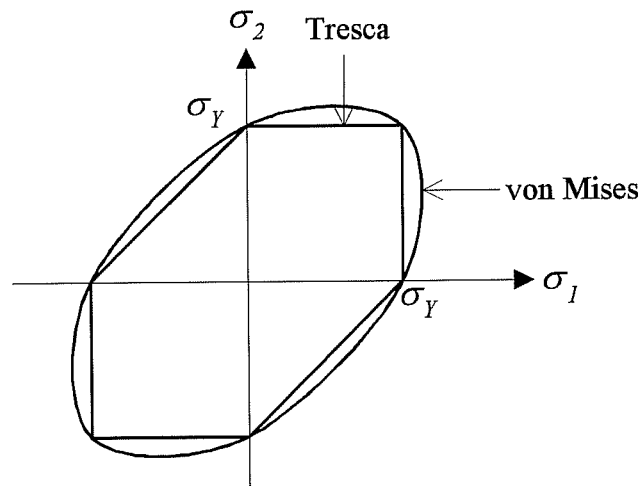


Figure 5.1 Tresca and von Mises Yield Surface

The Tresca yield criterion (Lubliner, 1990) assumes that plastic deformation occurs when the maximum shear stress over all planes reaches the value of the maximum shear stress in yielding in a tension test. The Tresca yield criterion F is expressed as

$$F = \frac{(\sigma_{\max} - \sigma_{\min})}{2} - \frac{\sigma_Y}{2} \quad (5.1)$$

where σ_{\max} and σ_{\min} represent the maximum and minimum principal stress and σ_Y is the tensile yield strength of the material. When F is less than zero, the material is in elastic state. The material is on the yield surface when F is equal to zero.

The von Mises yield criterion (Hunsaker, 1973) assumes that yielding occurs whenever the second invariant of the deviatoric stress tensor (J_2) exceeds a certain value. The von Mises yield criterion F from Tassoulas (1995) is expressed as

$$F = \sqrt{3J_2} - \sigma_Y \quad (5.2)$$

where J_2 is the second invariant of the deviatoric stress tensor which is defined as

$$J_2 = \frac{1}{2} \{S\}^T \{S\} \quad (5.3)$$

where $\{S\}$ is the deviatoric stress tensor. It is derived from

$$S_{ij} = \sigma_{ij} - \sigma_m \delta_{ij} \quad (5.4)$$

where σ_m is the hydrostatic stress which is the average of principal stresses, $\sigma_m = (\sigma_1 + \sigma_2 + \sigma_3)/3$, and δ_{ij} is the Kronecker delta which is defined as $\delta_{ij} = 1$ if $i = j$ and $\delta_{ij} = 0$ if $i \neq j$. The von Mises yield criterion is adopted in this study because it better represents material behavior than Tresca criterion for most metals. The plane stress version of the von Mises yield criterion (Crisfield, 1990) is given by

$$F = \left(\sigma_x^2 + \sigma_y^2 - \sigma_x \sigma_y + 3\tau_{xy}^2 \right) - \sigma_Y \quad (5.5)$$

5.2.2 Flow Rule

The incremental theory of plasticity which is also called the flow theory of plasticity assumes that plastic strain is governed by rate equations (Lubliner, 1990). In other words, the theory relates the plastic strain rate to the rate of yield criterion. The direction of plastic strain is determined by the flow rule.

The strain increment after yielding is composed of the elastic and plastic strain increments as follows:

$$d\{\varepsilon\} = d\{\varepsilon^e\} + d\{\varepsilon^p\} \quad (5.6)$$

where $d\{\varepsilon\}$ is the total strain increment, $d\{\varepsilon^e\}$ is the elastic strain increment, and $d\{\varepsilon^p\}$ is the plastic strain increment. The elastic strain increment is easily obtained using an elastic constitutive law like Hook's law. The flow rule determines the increment of plastic strain. The flow rule (Hunsaker, 1973) is expressed as follows:

$$d\{\varepsilon^p\} = d\lambda \frac{\partial g}{\partial \{\sigma\}} \quad (5.7)$$

where $d\lambda$ is the scalar multiplier, g is the plastic potential function, and $\{\sigma\}$ is the stress vector. If g is equal to the yield function F , the rule is called the associated flow rule. If g is not equal to F , then it is called the nonassociated flow rule. The associated flow rule is defined as

$$d\{\varepsilon^p\} = d\lambda \frac{\partial F}{\partial \{\sigma\}} \quad (5.8)$$

Equation 5.8 is also called the normality condition because, as shown in Figure 5.2, the vector $\partial F / \partial \{\sigma\}$ is normal to the yield surface $F = 0$. The normality condition means that the direction of plastic flow is normal to the yield surface. The normality condition is an acceptable assumption for metal (Owen and Hinton, 1980).

Hunsaker (1973) and Daye and Toridis (1991) define the scalar multiplier $d\lambda$ as

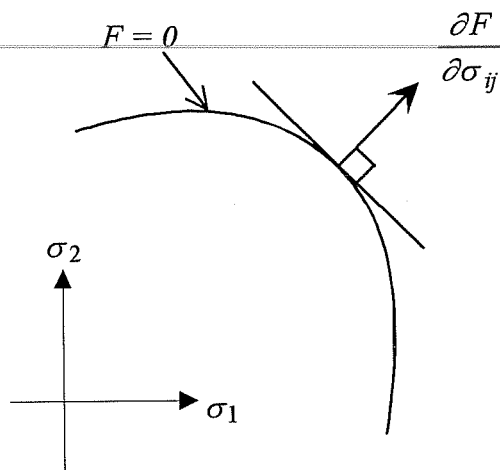


Figure 5.2 Normality Rule

$$d\lambda = \frac{d\bar{\varepsilon}^P}{2\bar{\sigma}} \quad (5.9)$$

where $d\bar{\varepsilon}^P$ is the increment of effective plastic strain and $\bar{\sigma}$ is the effective stress.

The increment $d\bar{\varepsilon}^P$ and the effective stress $\bar{\sigma}$ from Tassoulas (1995) is given by

$$d\bar{\varepsilon}^P = \sqrt{\frac{2}{3} \{d\varepsilon^P\}^T \{d\varepsilon^P\}} \quad (5.10.a)$$

$$\bar{\sigma} = \sqrt{3J_2} \quad (5.10.b)$$

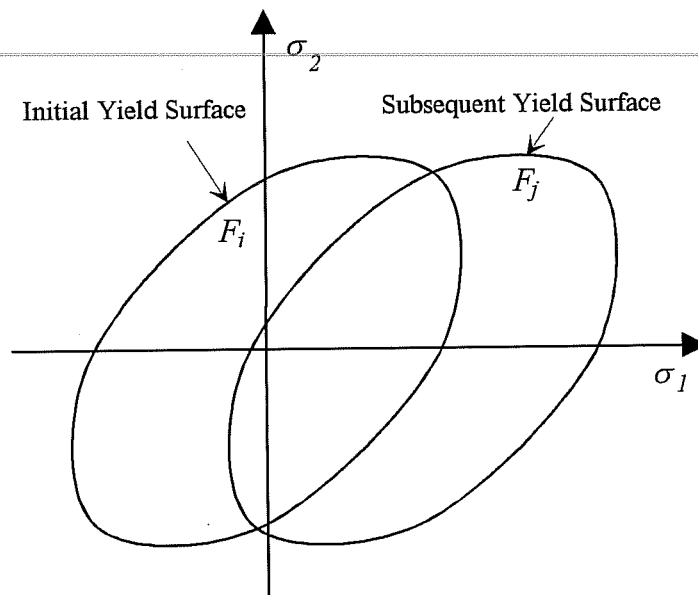


Figure 5.3 Kinematic Hardening

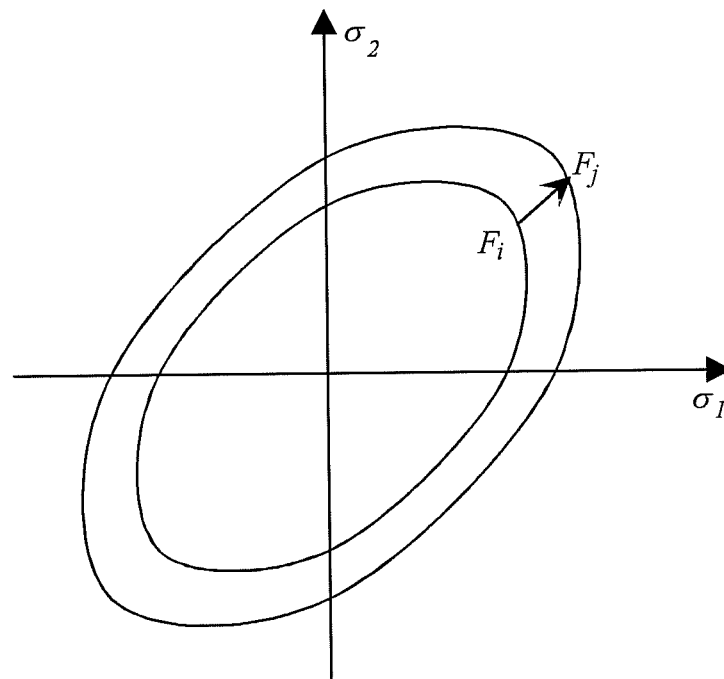


Figure 5.4 Isotropic Hardening

5.2.3 Hardening Rule

A hardening rule is used to describe the behavior of strain hardening materials. It relates strain hardening of arbitrary loading history to a simple loading history from experiments (Hunsaker, 1973). In general, tension test results are used as experimental stress-strain relationships.

Several hardening rules have been proposed and developed (Hunsaker (1973), Crisfield (1991), Tassoulas (1995), and Lubliner (1990)). Deformation, expansion, and translation of the yield surfaces are major factors that differentiate the various hardening rules. An isotropic hardening rule, a kinematic hardening rule, and a Mroz hardening rule are some of the proposed hardening rules.

The isotropic hardening rule assumes that the size of the yield surface is increased while the shape of the surface is not modified. The size of the yield surface depends only on the plastic strain history. The yield surface for kinematic hardening does not change in size and shape but the surface translates in the stress plane. Figure 5.3 illustrates kinematic hardening on two-dimensional stress space. Mroz (1967) proposed another kinematic hardening. The Mroz hardening rule assumes that the yield surface translates within a field of surfaces of constant work-hardening moduli. In this study, the isotropic hardening rule is employed. According to Hunsaker (1973), it is simple to use and it takes the least amount of computer storage for the loading history without unloading and load reversal.

Isotropic hardening in two-dimensional stress space is illustrated in Figure 5.4. The yield surface expands from the initial surface F_i to the subsequent yield surface F_j as the material is strain hardened. The von Mises yield surface was defined in Equation 5.2. The yield function F with isotropic hardening (Tassoulas, 1995) is defined as follows:

$$F(\{\sigma\}, \bar{\varepsilon}^p) = \bar{\sigma} - \sigma_Y(\bar{\varepsilon}^p) = \sqrt{3J_2} - \sigma_Y(\bar{\varepsilon}^p) \quad (5.11)$$

where $\bar{\varepsilon}^p$ is the effective plastic strain and $\sigma_Y(\bar{\varepsilon}^p)$ is the yield strength of the material that is the function of effective plastic strain. $\bar{\varepsilon}^p$ is obtained from the summation of the increment of uniaxial effective plastic strain $d\bar{\varepsilon}^p$ of Equation 5.10.a.

5.2.4. Elasto-Plastic Stiffness Matrix

When plastic deformation begins, the elasto-plastic incremental stress-strain relationship is used to define the plastic behavior of the material. Several references (Hunsaker (1973), Daye and Toridis (1991), Tassoulas(1995), Crisfield (1991), Meek and Lin (1990), Bushnell (1977), and Owen and Hinton (1980)) give procedures to derive the elasto-plastic stiffness matrix. The procedure used by Hunsaker (1973) is employed in this study.

The elastic incremental stress-strain relationship is defined as

$$d\{\sigma\} = [D_e]d\{\varepsilon^e\} \quad (5.12)$$

where $[D_e]$ is the elastic constitutive matrix. As discussed earlier, the total strain increment is composed of the elastic and plastic strain increment. The elastic strain increment is derived from Equation 5.6 as

$$d\{\varepsilon^e\} = d\{\varepsilon\} - d\{\varepsilon^p\} \quad (5.13)$$

and substituted into Equation 5.12. Then, the incremental stress-strain relationship becomes

$$d\{\sigma\} = [D_e] \left(d\{\varepsilon\} - d\{\varepsilon^p\} \right) \quad (5.14)$$

The plastic strain increment which is obtained using the associated flow rule, Equation 5.9, is given by

$$d\{\varepsilon^p\} = \frac{1}{2\bar{\sigma}} \frac{\partial F}{\partial \{\sigma\}} d\bar{\varepsilon}^p = \frac{\partial \bar{\sigma}}{\partial \{\sigma\}} d\bar{\varepsilon}^p \quad (5.15)$$

When Equation 5.14 is multiplied by the term $\left\{ \frac{\partial \bar{\sigma}}{\partial \{\sigma\}} \right\}$ on each side, the equation becomes

$$\left\{ \frac{\partial \bar{\sigma}}{\partial \{\sigma\}} \right\}^T d\{\sigma\} = d\bar{\sigma} = \left\{ \frac{\partial \bar{\sigma}}{\partial \{\sigma\}} \right\}^T [D_e] \left(d\{\varepsilon\} - \frac{\partial \bar{\sigma}}{\partial \{\sigma\}} d\bar{\varepsilon}^p \right) \quad (5.16)$$

The new term, a plastic modulus, is introduced to relate $d\bar{\sigma}$ and $d\bar{\varepsilon}^p$. The tangent modulus for the effective stress-strain relationship in the inelastic region is given by

$$E_T = \frac{d\bar{\sigma}}{d\bar{\varepsilon}} = \frac{d\bar{\sigma}}{d\bar{\varepsilon}^e + d\bar{\varepsilon}^p} = \frac{d\bar{\sigma}}{\frac{d\bar{\sigma}}{E} + d\bar{\varepsilon}^p} \quad (5.17)$$

The above equation yields the plastic modulus E_p which is defined as:

$$\frac{d\bar{\sigma}}{d\bar{\varepsilon}^p} = E_p = \frac{E E_T}{E - E_T} \quad (5.18)$$

If the plastic modulus, Equation 5.18, is substituted into Equation 5.16, the increment of effective plastic strain becomes

$$d\bar{\varepsilon}^p = \frac{\left\{ \frac{\partial \bar{\sigma}}{\partial \{\sigma\}} \right\}^T [D_e] d\{\varepsilon\}}{E_p + \left\{ \frac{\partial \bar{\sigma}}{\partial \{\sigma\}} \right\}^T [D_e] \frac{\partial \bar{\sigma}}{\partial \{\sigma\}}} d\{\varepsilon\} \quad (5.19)$$

From Equations 5.14, 5.15, and 5.19, the elasto-plastic constitutive matrix $[D_{ep}]$ for the incremental plasticity theory is obtained as

$$d\{\sigma\} = [D_{ep}] d\{\varepsilon\} = \left([D_e] - [D_p] \right) d\{\varepsilon\} \quad (5.20)$$

where

$$[D_p] = \frac{[D_e] \frac{\partial \bar{\sigma}}{\partial \{\sigma\}} \left\{ \frac{\partial \bar{\sigma}}{\partial \{\sigma\}} \right\}^T [D_e]}{E_p + \left\{ \frac{\partial \bar{\sigma}}{\partial \{\sigma\}} \right\}^T [D_e] \frac{\partial \bar{\sigma}}{\partial \{\sigma\}}} \quad (5.21)$$

The elasto-plastic stiffness matrix is used in the in-plane stress analysis and in the derivation of the out-of-plane plate stiffness matrix.

5.3 Deformation Theory of Plasticity

The deformation theory of plasticity which is sometimes called a total strain theory assumes that the plastic strain tensor is simply determined by the stress tensor (Lubliner, 1990). Because of its stress history independence, the development theory is mainly applied to proportional or radial loading cases and yields the exact solution (Lubliner, 1990). However, the response of structures under non-proportional loading, such as axial loading followed by torsion, is not predicted correctly. Budiansky (1959) showed that the theory is also suitable for near proportional loading. Despite its shortcoming, the deformation theory has been extensively used in the buckling analysis of plastic plates. Stowel (1948), Pride and Heimerl (1950), and Pifko and Isakson (1969) applied the deformation theory to describe plastic buckling of plates and reported good agreement with experimental results. Tests of long aluminum-alloy cruciform-section columns which were designed to buckle in torsion rather than flexure had been conducted by Gerard and Becker (1957). They reported that the inelastic modulus for pure twisting of plastic plate is very close to what the deformation theory predicts.

Stowell (1948) defined the stress-strain relationship for the deformation theory using the effective stress and strain. The effective stress $\bar{\sigma}$ and strain $\bar{\epsilon}$ for plane stress are defined as

$$\bar{\sigma} = \sqrt{(\sigma_x^2 + \sigma_y^2 - \sigma_x \sigma_y + 3\tau_{xy}^2)} \quad (5.22)$$

$$\bar{\epsilon} = \frac{2}{\sqrt{3}} \sqrt{\left(\epsilon_x^2 + \epsilon_y^2 + \epsilon_x \epsilon_y + \frac{\gamma_{xy}^2}{4} \right)} \quad (5.23)$$

The effective stress and strain are assumed to be related as follows:

$$\bar{\epsilon} = \frac{\bar{\sigma}}{E_s} \quad (5.24)$$

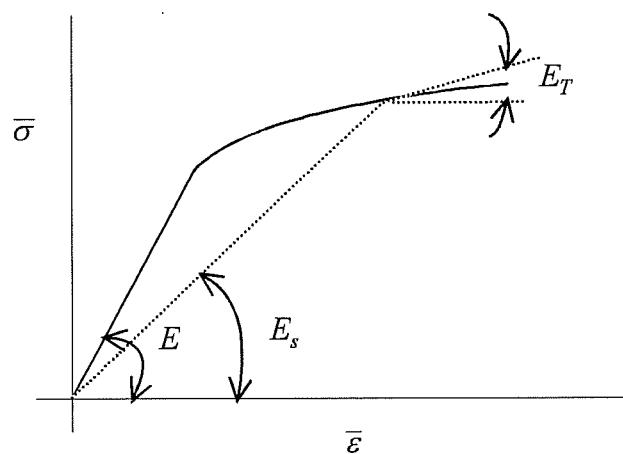


Figure 5.5 Effective Stress and Strain

where E_s is the secant modulus defined by the above equation and illustrated in Figure 5.5 . For strain hardening material, the secant modulus is larger than the tangent modulus E_T but smaller than the elastic modulus E . Then, stress-strain relationships for plane stress become

$$\varepsilon_x = \frac{1}{E_s} \left(\sigma_x - \frac{1}{2} \sigma_y \right) \quad \varepsilon_y = \frac{1}{E_s} \left(\sigma_y - \frac{1}{2} \sigma_x \right) \quad \gamma_{xy} = \frac{3 \tau_{xy}}{E_s} \quad (5.25)$$

The incremental stress-strain relationship for the deformation theory of plasticity was given by Stowel (1948) and Hutchinson(1974). The relationship from Stowel (1948) was used by Pifko and Isakson (1969) and El-Ghazaly et al. (1984) and employed in this study. The elasto-plastic constitutive matrix $[D_{ep}]$ is given by

$$[D_{ep}] = E_s \begin{bmatrix} \frac{4}{3} + \gamma \frac{\sigma_x^2}{\sigma^2} & \frac{2}{3} + \gamma \frac{\sigma_x \sigma_y}{\sigma^2} & \gamma \frac{\tau_{xy} \sigma_x}{\sigma^2} \\ & \frac{4}{3} + \gamma \frac{\sigma_y^2}{\sigma^2} & \gamma \frac{\tau_{xy} \sigma_y}{\sigma^2} \\ sym. & & \frac{1}{3} + \gamma \frac{\tau_{xy}^2}{\sigma^2} \end{bmatrix} \quad (5.26)$$

where $\gamma = \frac{E_T}{E_s} - 1$.

5.4 Plasticity of the Beam Element

The flanges of the member are modeled using layered beam elements as discussed in Chapter 4. When plastic deformation occurs, the spread of plasticity is monitored at each layer. Owen and Hinton (1980) assumed that a layer becomes plastic when the middle of the layer reaches the yield stress of the material.

The incremental inelastic stress-strain relationship of the layered beam will now be defined for finite element analysis. The total strain increment in the inelastic range is composed of elastic and plastic components as follows:

$$d\varepsilon = d\varepsilon_e + d\varepsilon_p \quad (5.27)$$

The increment of stress in the plastic range is defined as:

$$d\sigma = E d\varepsilon_e = E(d\varepsilon - d\varepsilon_p) \quad (5.28)$$

The plastic modulus E_p which relates the increment of stress to the increment of plastic strain was defined in Equation 5.18 and restated here as

$$E_p = \frac{d\sigma}{d\varepsilon_p} = \frac{E E_T}{E - E_T} \quad (5.29)$$

The plastic strain increment $d\varepsilon_p$ is derived from the above equation as $d\varepsilon_p = d\sigma/E_p$ and substituted into Equation 5.28. Then, the elasto-plastic stiffness E_{ep} can be derived as

$$E_{ep} = \frac{d\sigma}{d\varepsilon} = \frac{E E_p}{E + E_p} \quad (5.30)$$

The elasto-plastic stiffness is used in the derivation of the axial and bending stiffnesses of the yielded layer (Equation 4.29 and 4.30). Inelastic shear modulus which determines the torsional stiffness of the yielded layer will be discussed in next section.

5.5 Inelastic Shear Modulus

The inelastic shear modulus is the one of critical factors which influence the torsional and lateral flexural buckling capacities of beams. In previous sections, two plasticity theories were discussed. In this section, they are reviewed to define inelastic shear modulus. After the discussion of plasticity theories regarding shear modulus, literature dealing with the inelastic shear stiffness is reviewed.

5.5.1 Plasticity Theories

The deformation theory of plasticity predicts a decrease of the inelastic shear modulus in the plastic range when shear stresses do not exist. The tangent shear modulus is obtained from Equation 5.26 as follows:

$$G_T = (E_s / 3) + (\tau_{xy}^2 / \bar{\sigma})(E_s / E_T - 1) \quad (5.31)$$

Equation 5.31 shows that the inelastic shear modulus is only a function of the secant modulus when shear stress is absent ($\tau_{xy} = 0$).

Traditionally, the incremental theory of plasticity has been considered to have better theoretical backgrounds than the deformation theory. The incremental plasticity theory assumes that the increment of plastic strain is proportional to the corresponding deviatoric stress increment. If there is no shear stress in the inelastic member, inelastic shear strain is zero and the total shear strain of the inelastic member is equal to the elastic shear strain. As a result, inelastic and elastic shear modulus values are the same. Plate buckling loads predicted by the incremental theory (Damkilde, 1985) are reported to be higher than those from experimental results.

It is concluded that, when shear stresses exist in a member, both incremental and deformation plasticity theories state that the shear modulus is reduced in the plastic range. If there are no shear stresses in the member, the deformation theory predicts a decrease of the shear modulus as a function of the plasticity level. However, the incremental theory of plasticity indicates no difference between elastic and inelastic shear modulus.

5.5.2 Literature Review

Neal (1950) proposed an initial torsional rigidity of yielded beams through theoretical and experimental studies. He employed the incremental theory of plasticity to show theoretically that the initial inelastic shear modulus is equal to the elastic one. During experiments, flexural and torsional loading was applied to beams in sequence. Some beams were partially yielded by flexural loading before torsional loading was applied. The test results indicated that initial torsional

rigidities from partially yielded beams were very close to those from elastic beams. He concluded that the elastic shear modulus should be used as the initial inelastic shear modulus. Payne and Czyak (1960) tested thin-wall polycrystalline cylinders and reported the same results.

Haaijer (1957) suggested an inelastic shear modulus for A36 steel as 2400Ksi. The incremental theory of plasticity was used in the derivation of the modulus. The theory states that the inelastic shear modulus is initially equal to the elastic one but is reduced as the level of shear stress increases. Haaijer chose the reduced modulus from the strain hardening range as the inelastic shear modulus. He also carried out a few tests using structural tubes to find the relationship between shear strain and shear stress. Test results showed the non-linear shear stress-strain relationship when the member was compressed to strain-hardening range and then torsion was applied.

An often quoted inelastic shear modulus was suggested by Lay (1965). He used a slip line theory and local buckling tests to find the inelastic shear stress-strain relationship. The suggested shear modulus depends on the ratio of the elastic modulus E to the strain hardening modulus E_{ST} . The inelastic shear modulus G_T is defined as

$$G_T = G_E \left(2 / \left(1 + \frac{E/E_{ST}}{4(1+\nu)} \right) \right) \quad (5.32)$$

where E_{ST} is the strain hardening modulus and ν is the Poisson's ratio. However, Lay's recommended formula lacks generality and implies impossible values. For example, when the strain hardening modulus exceeds $(E/4(1+\nu))$, Equation 5.32

yields an inelastic shear modulus which is higher than the elastic modulus. On the other hand, the shear modulus will go to zero when the state of the material is in the yield plateau region ($E_{ST} = 0.0$).

Shammamy and Sidebottom (1967) tested three different materials to compare the incremental theory and the deformation theory under proportional and non-proportional loading. Tubes made from a non strain-hardening steel, a strain-hardening steel and a strain-hardening aluminum alloy were subjected to tension-torsion and torsion-tension loading. During non-proportional tension-torsion loading tests, tension was first applied up to a plastic range and held constant while torsion was applied. Results indicated that the initial plastic shear stiffness was the same as the elastic one both for strain-hardening and for non strain-hardening material. However, the shear stiffness dropped rapidly with an increase of torsion. Similar trends were observed also in torsion-tension loading tests. The axial stiffness of inelastic tubes was initially equal to the elastic stiffness but decreased as the axial stress was increased. Test data indicated that the incremental theory of plasticity was better suited to describe the response of strain-hardening and non strain-hardening material under non-proportional loading.

Popov and Petersson (1978) conducted a series of uniaxial loading and torque tests using structural tubes to find inelastic stiffness for general loading cases. Only individual loading, axial loading or torque, was applied to each specimen. No combined effects of axial loading and torque were measured during experiments. They found that the shear stress-strain curve generalized using effective stress and strain is similar to the axial stress-strain curve. It was concluded that the inelastic shear modulus depended on the tangent modulus of uniaxial stress-strain curves and defined as:

$$G_T = \frac{E_T}{E} G \quad (5.33)$$

The suggested shear modulus was not applicable to inelastic buckling analysis because the modulus was found from “shear only” tests with substantial shear strain. During buckling, the main source of inelasticity was not from shear strain but from axial deformation.

Inelastic beam buckling equations by Timoshenko and Gere (1963) were modified from the elastic buckling one (Equation 2.2) by multiplying the ratio of (E_T/E). The underlying assumption of these beam inelastic buckling equations is that, in the inelastic range, the flexural and torsional rigidities are reduced in the same proportion. This assumption would lead to under valued buckling capacities when applied to test data by Neal (1950) and Shammamy and Sidebottom (1967). The data showed no decrease in the initial plastic shear stiffness.

In the development of the program IBASP, both the incremental theory and the deformation theory were tested. When the incremental theory was employed, it was assumed that the inelastic shear modulus of the beam element was equal to the elastic value. The shear modulus was automatically reduced when the deformation theory was used.

5.6 Solution Method for Non-Linear Problems

Non-linear problems generally arise from material and/or geometric non-linearity. In this section, the method and algorithm used to solve non-linear problems will be discussed. Plasticity theories have been discussed and inelastic

stiffness matrices associated with theories have been generated in previous sections. Those matrices will now be used in the non-linear solution process.

The solution process for non-linear problems is divided into two phases. One phase is the iteration method for non-linear problems. Within each iteration, another routine called a ‘plasticity algorithm’ (Crisfield, 1991) is used to determine the state of the material. The plasticity algorithm is the inner loop of the first phase.

The finite element equation for material non-linearity (Tassoulas, 1995) is defined as follows:

$$\left[\int_V [B]^T [D][B] dV \right] d\{\Delta U\} = (\beta + \Delta\beta)\{P\} - \int_V [B]^T (\{\sigma\} + \{\Delta\sigma\}) dV \quad (5.34)$$

where $\int_V [B]^T [D][B] dV$ is the tangent stiffness matrix $[K]$, $d\{\Delta U\}$ is the increment of displacements, $(\beta + \Delta\beta)\{P\}$ is the external or applied load, β and $\Delta\beta$ are the load parameters, and $\int_V [B]^T (\{\sigma\} + \{\Delta\sigma\}) dV$ is the internal load.

The right hand side of Equation 5.34 represents out-of-balance load $\{R\}$. The matrix $[D]$ of the tangent stiffness matrix $[K]$ is the constitutive matrix and is a function of the state of the material. Figure 5.6 illustrates the non-linear finite element equation.

Equation 5.34 cannot be solved directly because the stiffness matrix depends on the state of the material as shown in Figure 5.6. Iteration methods are required to solve Equation 5.34. At i th iteration, the tangent stiffness matrix and the out-of-balance load vector are

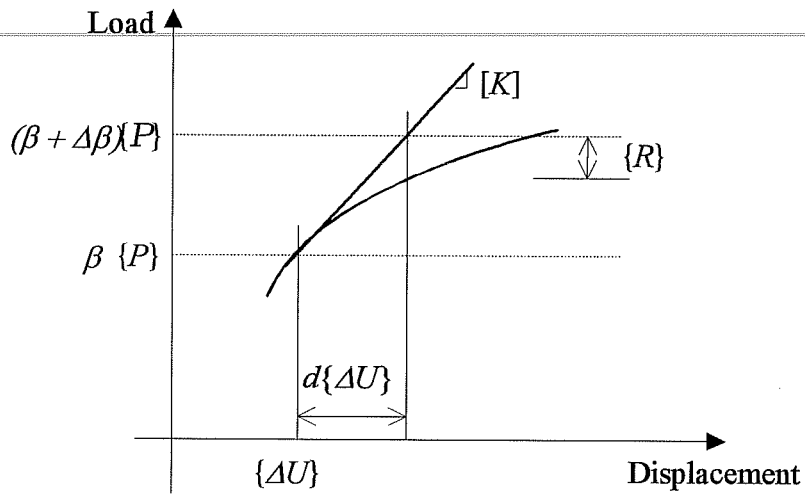


Figure 5.6 Non-Linear Problem Solution Procedure

$$[K^{(i)}] = \int_V [B]^T [D^{(i)}] [B] dV \quad (5.35)$$

$$\{R^{(i)}\} = (\lambda + \Delta\lambda)\{P\} - \int_V [B]^T (\{\sigma\} + \{\Delta\sigma\}^{(i)}) dV \quad (5.36)$$

Then, Equation 5.34 becomes

$$[K^{(i)}] d\{\Delta U\} = \{R^{(i)}\} \quad (5.37)$$

The above equation is solved for $d\{\Delta U\}$. The updated displacements and strains are

$$\{\Delta U^{(i+1)}\} = \{\Delta U^{(i)}\} + d\{\Delta U\} \quad (5.38)$$

$$\{\Delta \varepsilon^{(i+1)}\} = [B]\{\Delta U^{(i+1)}\} \quad (5.39)$$

The new state of material is determined from the strain vector $\{\Delta \varepsilon^{(i+1)}\}$. The process is iterated until convergence criteria are satisfied.

Bushnell (1977), Bathe and Cimento (1979), Cook et al. (1989), and Crisfield (1991) suggested iteration methods for non-linear problems like Equation 5.34. They recommended methods such as a Newton-Raphson method, a modified Newton-Raphson method, a quasi Newton-Raphson method, and an arc-length method. The main difference between the iteration methods lies in the formulation and update scheme of the tangent stiffness matrix. The modified Newton-Raphson method which updates the tangent stiffness matrix infrequently is employed in this study. It is easy to implement and less influenced by the load increment but is slow to converge. It also takes more iteration cycles than the other methods.

Another routine, the plasticity algorithm, is needed to determine the material state and form the corresponding tangent stiffness matrix. Stresses are updated through the integration of an elastic-plastic constitutive law in the plasticity algorithm. Krieg and Krieg (1977) reviewed algorithms for elastic-perfectly plastic material. Schreyer et al. (1979) studied a number of plasticity routines for isotropic hardening material. Dodds (1987) studied plasticity algorithms and recommended the elastic predictor-radial return algorithm over other routines. He suggested that the best convergence is achieved when the constitutive matrix $[D]$, which is consistent with the elastic predictor-radial return

algorithm, is used. Tassoulas (1995) also used the elastic predictor-radial return algorithm for isotropic hardening.

The elastic predictor-radial return algorithm is used in this study. The ‘elastic predictor’ means that, initially, the elastic stress-strain relationship is assumed. Thus, stresses are calculated using the elastic constitutive law. If the state of material is not elastic, stresses are returned to the yield surface. It is also assumed that the effective stress and strain follow the uniaxial test results. The procedure suggested by Tassoulas (1995) and Dodds (1987) is employed.

First, terms related with the stresses and strains are defined. Stresses are divided into deviatoric and hydrostatic stresses as defined in Equation 5.3. The strain increment is also split into two parts: the deviatoric and the volumetric strain increment. The stresses and increments of strains are expressed as follows

$$\sigma = \frac{1}{3} \{i\}^T \{\sigma\} \quad \{S\} = \{\sigma\} - \{i\} \sigma \quad (5.40)$$

$$\Delta\varepsilon = \{i\}^T \{\Delta\varepsilon\} \quad \{\Delta e\} = \{\Delta\varepsilon\} - \frac{1}{3} \{i\} \Delta\varepsilon \quad (5.41)$$

where $\{i\}^T = [1 \ 1 \ 1 \ 0 \ 0 \ 0]$, σ and $\{S\}$ represents hydrostatic stress and deviatoric stress, $\Delta\varepsilon$ and $\{\Delta\varepsilon\}$ are the volumetric and deviatoric strain increments. The relationships between stresses and strains are defined as

$$\sigma = K \varepsilon \quad (5.42)$$

$$\{S\} = 2G \{e\} \quad (5.43)$$

where ε is volumetric strain, K is the bulk modulus, and G is the shear modulus.

As shown in Equation 5.39, the incremental strain $\{\Delta\varepsilon\}$ is obtained from the displacement increment $\{\Delta U\}$. Because an elastic stress-strain relationship is initially assumed in the elastic predictor-radial return algorithm, trial stresses are calculated using the elastic constitutive law and added to the existing stresses (σ and $\{S^T\}$).

$$\sigma^T = \sigma + K \Delta\varepsilon \quad (5.44)$$

$$\{S^T\} = \{S\} + 2G\{\Delta e\} \quad (5.45)$$

where the superscript T represents *trial* state. The trial effective stress becomes

$$\bar{\sigma}^T = \sqrt{\frac{3}{2} \{S^T\}^T \{S^T\}} \quad (5.46)$$

If $\bar{\sigma}^T < \sigma_y(\bar{\varepsilon}^P)$ that means $\bar{\sigma}^T$ is less than the current yield stress, the material is still elastic. Then, the stresses and plastic strain become

$$\{\sigma\} + \{\Delta\sigma\} = \{S^T\} + \{i\}\sigma^T \quad (5.47)$$

$$\bar{\varepsilon}^P = \bar{\varepsilon}^P \quad (5.48)$$

The above equations mean that the elastic trial stresses become a new level of stresses and effective plastic strain is not increased. The elastic constitutive matrix is used in the calculation of the tangent stiffness matrix.

If $\bar{\sigma}^T \geq \sigma_Y(\bar{\varepsilon}^p)$, then plastic deformation is started. Elastically predicted trial stresses need to be modified to satisfy the yield criteria. The increment of effective plastic strain $\Delta\bar{\varepsilon}^p$ is obtained from the following equation:

$$\sigma_Y(\bar{\varepsilon}^p + \Delta\bar{\varepsilon}^p) + 3G\Delta\bar{\varepsilon}^p = \bar{\sigma}^T \quad (5.49)$$

The increased effective plastic strain $\bar{\varepsilon}^p + \Delta\bar{\varepsilon}^p$ leads to higher yield strength $\sigma_Y(\bar{\varepsilon}^p + \Delta\bar{\varepsilon}^p)$. Then, the increments of stresses are determined and added to previous stresses as follows

$$\{S\} + \{\Delta S\} = \frac{\sigma_Y(\bar{\varepsilon}^p + \Delta\bar{\varepsilon}^p)}{\bar{\sigma}^T} \{S^T\} \quad (5.50)$$

$$\{\sigma\} + \{\Delta\sigma\} = \{S\} + \{\Delta S\} + \{i\}(\sigma + \Delta\sigma) \quad (5.51)$$

$$\bar{\varepsilon}^p = \bar{\varepsilon}^p + \Delta\bar{\varepsilon}^p \quad (5.52)$$

The above algorithm is derived for three-dimensional stress-strain relationships. The elastic predictor-radial return algorithm for a plane stress condition is more complex than the above derivation because $\Delta\varepsilon_z$ is required for the calculation of trial stresses while $\Delta\sigma_z$ should be zero. The algorithm which satisfies the plane stress condition and the consistent constitutive matrix recommended by Dodds (1987) is given in Appendix A.

5.7 Eigenproblem Solution Routine

Because buckling equations are considered as standard eigenproblems, eigenproblem solution methods are used to solve buckling equations. Eigenvalues and eigenvectors of the buckling equation represent buckling loads and mode shapes respectively. Iteration methods are generally preferred for solving large size eigenproblems. A power method, an inverse iteration method, a subspace iteration, a Lanzos method are generally recommended iteration methods for large size problems (Humar, 1990). An appropriate iteration method is selected depending on the solution requirements.

The conventional and geometric stiffness matrices are obtained from the in-plane and out-of-plane analyses as discussed in Chapter 4. The buckling equation is restated here as

$$([K] + \lambda[K_G])\{U\} = 0 \quad (5.53)$$

The nontrivial solution of the above equation exists only when the determinant of stiffness matrices is equal to zero. The determinant is expressed as follows:

$$|[K] + \lambda[K_G]| = 0 \quad (5.54)$$

For the given state of stress, the eigenvalue λ assumes certain values to satisfy the above equation. When the critical (buckling) state of stresses is reached, the eigenvalue λ is equal to one (Gupta, 1978). Thus, it can be stated that buckling happens when $\lambda = 1$.

A Sturm sequence property (Gupta, 1973 & 1978) is used to determine whether or not the critical state is reached. This property states that the number of changes in signs of leading principal minors of a standard eigenproblem like $([A] - \lambda[B])$ is equal to the number of eigenvalues less than the current λ . Leading principle minors are obtained by factorizing the matrix. The matrix $([K] + \lambda[K_G])$ is factorized into $[L][D][L]^T$ where $[L]$ is the lower triangular matrix and $[D]$ is the diagonal matrix: $[D]=d_{ii}[I]$ where $[I]$ is the identity matrix. The diagonal elements of the matrix $[D]$ represent leading principal minors. The Sturm sequence property can be restated as the number of negative elements in $[D]$ equals to the number of eigenvalues smaller than λ . When the critical state $\lambda = 1$ is reached, a slight increase of λ , say $\lambda + \alpha$, results in *one* negative element in the matrix $[D]$. The slight decrease of λ , $\lambda - \alpha$, will lead all positive elements in $[D]$. α represents the solution tolerance and can be changed. By using the Sturm sequence property, the buckling load can be determined by just looking at the leading principal minors of stiffness matrices rather than calculating eigenvectors as well as eigenvalues to see whether $\lambda = 1$. The algorithm given below is used to find the buckling load.

- 1) read or set the load increment $\Delta\beta\{P\}$
- 2) the total load becomes $(\beta + \Delta\beta)\{P\}$
- 3) perform in-plane and out-of-plane analysis and form $[K]$ and $[K_G]$
- 4) add two matrices to form $[K_s] = [K] + (\lambda + \alpha)[K_G]$ where $\lambda = 1$ and α is the allowable error
- 5) factorize the matrix $[K_s]$

- 6) determine whether all leading principal minors are positive
 - If yes, then increase the load by going back to step (1) and start the procedure again with the increased load
 - If not, the buckling load may be obtained; go to step (7)
- 7) form a new matrix $[K_s] = [K] + (\lambda - \alpha)[K_G]$ with $\lambda = 1$
- 8) determine whether all leading principal minors are positive
 - If yes, then the critical buckling state is reached; stop routine
 - If not, the buckling load is passed; go to step (9)
- 9) reduce the load increment by half $\Delta\beta = \frac{\Delta\beta}{2}$ and go back to step (3)

After finding the buckling load, a corresponding buckling shape is determined using the subspace iteration method with shifts (Humar, 1990). A few iterations would be enough to find the buckled shape when the true critical state is reached.

As shown in the above routine, the load increment is reduced by half when the increased load exceeds the buckling load. The increment is also reduced when the in-plane stress analysis routine does not converge in a given number of in-plane iterations. When the load increment is less than 1×10^{-10} , the program is stopped but still calculates a buckled shape. The program will issue a warning when that happens.

5.8 IBASP Program

The details of inelastic finite element analysis have been discussed. In this section, programming details and the limit of IBASP are discussed. The residual stress option in IBASP is also discussed. The sample input file for IBASP is given in Appendix B.

5.8.1 IBASP Programming and Limit

IBASP was programmed using FORTRAN 77 and compiled using a WATCOM FORTRAN 77³² compiler (WATCOM, 1993). The graphic routines from the compiler were also used to draw a buckled shape. The program was compiled for MS-DOS and needs a DOS extender file, *DOS4GW.EXE*, in the directory which is running. A Personal Computer with 486 or Pentium chips is preferred to run IBASP. The examples of Chapter 6 are executed on a 486 Personal Computer. The maximum number of elements and nodes allowed in IBASP is 40 nine-node elements and 200 nodes. The 200 beam elements used to model the stiffeners and flanges are allowed in IBASP.

The program generates two output files. One is a '*ibo*' which has general information like boundary conditions, coordinates of nodes, buckling load, stress distributions, and in-plane displacements. The buckled shape of the member is given in a file, '*deform.dat*' which can be imported to spread sheet programs.

5.8.2 Residual Stress

Residual stresses generated from different cooling rates on different parts of a cross-section reduce the buckling capacities of inelastic beams and columns. In IBASP, a user can decide whether residual stresses need to be included or not.

Compressive residual stresses occur at a more exposed area like flange tips for rolled I-shaped sections. The junction of a flange and a web in I-shaped sections cools later and has tensile residual stresses. The residual stress model (Galambos and Ketter, 1959) shown in Figure 5.7 is widely used and employed here. In Figure 5.7, T and C represent the area with tensile and compressive residual stresses respectively. The magnitude of tensile residual stresses is given by

$$\sigma_{rt} = \left(\frac{B t_f}{B t_f + t_w (D - 2 t_f)} \right) \sigma_{rc} \quad (5.55)$$

where σ_{rt} is the maximum tensile residual stress and σ_{rc} is the maximum compressive residual stress. The amount of the maximum compressive residual stress is given by a user.

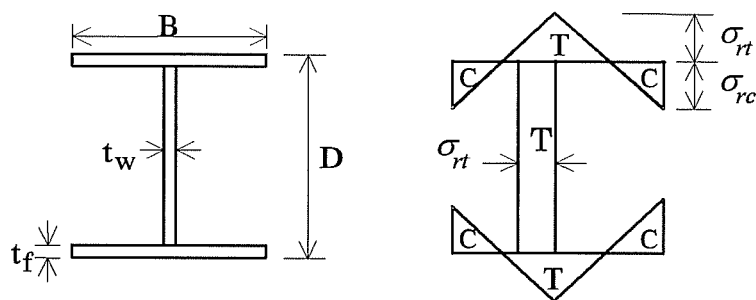


Figure 5.7 Assumed Residual Stresses Distribution

CHAPTER 6:

IBASP Calibration

6.1 Introduction

The inelastic buckling analysis program, IBASP, was developed as explained in Chapter 4 & 5. The program can predict elastic and inelastic buckling capacities of the members. In this chapter, the program is tested using theoretical solutions and experimental results. Two different plasticity theories are compared with experimental and theoretical results. Both the eight-node and the nine-node element are used.

Four different sets of inelastic buckling solutions and test results are adopted to demonstrate the accuracy of the IBASP program. First, the buckling loads of a cantilever column and the buckling moments of a simply supported beam are calculated and compared with theoretical solutions. A bilinear stress-strain relationship is assumed for the column and the beam. Second, continuous beam tests by Bansal (1971) are used where the beams failed by lateral buckling. Third, Elgaaly and Salkar's (1990) in-plane edge loading tests are employed for a comparison with the tested sections which failed by web crippling. Last, the results from Ales and Yura's (1993) braced beam buckling tests are compared with the IBASP results.

The simple parametric study is performed to show that IBASP can be the effective tool to find the brace stiffness requirements of inelastic as well as elastic members.

6.2 Inelastic Buckling Examples

In this section, elastic and inelastic buckling loads of cantilever columns and buckling moments of simply supported beams are determined using IBASP. The results from IBASP are compared with theoretical solutions. The cross-section dimensions shown in Figure 6.1 and the idealized bilinear stress-strain relationship shown in Figure 6.2 are used for both the columns and beams. The material is assumed to become inelastic at 30 ksi as shown in Figure 6.2.

6.2.1. Cantilever Column

The elastic buckling load for the column is expressed as

$$P_{cr} = \frac{\pi^2 EI}{(kL^2)} \quad (6.1)$$

where the k is the effective length factor. For a cantilever column of Figure 6.3, the k factor is equal to 2. According to the tangent modulus theory, the inelastic

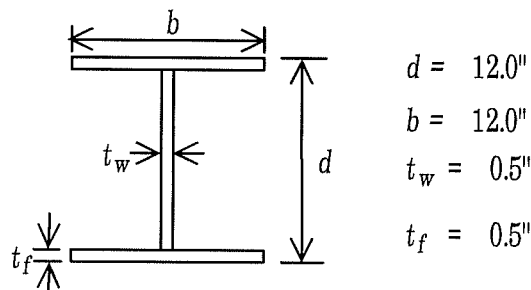


Figure 6.1 Cross-section Properties

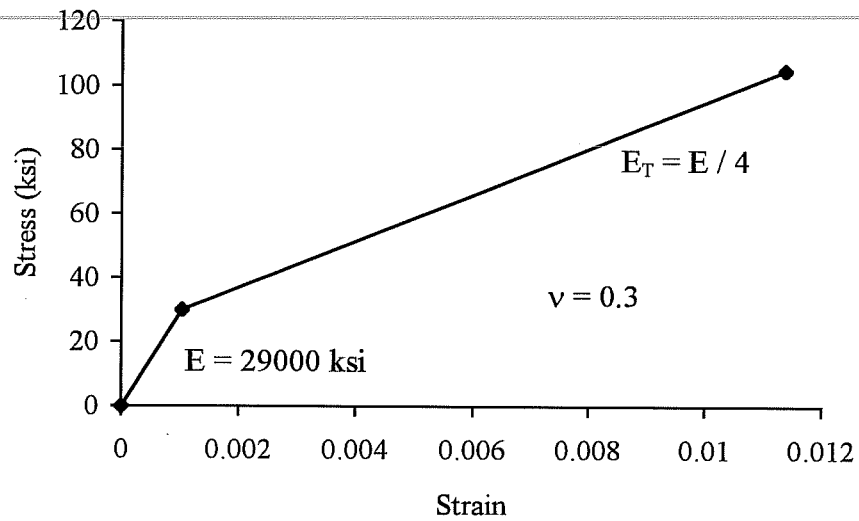


Figure 6.2 Material Properties

buckling load is determined by multiplying the inelasticity ratio τ by the elastic buckling load. The inelasticity ratio τ is defined as

$$\tau = \frac{E_T}{E} \quad (6.2)$$

Then, the inelastic buckling load of a given column is expressed as

$$P_{cr} = \tau \frac{\pi^2 E I}{(k L^2)} \quad (6.3)$$

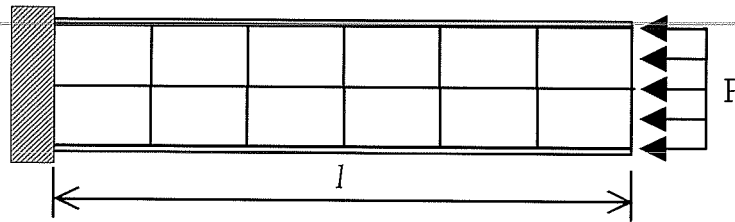


Figure 6.3 Cantilever Column Model

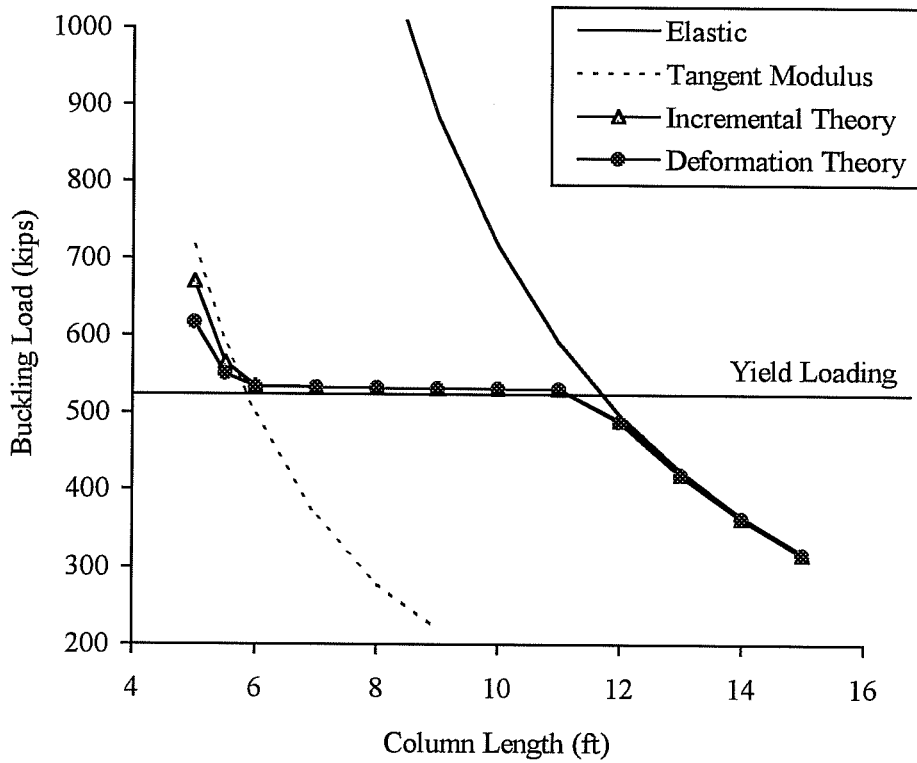


Figure 6.4 Column Strength Curve

Different meshes were tried to check the convergence. It was observed that, with mesh refinements, the IBASP results converged to theoretical solutions. The results shown in Figure 6.4 were obtained using a 2x6 mesh. The results from IBASP using two different plasticity theories and the elastic and tangent modulus buckling loads are shown in Figure 6.4. In the elastic range, the IBASP results are almost equal to the theoretical values from Equation 6.1. In the inelastic state, buckling loads from IBASP are lower than those from the tangent modulus theory. This may be due to the stress concentration right under the applied load. The stress concentration causes localized large plastic deformation which reduces the stiffness of the column. The IBASP results also indicate that the incremental theory of plasticity yields higher buckling loads than the deformation theory.

6.2.2 Simply Supported Beam with Constant Moment

The simply supported beam under a constant moment as shown in Figure 6.5 is used to compare the results from the IBASP to the theoretical solutions by Timoshenko and Gere (1961). The elastic and inelastic lateral-torsional buckling moments which were discussed in Chapter 2 are briefly reviewed here. The elastic buckling moment, M_{cr}^E , is expressed as

$$M_{cr}^E = \frac{\pi}{l} \sqrt{EI_y \left(GJ + EC_w \frac{\pi^2}{l^2} \right)} \quad (6.4)$$

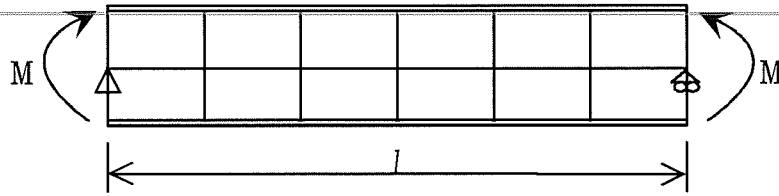


Figure 6.5 Simply Supported Beam Model under the Constant Moment

Timoshenko and Gere (1961) suggested that the inelastic buckling moment is obtained by multiplying the inelasticity ratio, τ , to the above equation. Then, the inelastic buckling moment, M_{cr}^I , is expressed as follows,

$$M_{cr}^I = \tau M_{cr}^E \quad (6.5)$$

As discussed in Chapter 2, the above equation is too conservative because the shear modulus is assumed to be reduced in the inelastic range. If the elastic shear modulus is used as the inelastic shear modulus, the inelastic buckling moment becomes

$$M_{cr}^I = \frac{\pi}{l} \sqrt{E_T I_y (GJ + E_T C_w \frac{\pi^2}{l^2})} \quad (6.6)$$

The analysis results along with the theoretical solutions are plotted in Figure 6.6. It shows the relationship between the lateral-torsional buckling moments and the beam lengths. The buckled shape and cross-section deformation are shown in Figure 6.7.

Figure 6.6 shows that, as in the column buckling problems, the deformation theory yields lower buckling moments than the incremental theory in the inelastic range. The difference between two plasticity theories is more evident as the level of the inelasticity is increased. It also shows that the inelastic buckling moments from Equation 6.6 closely match with those from the incremental theory.

In general, the eight-node element yielded lower buckling moments and loads than the nine-node element. However, the difference between two elements was small.

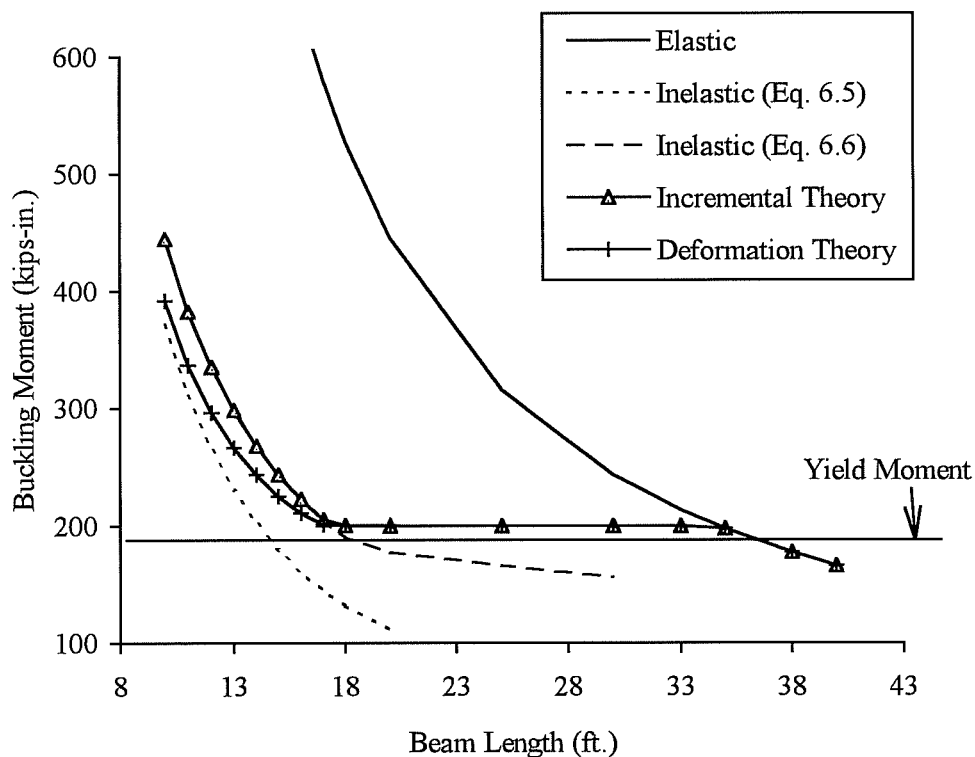
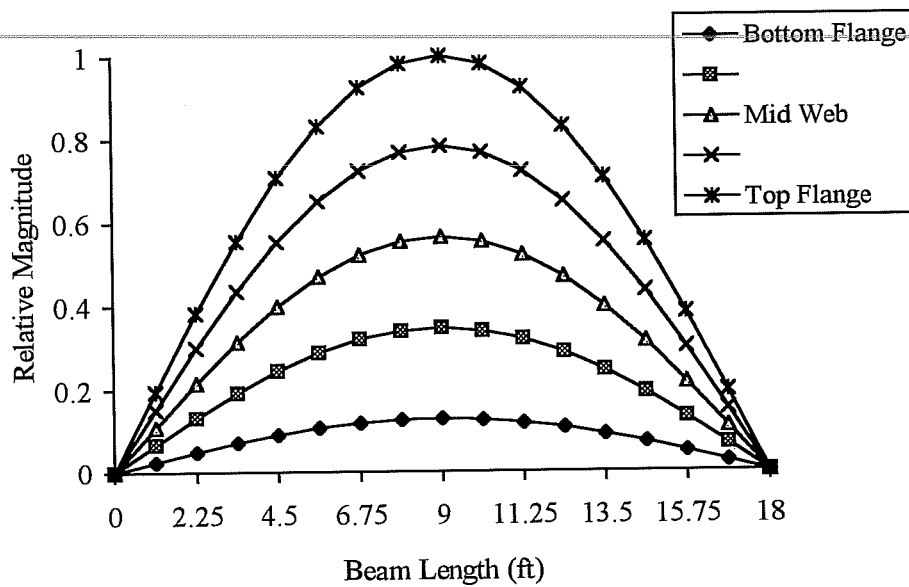
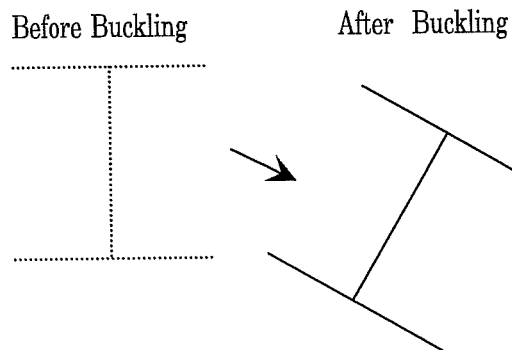


Figure 6.6 Buckling Moments of Simply Supported Beam



(a) Lateral-Torsional Buckling Shape



(b) Cross-section of the Buckled Beam at Midspan

Figure 6.7 Buckling Shapes of Simply Supported Beams and Cross-section Displacement

6.3 Bansal's Test

Bansal (1971) conducted a total of 37 buckling tests using three span continuous steel beams to study elastic and inelastic instability behavior. Rolled I-shaped beams and plate girders were used in tests. The results from the five tests which failed by lateral buckling are used here to compare with those from the program, IBASP. It was reported (Bansal, 1971) that all five beams except Test #4 buckled in the inelastic range. The cross-section dimensions for each test are given in Table 6.1. Table 6.2 shows the material properties of the beams.

Test setups for each test are illustrated in Figures 6.8. The differences between tests were the beam slenderness ratio, number of loads, and the placement of braces and stiffeners. A total of 32 elements (2x16) was used to model the continuous beams. The eight-node and nine-node elements as well as two different plasticity theories were used during the analytical studies. Residual stress was not used.

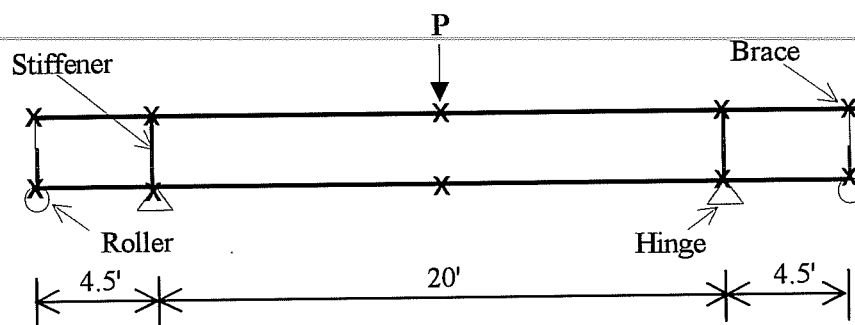
The load vs. the vertical displacement at the midspan curves from experiments and analysis using the incremental theory are plotted in Figure 6.9 through 6.13. The buckled shapes from IBASP are also shown in the figures. The *lateral buckling load* in the figures represents the observed lateral buckling loads from the experiments. The load-displacement curves from experiments show that the buckled beam had some post buckling strength. However, IBASP predicts the buckling load of the beams but not the post buckling strength.

Table 6.1 Material Properties of Tested Beams from Bansal (1971)

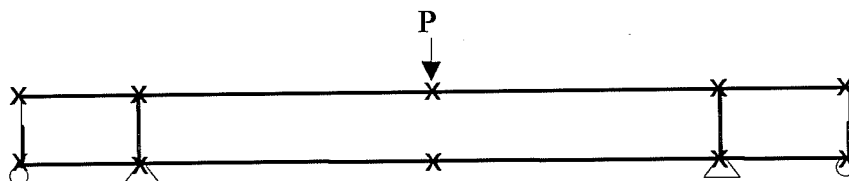
Test No.	Section	Yield Stress, ksi	Strain Hardening Strain	Strain Hardening Modulus
4	W12 x 14	65.35	22000	394
6	W12 x 16.5	48.35	-	-
10	W12 x 22	57.25	12000	570
15	W16 x 26	63.75	18000	567
17	W12 x 14	43.75	15000	1045

Table 6.2 Cross-section Properties of Tested Beams from Bansal (1971)

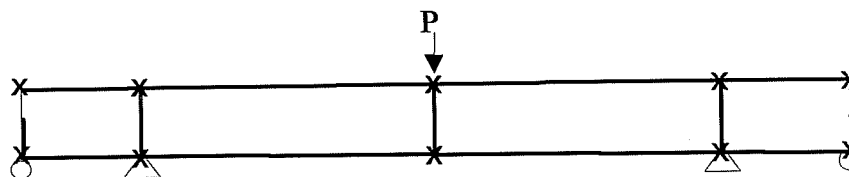
Test No	Section	Depth	Flange Width	Flange Thickness	Web Thickness
4	W12 x 14	11.98	3.99	0.229	0.200
6	W12 x 16.5	12.10	4.04	0.273	0.230
10	W12 x 22	12.34	3.98	0.425	0.260
15	W16 x 26	15.69	5.63	0.337	0.257
17	W12 x 14	11.93	3.98	0.256	0.212



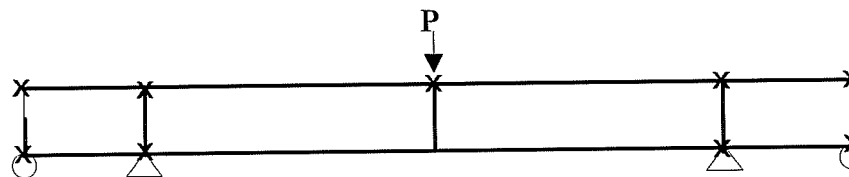
(a) Test Number 4



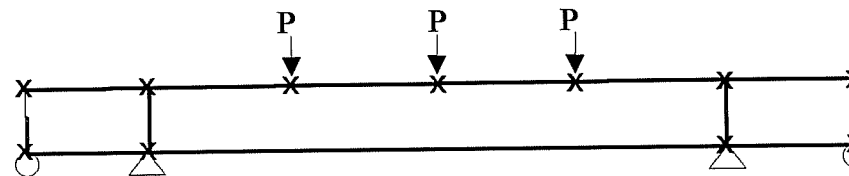
(b) Test Number 6



(c) Test Number 10

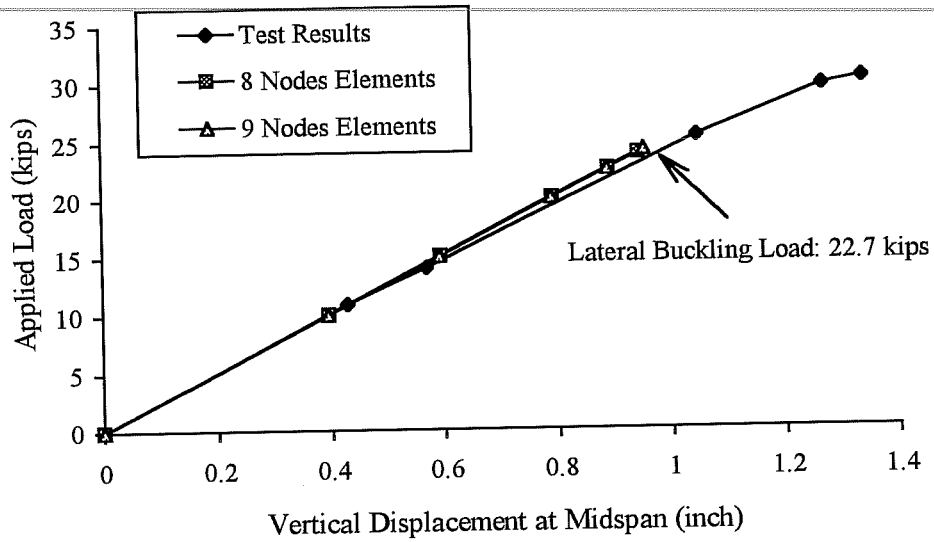


(d) Test Number 15

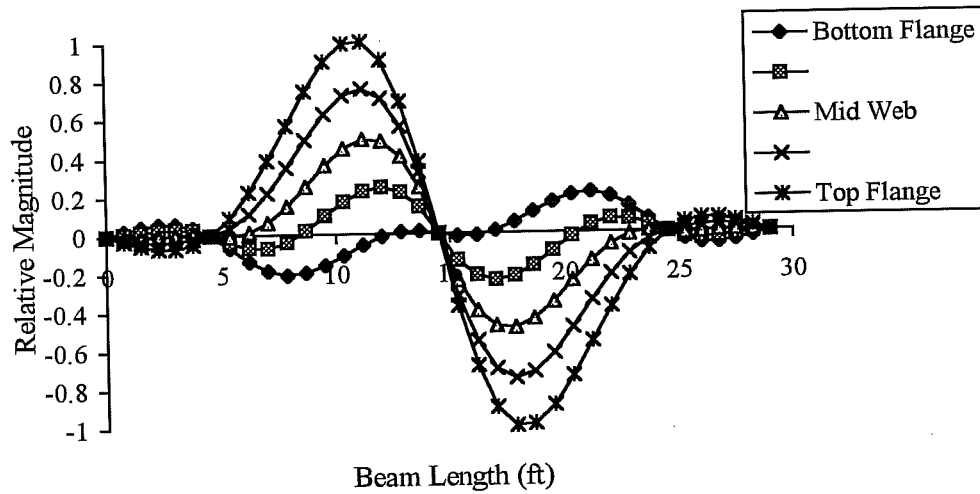


(e) Test Number 17

Figure 6.8 Bansal's Test Setups

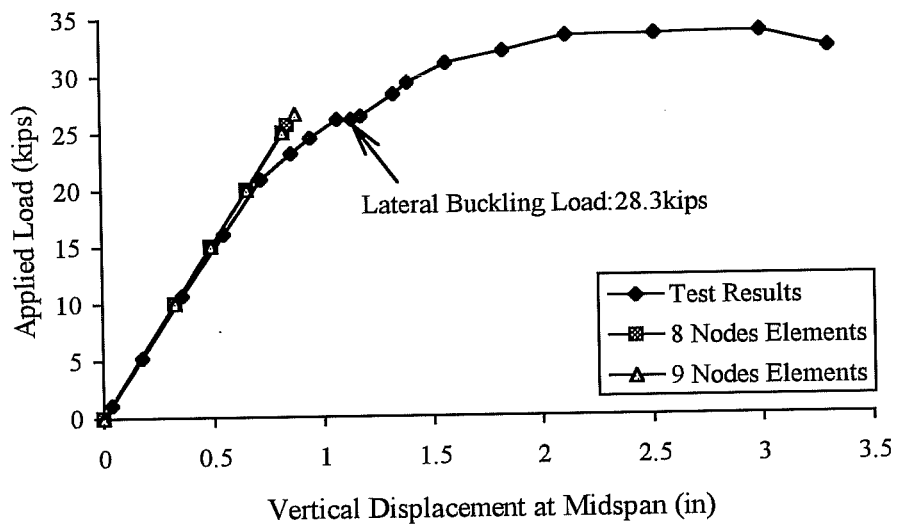


(a) Load. Vs. Displacement

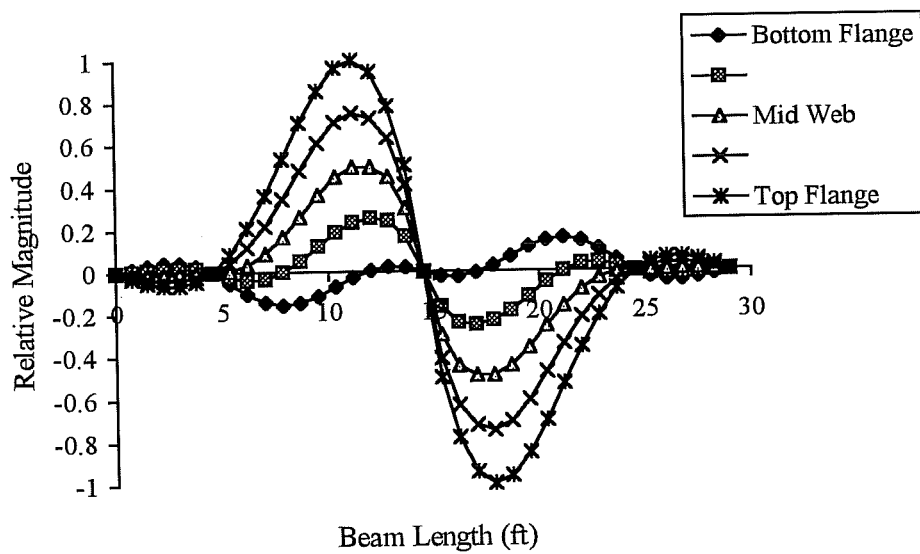


(b) Buckled Shape

Figure 6.9 Bansal's Test # 4

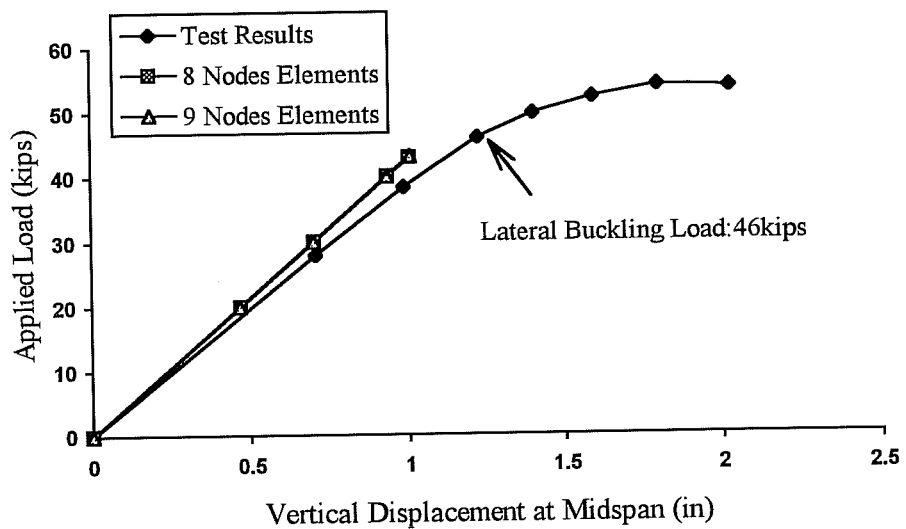


(a) Load vs. Displacement

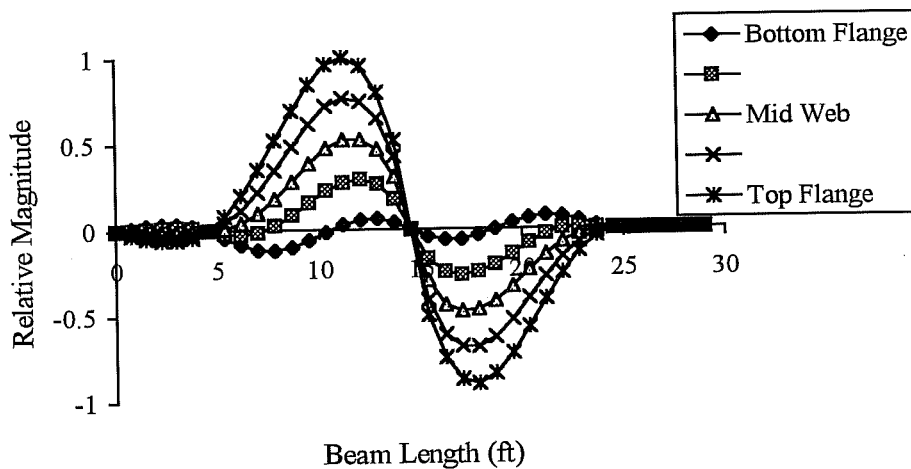


(b) Buckled Shape

Figure 6.10 Bansal's Test # 6

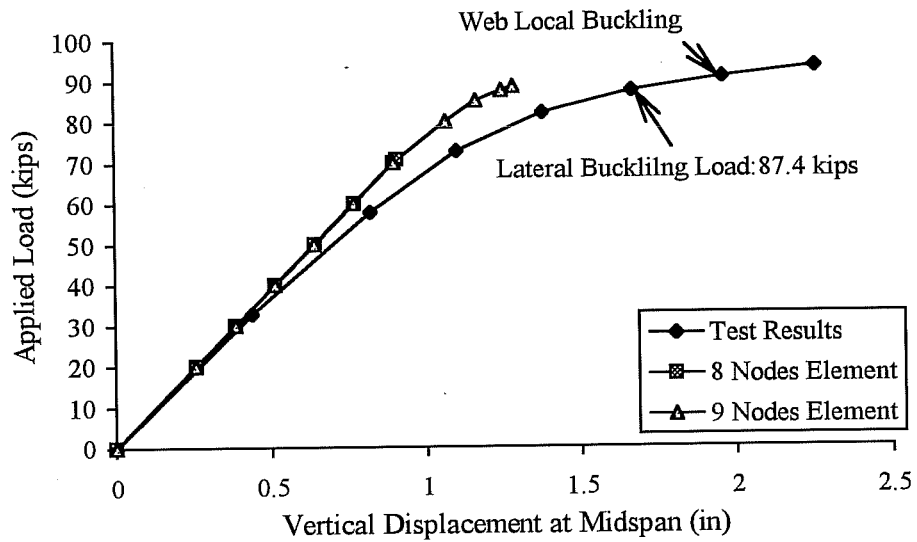


(a) Load vs. Displacement

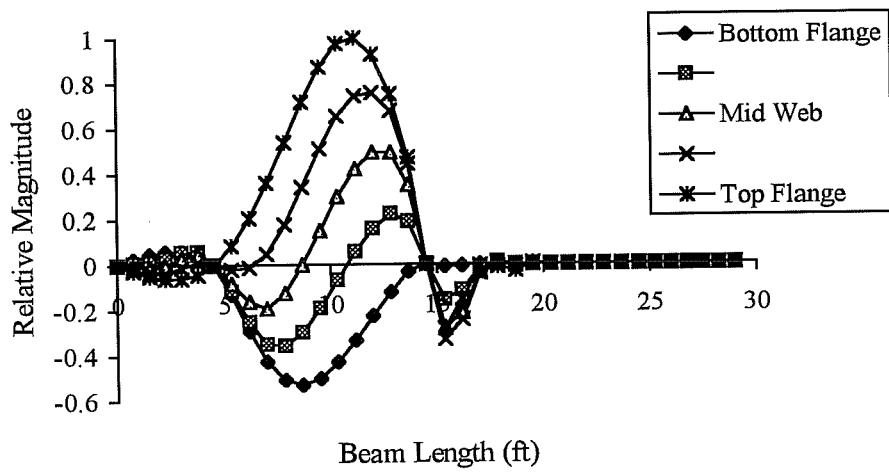


(b) Buckled Shape

Figure 6.11 Bansal's Test # 10

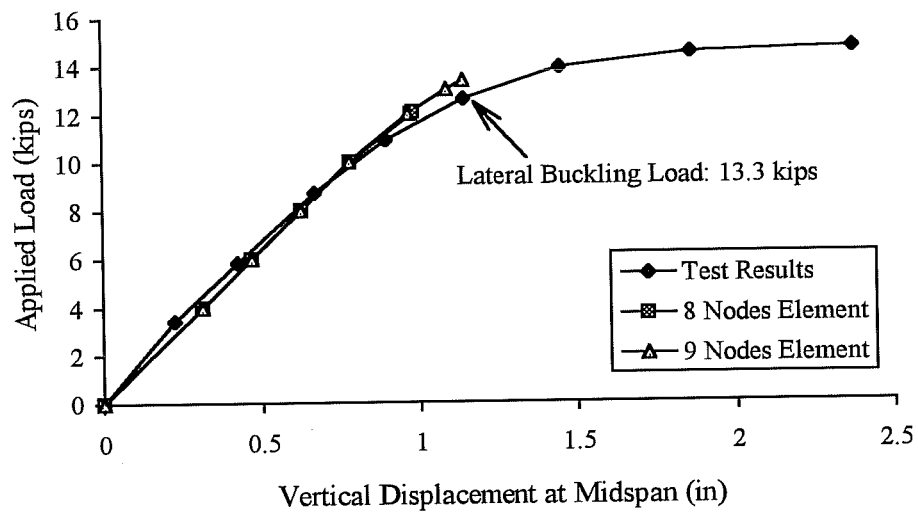


(a) Load vs. Displacement

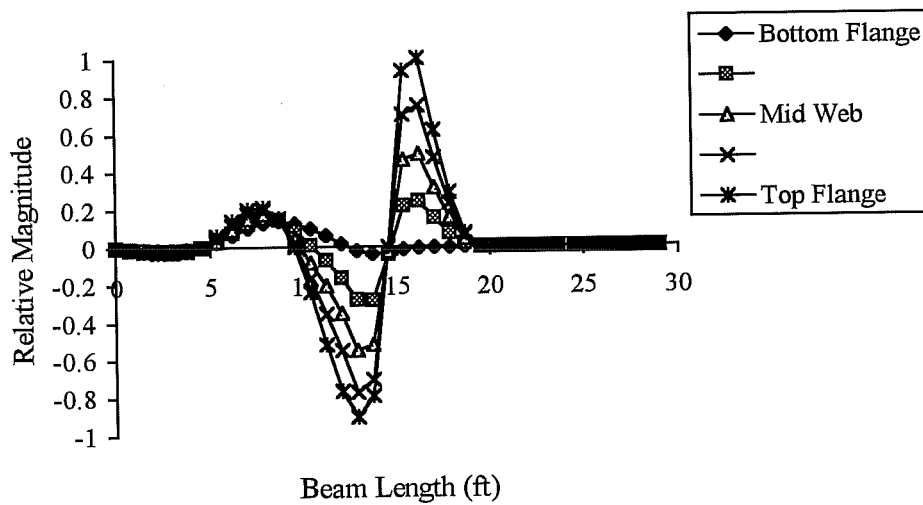


(b) Buckled Shape

Figure 6.12 Bansal's Test # 15



(a) Load vs. Displacement



(b) Buckled Shape

Figure 6.13 Bansal's Test # 17

Table 6.3 Buckling Loads from Experiments and IBASP (kips)

Test No.	Experimental Results	Incremental Eight-Node Element	Incremental Nine-Node Element	Deformation Eight-Node Element	Deformation Nine-Node Element
4	22.7	23.8	24.1	23.8	24.1
6	28.3	25.7	26.6	25.7	26.6
10	46.0	42.9	43.1	42.9	43.1
15	87.2	70.7	88.5	70.7	87.4
17	13.3	12.1	13.4	12.1	13.4

The lateral buckling loads from Bansal (1971) and the IBASP are compared in Table 6.3. In the table, *incremental* and *deformation* mean the incremental theory of plasticity and the deformation theory of plasticity, respectively. Overall, the differences between analytical results from the nine-node element and experimental results are less than 6 %.

In general, the nine-node element yielded higher buckling loads than the eight-node elements did regardless of plasticity theories. The buckling loads from the nine-node element were closer to the experimental buckling loads.

As discussed earlier, the deformation theory of plasticity was reported to yield lower buckling loads than the incremental theory (El-Ghazaly *at al*, 1984 a & b). It was also reported (Damkilde, 1985) that plate buckling loads by the deformation theory were closer to experimental buckling loads. However, Table 6.3 does not show any significant difference between two plasticity theories except Test # 15.

The buckled shape of Test # 15 was unsymmetrical as shown in Figure 6.12.b. It was reported by Bansal (1971) that, in Test # 15, lateral-torsional buckling was occurred first, then followed by web local buckling. The buckled shape from IBASP might show the combination of those two buckling modes.

6.4 Elgaaly and Salkar's Test

Elgaaly and Salkar (1990) performed a series of tests to study local web yielding and crippling behavior of I-shaped beams under in-plane edge loads. Tests were performed on short beams with a concentrated load at the midspan. In this section, results from 2 tests are compared with those from IBASP to see whether IBASP can predict local crippling buckling loads.

The stress-strain relationship of Figure 6.14 was used as material data. The yield strength of the material was measured by Elgaaly and Salkar (1990). The strain hardening strain and modulus were assumed for the analysis. It was also assumed that the material continues to deform with no fracture.

Figure 6.15 shows the test setup and measured cross-section dimensions of a W16x31 section. During experiments, the ratios of the length of applied load (N) to the web depth (d), N/d , were varied from 0.2 to 0.6. The ratios, N/d , of 0.2 and 0.4 were used for the analytical study. The beam was braced against out-of-plane displacements and rotations at supports and at the applied load points (N).

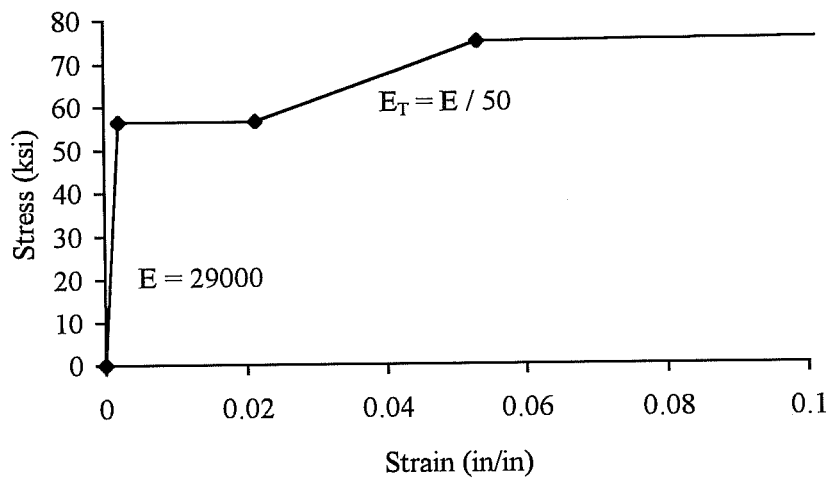
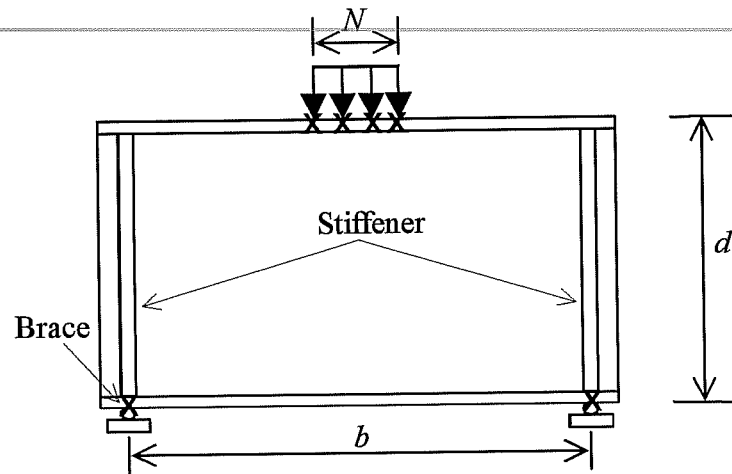
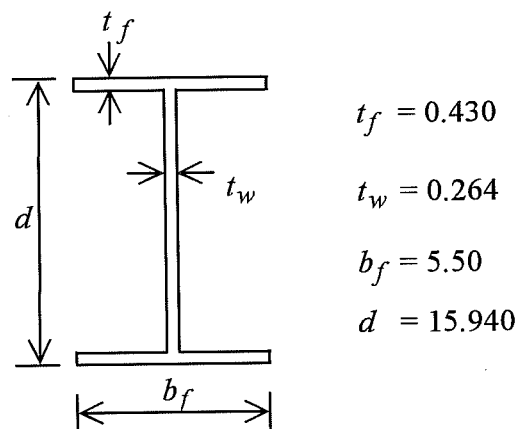


Figure 6.14 Stress-Strain Relationship for W16x31



(a) Test Setup



(b) Cross-section Dimension

Figure 6.15 Test Setup and Cross-section Dimension of W16x31 (Elgaaly & Salkar, 1991)

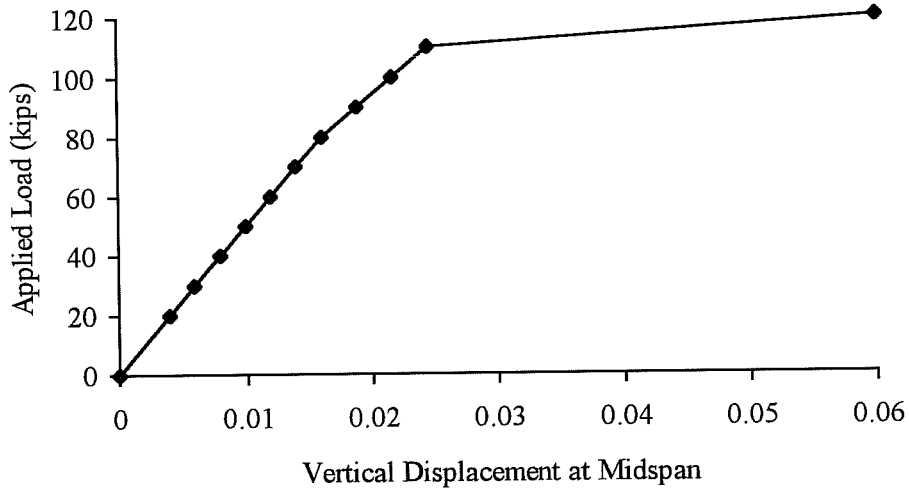
A total of 24 (3x8) nine-node elements were used to model the beam. For $N/d = 0.2$, IBASP did not converge in the in-plane analysis routine. It might be due to the localized large plastic deformation at the loading points. As discussed in Chapter 5.7, the program was stopped when the load increment was small enough. The load at the last iteration was taken as the buckling capacity of the beam and the buckled shape was calculated. IBASP did converge when the ratio N/d was 0.4. The load vs. the vertical displacement at a mid-span curves are shown in Figure 6.16 and 6.17. The figures show that the large degree of plastic deformation had occurred before buckling.

The buckled shapes are also shown in Figure 6.16 and 6.17. The cross-section of the buckled beam at the quarter span and the mid-span is given in Figure 6.18. The buckled cross-section shape of Figure 6.18 (b) indicates that the distortional buckling occurred rather than the lateral-torsional buckling. It also demonstrates the capacity of the IBASP to predict the distortional buckling as well as the lateral torsional buckling.

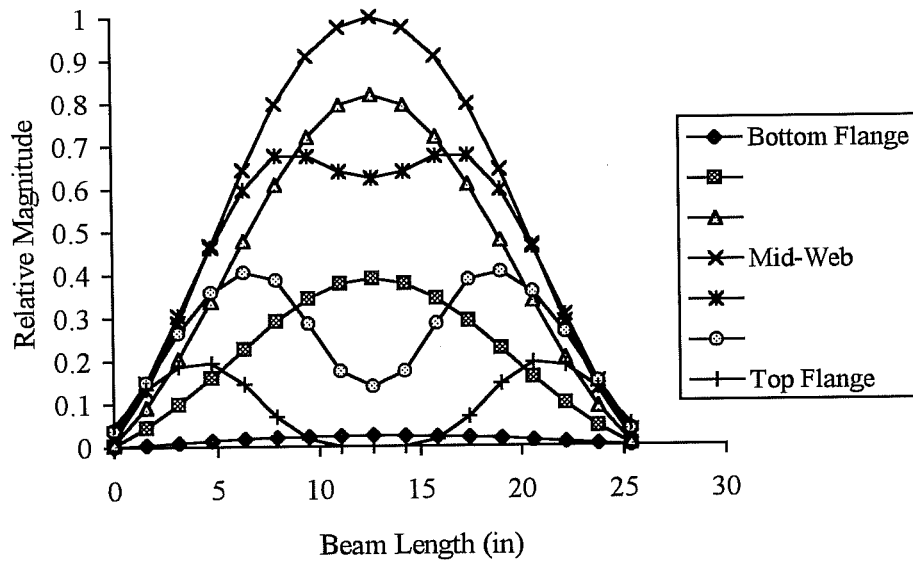
Table 6.4 shows buckling loads from experiments and IBASP. The analytical buckling loads are larger than those from experiments. This may be due to the fact that the stress-strain relationship after yielding is assumed for the analytical study since a complete stress-strain relationship was not reported.

Table 6.4 Experimental and IBASP Results

N/d	Experimental Results	IBASP Results
0.2	112.0	120.0
0.4	145.0	155.7

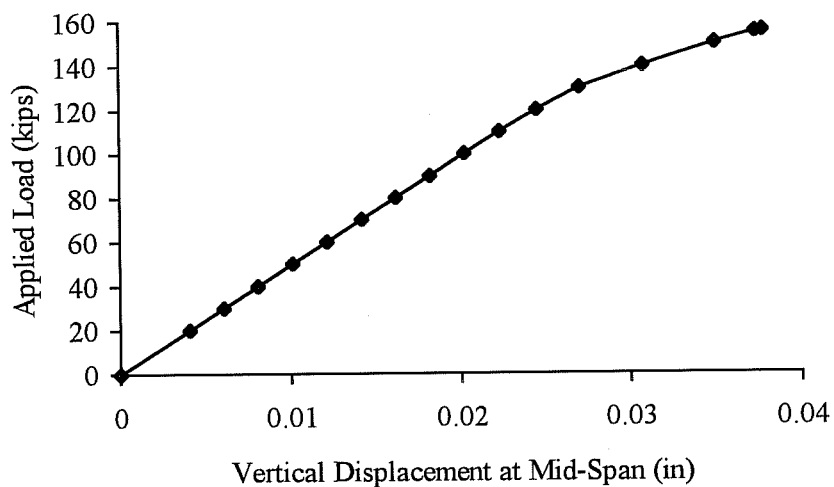


(a) Load-Displacement Curve

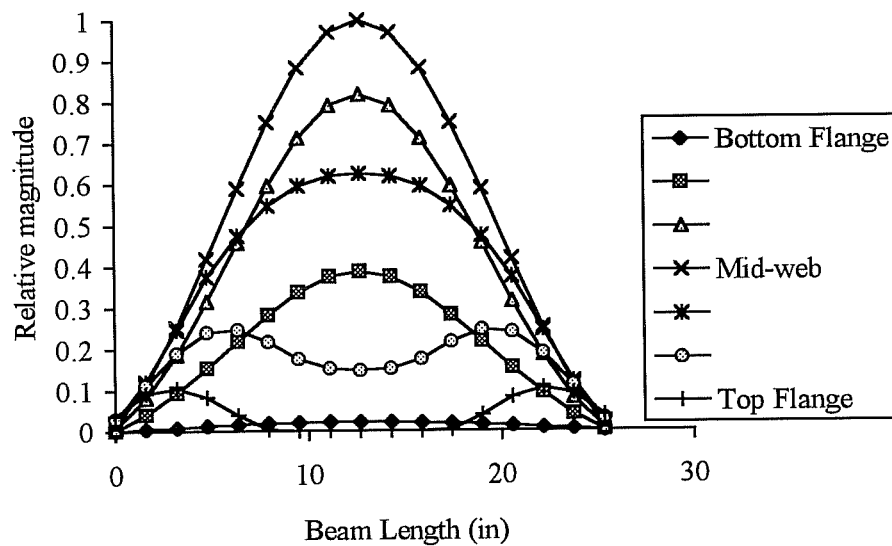


(b) Buckled Shape

Figure 6.16 Results from the Beam with $N/d = 0.2$



(a) Load-Displacement Curve



(b) Buckled Shape

Figure 6.17 Results from the Beam with $N/d = 0.4$

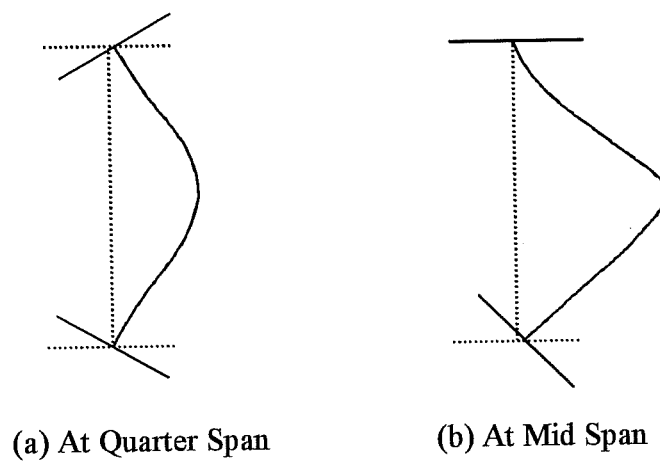


**Figure 6.18 The Cross-section View of the Buckled
Beam for $N/d = 0.4$**

6.5 Ales and Yura's Test

Ales and Yura (1993) performed inelastic beam buckling tests using a S6x12.5 shown in Figure 6.19. The main purpose of the experiments was to determine if Winter's (Winter, 1958) brace requirements could be applied to inelastic beams. As shown in Figure 6.20 (a), the simply supported beam was under constant moment at the center of the beam (Figure 6.20 (b)). The beams were rigidly braced at the supports and loading points against the out-of-plane displacements and rotations. At the midspan, the beam was braced only at the top flange. Two different brace schemes were used for the center brace: a rigid brace and the elastic brace with finite stiffness. The elastic brace is 1.2 times stiffer than the one recommended by Winter (1958). The stress-strain relationship from tension coupon tests was simplified as shown in Figure 6.21 and used as material data for IBASP.

The buckling moments from both the rigidly and the elastically braced beams were the same (355 kips-in.). It was reported by Ales and Yura that the beams buckled in an S-shape at both tests.

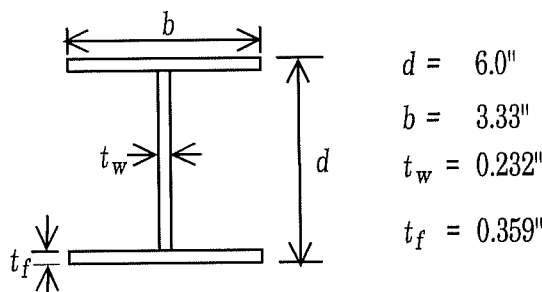
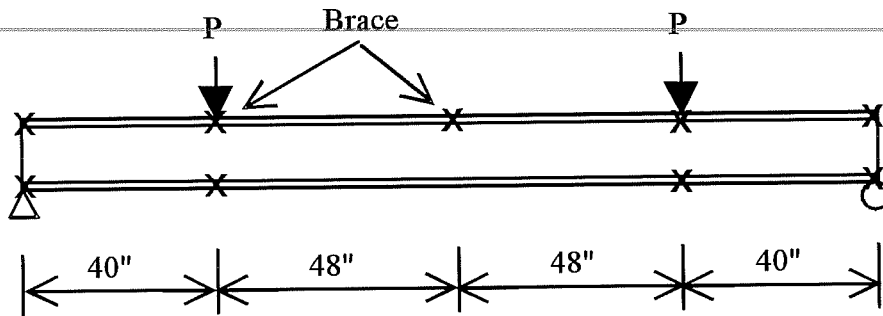
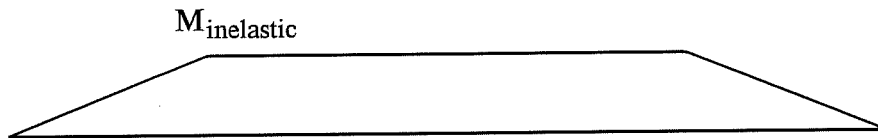


Figure 6.19 Cross-section Dimensions of S6x12.5



(a) Test Setup from Ales and Yura (1994)



(b) Moment Diagram

Figure 6.20 Test Setup and Moment Diagram for Ales and Yura Tests

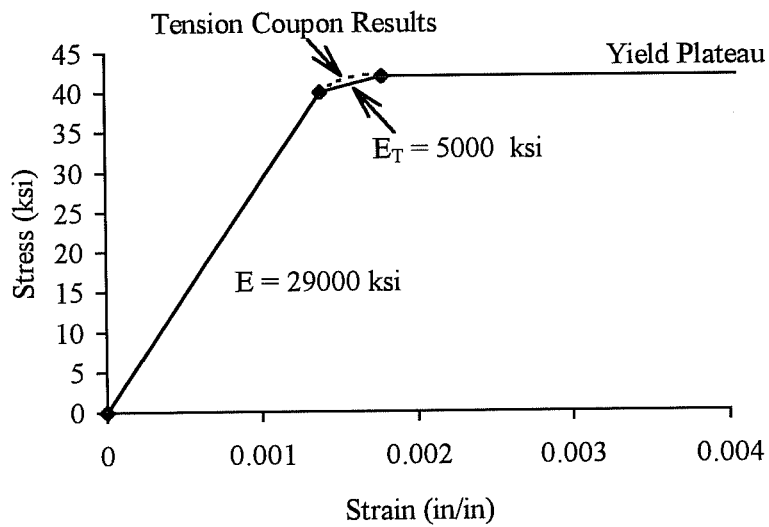


Figure 6.21 Stress-Strain Diagram

The applied moment versus the vertical displacement at the midspan of the beam is shown in Figure 6.22. It shows that the analytical results closely follow the experimental values. The buckled shape from IBASP is also shown in Figure 6.23. The buckling moment from IBASP (342 kips-in) is slightly lower than that from the experiments (355 kips-in).

Figure 6.22 also shows the difference between the beam without residual stress and the beam with assumed residual stress. As expected, the residual stresses reduce the buckling moments to 314 kips-in.

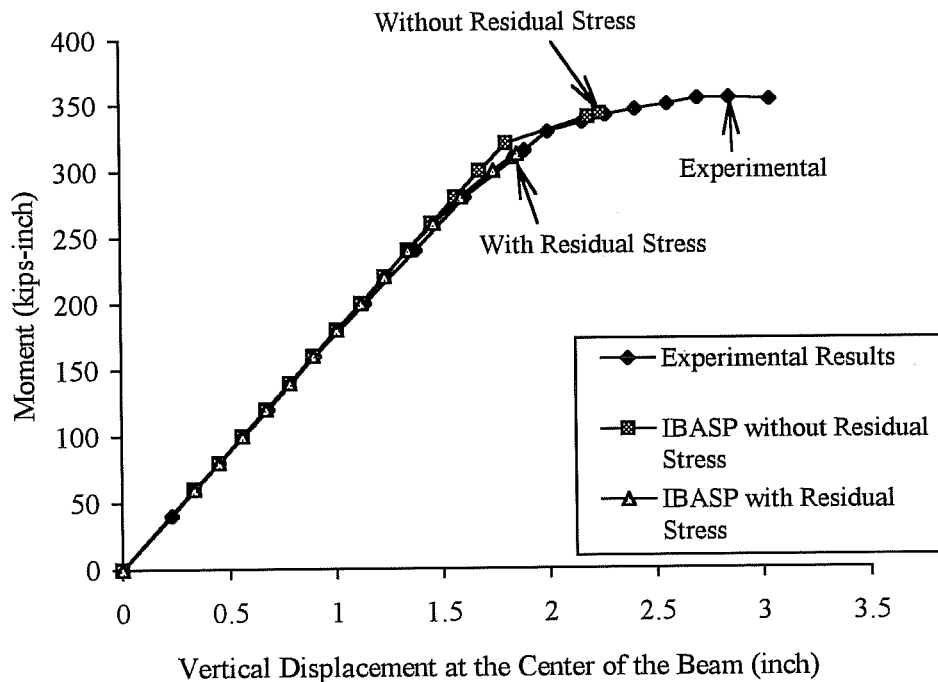


Figure 6.22 Moment vs. Displacement of Simply Supported Beam

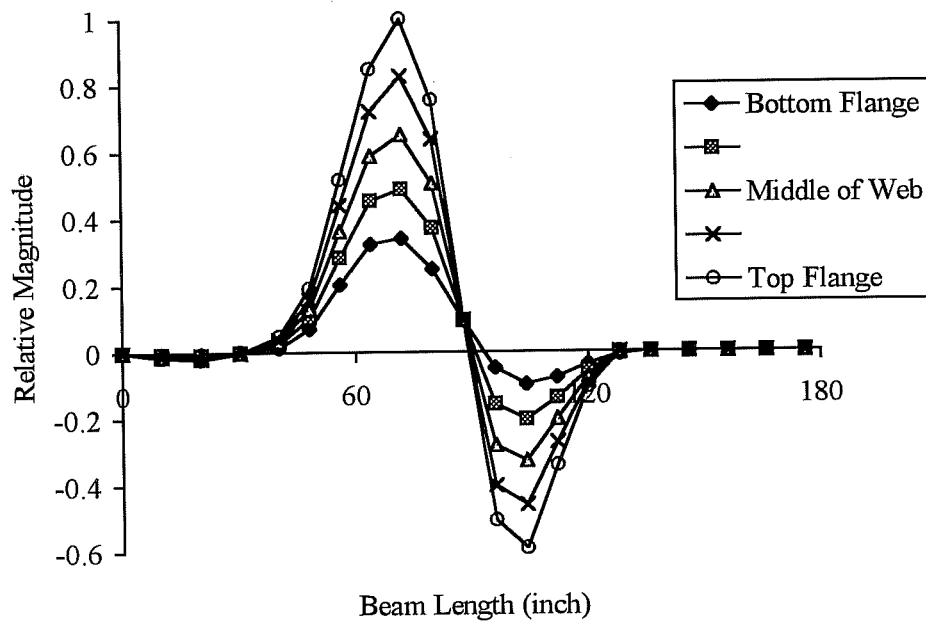


Figure 6.23 Buckled Shape of Fully Braced Beam

6.6 Parametric Study

The use of IBASP to determine the brace requirements of members is demonstrated in this section. The material properties and cross-section dimensions from Ales and Yura (Figure 6.19 & 6.21) are used again as input data for IBASP. A simply supported beam under a constant moment was used as the example. Two types of braces, the lateral brace and the torsional brace, were studied.

The 10 ft. long simply supported beam was assumed to be braced at both ends for the out-of-plane displacement and rotation as shown in Figure 6.24. At midspan, the beam was braced at the top flange only. A lateral brace and then a torsional brace were used as the midspan brace. The stiffness of the braces was changed to find the relationship between the buckling moments and the brace stiffness. A total of 20 nine-node elements and the incremental theory of plasticity were used.

When the stiffness of the mid span brace was equal to zero, the beam buckled in the elastic range with the buckling moment of 271.6 kips-in. The buckling moment of a one half beam (60") or the fully braced beam was 319 kips-

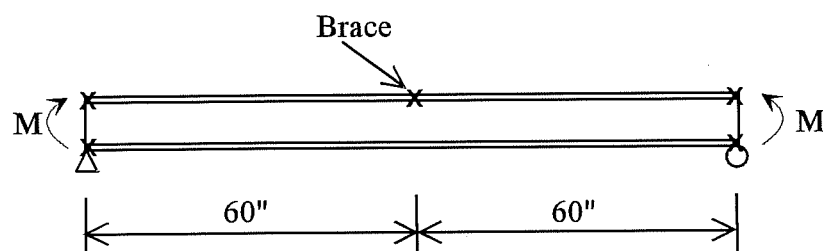


Figure 6.24 Braced Beam under the Constant Moment

in. by IBASP. This buckling moment was greater than the yield moment of the beam. The buckling moment of the fully braced member was not twice as much as that of the unbraced beam due to inelasticity. As the brace stiffness was increased, the state of material changed from elastic to inelastic.

The results from IBASP are shown in Figure 6.25 and Figure 6.26. M_y in the figures represents the yield moment of the section. Figure 6.25 shows the influence of the lateral brace stiffness on the buckling moment of the beam. The relationship between the buckling moments of the braced beam and the torsional braces stiffness is shown in Figure 6.26. Both beams behave similarly. When the

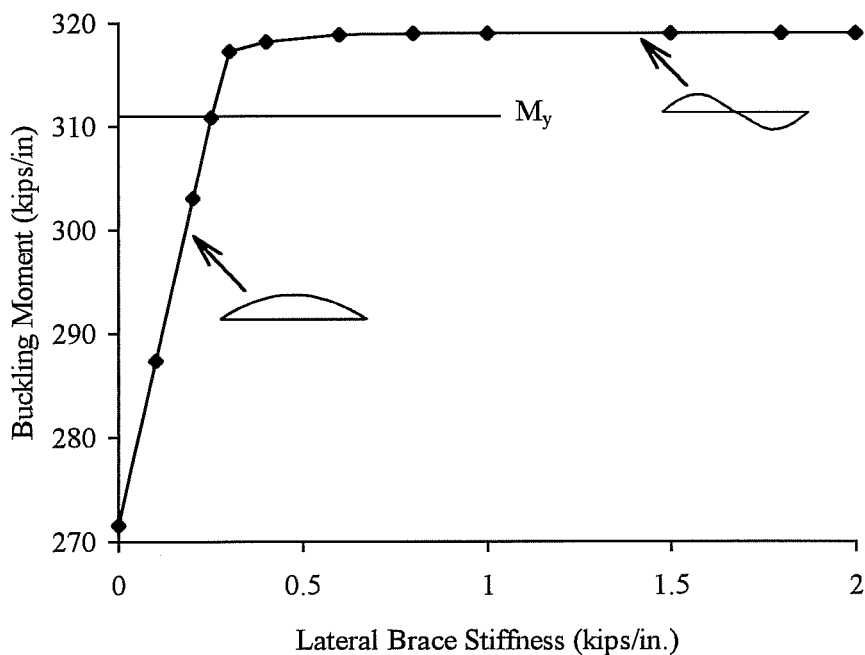


Figure 6.25 Buckling Moment vs. Lateral Brace Stiffness for a Simply Supported Beam

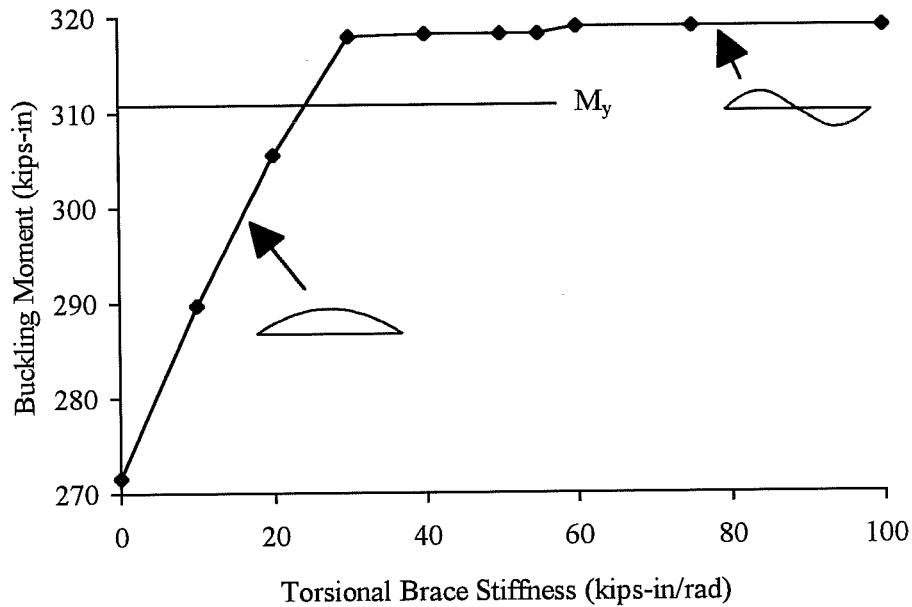


Figure 6.26 Buckling Moment vs. Torsional Brace Stiffness for a Simply Supported Beam

beam is under braced, the buckling capacity increases as a function of the brace stiffness in the elastic and inelastic range. The buckling capacity vs. brace stiffness relationship indicates that, as Winter (1958) stated, the brace stiffness requirements depend on the buckling loads but not on the state of the material.

For the given member, the full brace requirements as well as the buckling loads or moments can be determined by the above procedure.

6.7 Summary

In Chapter 6, a comparison was made between the results from IBASP and experiments. Those examples were used to show the accuracy of the IBASP program. The following observations are made;

- 1) the inelastic stress-strain relationship greatly influences the buckling loads of the inelastic members
- 2) There is not much difference between the incremental theory of plasticity and the deformation theory of plasticity.
- 3) The buckling loads from the eight-node element were smaller than those from the nine-node element and experiments.
- 4) The nine-node element with the incremental theory of plasticity yielded the best results. The maximum difference between the results from IBASP and experiments was 6%
- 5) The IBASP program can predict the lateral-torsional as well as local buckling capacities of the members.

Chapter 7:

Summary, Conclusion, and Future Research

7.1 Summary and Conclusion

This study on the bracing requirements for inelastic members was composed of experimental and theoretical works.

In the experimental phase, composite columns were fabricated from three steel bars with two different yield strengths. A total of nine braced columns with the elastic brace at the mid height was tested. The elastic brace had four different stiffnesses. The columns buckled in double curvature when the brace was stiff. When the stiffness of the brace was low, the columns buckled in a single curvature. The results from buckling tests confirmed that Winter's bracing requirements were valid for inelastic members. Winter specified that the bracing requirements are only a function of buckling loads and member length but not the state of material.

The inelastic columns were modeled and analyzed by ABAQUS. The analytical results were compared with experimental ones. The results were also compared with the bracing requirements for elastic members. The buckling loads from ABAQUS were lower than those from experiments. The ABAQUS results also showed that the brace stiffness and strength requirements for the elastic members can be applied to inelastic members.

Winter's method is directly applicable to a single column under a constant axial load and a beam with a constant moment. However, most actual loading conditions, especially for beams, have variable stresses along the length so that Winter's method is not directly applicable. While there are programs such as BASP to handle complex elastic loading conditions, there are no programs for

inelastic members. In Part II, an inelastic buckling analysis program, IBASP, using the finite element method was developed to predict inelastic buckling loads of braced and unbraced members. The program can consider lateral-torsional, flexural, and local buckling.

In the program, the in-plane analysis to determine the stress distribution of the member was performed first. Then, the tangent modulus theory which specifies that the buckling capacities of inelastic members depend on the tangent modulus of the material, was utilized to determine the stiffness of the member. Last, an eigenproblem solution routine was employed to determine the buckling load and the buckled shape. The elastoplastic behavior of the material was considered if the stresses at buckling exceeded the yield strength of the material. The modified Newton-Raphson method was employed to solve non-linear problems due to inelasticity. Two plasticity theories, the incremental theory of plasticity and the deformation theory of plasticity, were tried. The eight-node and nine-node isoparametric plate elements were also tested.

The theoretical solutions and experimental results of determinant and non-determinant members were used to test the accuracy of the program. The comparison of two plasticity theories showed that the incremental theory yielded the buckling loads which were closer to the theoretical solutions. When the results from two theories were compared with experimental buckling loads, not much difference between two theories was observed. The buckling loads from the nine-node element were higher than those from the eight-node one. They were also closer to experimental results.

The nine-node plate element with the incremental theory of plasticity yielded the best results. The comparison with experimental results showed that the

difference was less than 6%. It was also shown that the program can follow local as well as lateral torsional buckling behavior.

7.2 Future Research

There have not been many inelastic buckling tests of braced structures. In this study, small scale buckling tests were conducted to find the bracing requirements of inelastic columns. Full scale inelastic buckling tests need to be performed to verify those requirements in future studies.

The parametric studies using IBASP are suggested to better understand the behavior of braced inelastic members and the bracing requirements. Design guidelines can be developed through those studies.

By changing the input formats, buckling capacities of tapered members can be determined using IBASP. IBASP which is currently limited to symmetric cross-sections can be extended to include non-symmetrical cross-sections such as a Z-shaped cross-section. The inelastic buckling analysis program should be improved to take account of initial in-plane and out-of-plane imperfections and eccentric loading.

Appendix A:

Consistent Constitutive Matrix and Elastic Predictor-Radial Return Algorithm for Plane Stress

Consistent Constitutive Matrix

The elastic predictor-radial return algorithm used in the plasticity routine to determine the state of the material when the stresses were over the yield strength of the material. As discussed in Chapter 5, the convergence of the algorithm would improve if the consistent constitutive matrix was used. The matrix, $[D_{ep}^c]$, given by Tassoulas (1995) is shown here. The relationship between the stress and strain increment is

$$d\{\Delta\sigma\} = [D_{ep}^c] d\{\Delta\varepsilon\} \quad (\text{A.1})$$

where

$$[D_{ep}^c] = [D_e] - \frac{3G\Delta\bar{\varepsilon}^P}{\sigma_Y + 3G\Delta\bar{\varepsilon}^P} \left[2G \left([I] - \frac{1}{3} \{I\} \{I\}^T \right) \right] - \frac{\sqrt{3}G}{\sigma_Y \bar{\sigma}^T} \left[\frac{1 - \left(\frac{1}{\sigma_Y} \right) \left(\frac{d\sigma_Y}{d\bar{\varepsilon}^P} \right) \Delta\bar{\varepsilon}^P}{\left[1 + \frac{3G\Delta\bar{\varepsilon}^P}{\sigma_Y} \right]^2} \right] \left[\frac{1}{1 + \frac{1}{3G} \frac{d\sigma_Y}{d\bar{\varepsilon}^P}} \right] \{S^T\} \{S^T\}^T \quad (\text{A.2})$$

Elastic Predictor-Radial Return Routine for Plane Stress

For plane stress problems, the plane stress condition, $\sigma_z = 0$, needs to be satisfied while the strain increment in z-direction, $\Delta\varepsilon_z$, is not zero. Dodds (1987) and Tassoulas (1995) described the iterative procedure for plane stress problems. If the stress in z-direction, σ_z , was not zero, the strain increment in z-direction, $\Delta\varepsilon_z$, was iteratively adjusted using a Newton-Raphson method.

Do the following steps if a plastic deformation occurred,

- 1) assume $\Delta\varepsilon_z^0$ for the initial iteration as follows

$$\Delta\varepsilon_z^0 = -\frac{\nu}{(1-\nu)}(\Delta\varepsilon_x + \Delta\varepsilon_y) \quad (\text{A.3})$$

the above equation is derived from plane stress condition

- 2) The new state of stresses is calculated using the elastic predictor-radial return algorithm. The new stresses given in Equation 5.51 are shown again

$$\{\sigma\} + \{\Delta\sigma\} = \{S\} + \{\Delta S\} + \{i\}(\sigma + \Delta\sigma) \quad (\text{A.4})$$

If $(\sigma_z + \Delta\sigma_z) \leq tol$, then the plane stress condition is satisfied and the new state of stress has been determined

If $(\sigma_z + \Delta\sigma_z) > tol$, the plane stress condition is not satisfied and a Newton-Raphson method is employed to find the state of stress

3) Derive the i th z-direction stress increment, $\Delta\sigma_z^i$, which is the function of $\Delta\varepsilon_z$ and the i th derivation of the z-direction stress increment with respect to $\Delta\varepsilon_z$ as follows

$$\Delta\sigma_z^i(\Delta\varepsilon_z^{i-1}) = \left(\frac{1}{1+2G\Delta\lambda} S_z^T - S_z \right) + \Delta\sigma \quad (\text{A.5})$$

$$\left. \frac{\partial \Delta\sigma_z}{\partial \Delta\varepsilon_z} \right|_{\Delta\varepsilon_z^{i-1}} \quad (\text{A.6})$$

where

$$\frac{\partial \Delta\sigma_z}{\partial \Delta\varepsilon_z} = \frac{\partial}{\partial \Delta\varepsilon_z} \left(\frac{1}{1+2G\Delta\lambda} S_z^T - S_z + \Delta\sigma \right) \quad (\text{A.7.a})$$

$$= - \frac{1}{(1+2G\Delta\lambda)^2} 2G \frac{\partial(\Delta\lambda)}{\partial \Delta\varepsilon_z} S_z^T + \frac{1}{(1+2G\Delta\lambda)} \frac{\partial S_z^T}{\partial \Delta\varepsilon_z} + \frac{\partial \Delta\sigma}{\partial \Delta\varepsilon_z} \quad (\text{A.7.b})$$

4) the new strain increment in z-direction is

$$\Delta\varepsilon_z^i = \Delta\varepsilon_z^{i-1} - \frac{\Delta\sigma_z^i(\Delta\varepsilon_z^{i-1})}{\left. \frac{\partial \Delta\sigma_z}{\partial \Delta\varepsilon_z} \right|_{\Delta\varepsilon_z^{i-1}}} \quad (\text{A.8})$$

5) Go back to Step 2

The above steps are repeated until the $\Delta\sigma_z$ is less than the tolerance value

Appendix B:

Input Manual and A Example Input File for IBASP

Input Manual

18 input items are needed

1. IO, IGSTF, ISHEAR, IRES

IO : output options

If IO .EQ. 2, short output option

If IO .EQ. 1, medium output option

If IO .EQ. 0, large output option

IGSTF : torsional geometric stiffness option

If IGSTF .EQ. 0, no torsional geometric stiffness

If IGSTF .EQ. 1, include torsional geometric stiffness

ISHEAR : shear distortion option

If ISHEAR .EQ. 0, no shear distortion

If ISHEAR .EQ. 1, include shear distortion

IRES : residual stress option

If IRES .EQ. 0, include residual stress and enter the amount in item 15

If IRES .EQ. 1, no residual stress

2. Annotation of Problem: first line

3. Annotation of Problem: second line

4. NUMELX, NUMELY, XLEN, YLEN, NLPTS, NMBPTS, NSPRM, NBBPTS,

NSPRB

NUMELX : number of elements in a horizontal direction (x-axis)

NUMELY: number of elements in a vertical direction (y-axis)

XLEN : the length of the member in a horizontal direction (x-axis)

YLEN : the length of the member in a vertical direction (y-axis)

NLPTS : number of nodes with in-plane loads

NMBPTS : number of nodes with the in-plane boundary conditions

NSPRM : number of nodes with in-plane springs

NBBPTS : number of nodes with the out-of-plane boundary conditions

NSPRB : number of nodes with out-of-plane springs

5. YNG, PSN

YNG : elastic modulus

PSN : Poisson's ratio

6. NMD : number of material data (must be greater than 1 and less than 10)

7. CONST(1,I), CONST(2,I) : material constants (I=1, NMD)

CONST (1,I) : plastic strain (total strain - inelastic stress/elastic modulus)

CONST (2,I) : yield stress

8. THIW, THIB, WIDB, THIT, WIDT

THIW : thickness of web

THIB : thickness of bottom flange

WIDB : width of bottom flange

THIT : thickness of top flange

WIDT : width of bottom flange

9. NSTF : number of stiffeners

If NSTF = 0, skip item 10 and go to item 11

10. for each stiffener:

KQB(1,I), KQB(2,I), TB(I), H(I); I=1,NSTF

KQB(1,I) and KQB(2,I) : node number for the stiffener

TB (I) : thickness of the stiffener

$H(I)$: width of the stiffener

11. in-plane loading conditions

$I1, I2, INCR, R(1), R(2)$

$I1$: node number 1

$I2$: node number 2

$INCR$: the node increment from $I1$ to $I2$

$R(1)$: the applied load in a horizontal direction (x-axis)

$R(2)$: the applied load in a vertical direction (y-axis)

12. in-plane boundary conditions

$I1, I2, INCR, IB(1), IB(2), BV(1), BV(2)$

If $IB(1) = 1$, horizontal displacement is limited

If $IB(1) = 0$, horizontal displacement is allowed

If $IB(2) = 1$, vertical displacement is limited

If $IB(2) = 0$, vertical displacement is allowed

$BV(1)$: prescribed horizontal displacement (x-axis)

$BV(2)$: prescribed vertical displacement (y-axis)

13 in-plane springs

$I1, I2, INCR, SPR(1), SPR(2)$

$SPR(1)$: spring stiffness in a horizontal direction (x-axis)

$SPR(2)$: spring stiffness in a vertical direction (y-axis)

14 out-of-plane boundary conditions

$I1, I1, INCR, IB(1), IB(2), IB(3)$

If $IB(1) = 1$, out-of-plane displacement is prohibited

If $IB(1) = 0$, out-of-plane displacement is allowed

If $IB(2) = 1$, rotation about z-axis is prohibited

If $IB(2) = 0$, rotation about z-axis is allowed

If $IB(3) = 1$, torsion (rotation about x-axis) is prohibited

If $IB(3) = 0$, torsion (rotation about x-axis) is allowed

15. out-of-plane springs

I1, I2, INCR, SPR(1), SPR(2), SPR(3)

SPR(1) : spring stiffness against out-of-plane displacement

SPR(2) : spring stiffness against rotation about z-axis

SPR(3) : spring stiffness against torsion (rotation about x-axis)

16. this item is skipped if IRES = 1 in item 1,

GRES : the amount of maximum compressive residual stresses

17. NSTEP, MCYCLE, TOL

NSTEP : number of load steps allowed

MCYCLE : number of iterations allowed for in-plane analysis

TOL : tolerance for a buckling load

18. DLOADI, DLOAD

DLOADI : the initial load increment

DLOAD : the load increment

Example Input File

An example input file is given below. The cross-section dimension and the member are shown in Figure B.2 and B.3. The numbering sequence of nodes and elements are also shown. The material behavior is shown in Figure B.1. In the yield plateau, the tangent modulus of 10.0(ksi) is used rather than 0.0(ksi) for faster convergence. The comparison of total strain and plastic strain is shown in Table B.1.

Table B.1 Total and Plastic Strain

Stress (ksi)	Total Strain (in./in.)	Plastic Strain (in./in.)
40.0	0.001379	0.0
42.0	0.001779	0.000331
42.178	0.019572	0.018118

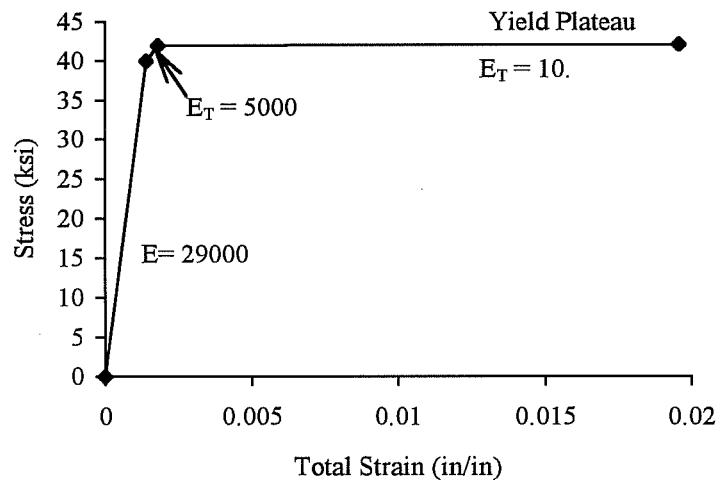


Figure B.1 Material Data

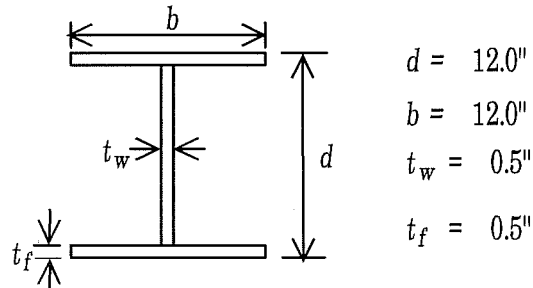
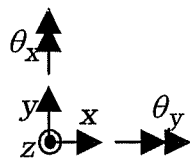
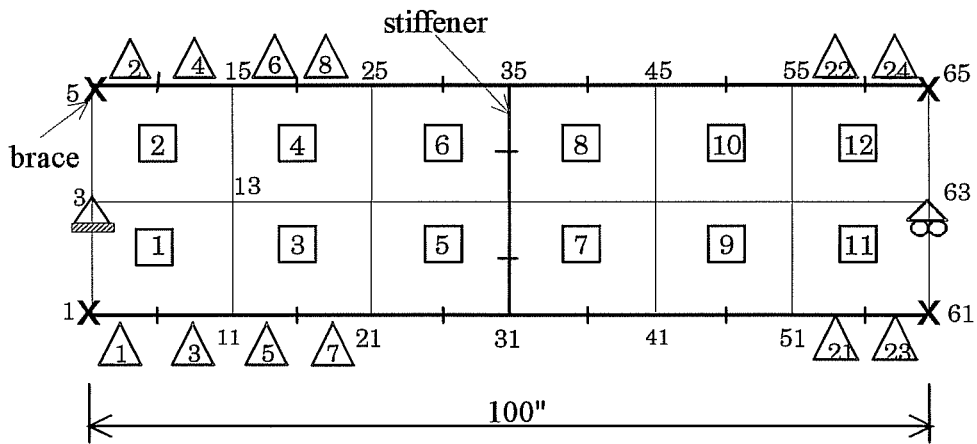


Figure B.2 A Cross-section Dimension



- 1 represents the node number
- 1 represents the web element number
- 1 represents the flange and stiffener beam element number

Figure B.3 A Example Problem

Example Input file

(Option: shorter outputs, no torsional geometric stiffness, no shear distortion, and include residual stresses with 12.0 ksi as maximum compressive residual stress)

2, 0, 0, 0	item 1
Length of the Member: 100"	item 2
Depth of Member : 12"	item 3
6, 2, 100.0, 11.5, 1, 2, 0, 4, 0	item 4
29000.0, 0.3	item 5
3	item 6
0.0, 42.0	item 7
0.000331, 42.0		
0.018118, 42.178		
0.5, 0.5, 12.0, 0.5, 12.0	item 8
4	item 9
31, 32, 1, 0.25, 6.0	item 10
32, 33, 1, 0.25, 6.0		
33, 34, 1, 0.25, 6.0		
34, 35, 1, 0.25, 6.0		
35, 35, 1, 0, -1.0	item 11
3, 3, 1, 1, 1, 0.0, 0.0	item 12
63, 63, 1, 0, 1, 0.0, 0.0		
1, 5, 4, 1, 0, 1	item 14
61, 65, 4, 1, 0, 1		
12.0	item 16
100, 500, 0.0000001	item 17
20.0, 10.0	item 18

BIBLIOGRAPHY

- ABAQUS User's Manual Version 5.2 (1995), Hibbitt, Karlsson, & Sorensen, Inc.
- Ahmad, S., Irons, B. M., and Zienkiwicz, O. C. (1970), "Analysis of Thick and Thin Shell Structures by Curved Finite Elements," *International Journal for Numerical Methods in Engineering*, Vol. 3, pp. 419-451
- Akay, H. U., Johnson, P., and Will, K.M., (1977), "Lateral and Local Buckling of Beams and Frames," *ASCE, Journal of Structural Division*, ST. 9
- Akay, H. U. (1974), "Linear Buckling and Geometrically Nonlinear Analysis of Planar-Stiffener Type Structures by the Finite Element Method," Ph. D. Dissertation, Dept. of Civil Eng., The University of Texas at Austin
- Ales Jr., J. M. and Yura, J. A. (1993), "Bracing Design for Inelastic Structures," *Structural Stability Research Council, 1993 Conference, "Is Your Structure Suitably Braced"*, SSRC
- ANSYS User's Manual (1992), Swanson Analysis Systems, Inc.
- Bansal, J. P. (1971), "The Lateral Instability of Continuous Steel Beams," Dept. of Civil Engg., Structural Research Laboratory, The University of Texas at Austin
- Barsoum, R. S. and Gallagher, R. H. (1970), "Finite Element Analysis of Torsional and Torsional-Flexural Stability Problems," *International Journal of Numerical Methods in Engineering*, Vol. 2, pp. 335-352
- Bathe, K. J. and Cimento, A. P. (1980), "Some Practical Procedures for the Solution of Nonlinear Finite Element Equations," *Computer Methods in Applied Mechanics and Engineering*, Vol. 22, pp. 59-85
- Bradford, M. A. and Trahair, N. S. (1981), "Distorsional Buckling of I-beams," *Journal of the Structural Division, ASCE*, Vol. 107, No. ST2, pp.355-370

- Bradford, M. A. (1985), "Distorsional Buckling of Monosymmetric I-Beams,"
Journal of Constructional Steel Research, Vol. 5, pp. 123-136
- Bradford, M. A. (1992), "Lateral-Distorsional Buckling of Steel I-Section
Members," Journal of Constructional Steel Research, Vol. 23, pp. 97-116
- Budiansky, B. (1959), "A Reassessment of Deformation Theories of Plasticity,"
ASME, Journal of Applied Mechanics, June, pp. 259-264
- Bushnell, D. (1977), "A Strategy for the Solution of Problems involving Large
Deflections, Plasticity, and Creep," International Journal for Numerical
Methods in Engineering, Vol. 11, pp.683-708
- Chin, C. K., Al-Bermani, F. G. A., & Kitipornchai, S. (1990), "Stability of Thin-
Walled Members with Arbitrary Flange Shape and Flexible Web," Research
Report No. CE119, Dept. of Civil Eng. The University of Queensland
- Cook, R. D., Malkus, D. S., and Plesha, M. E. (1989), "Concepts and Applications
of Finite Element Analysis," John Wiley & Sons, Inc., New York
- Clark, J. W. and Hill, H. N. (1960), "Lateral Buckling of Beams," Journal of the
Structural Division, ASCE, July
- Crisfield, M. A. (1991), "Non-Linear Finite Element Analysis of Solids and
Structures Vol. 1," John Wiley & Sons, Inc., Chichester, England
- Damkilde, L. (1985), "Elastic-Plastic Buckling of a Finite Length Cruciform
Column," Computers and Structures, Vol. 21, No. 3, pp. 521-528
- Daye, M.A. and Toridis, T. G. (1991), "Elasto-Plastic Algorithms for Plates and
Shells Under Static and Dynamic Loads," Computers and Structures, Vol.
39, No. 1/2, pp. 195-205
- Dodds, R. H. (1986), "Numerical Techniques for Plasticity Computations in
Finite Element Analysis," Computers & Structures, Vol. 26, No. 5,
pp.767-779

- Elgaaly, M. and Salkar, R. (1990), "Behavior of Webs of Rolled Sections under In-plane Compressive Edge Loads," Department of Civil Engineering, University of Maine
- El-Ghazaly, H. A., Dubey, R. N., and Sherbourne, A. N. (1984a), "Elasto-Plastic Buckling of Stiffener Plates in Beam-To-Column Flange Connections," *Computers and Structures*, Vol. 18, No. 2, pp. 201-213
- El-Ghazaly, H. A., Sherbourne, A. N., and Dubey, R. N. (1984b), "Inelastic Interactive Distorsional Buckling of W-Shape Steel Beams," *Computers and Structures*, Vol. 19, No. 3, pp. 351-368
- El-Ghazaly, H. A. and Sherbourne, A. N. (1986), "Deformation Theory for Elastic-Plastic Buckling Analysis of Plates Under Non-Proportional Planar Loading," *Computers and Structures*, Vol. 22, No. 2, pp. 131-149
- Galambos, T. V. and Ketter R. L. (1959), "Columns Under Combined Bending and Thrust," *ASCE, Journal of Engineering Mechanics Division*, Vol. 85
- Galambos, T. V. (1963), "Inelastic Lateral Buckling of Beams," *ASCE, Journal of the Structural Division*, Vol. 89, No. ST5, October, pp. 217-242
- Gerard, G. and Becker, H. (1957), "Handbook of Structural Stability, Part I," NACA Tech Note 3781
- Gupta, K. K. (1973), "Eigenproblem Solution by a Combined Sturm Sequence and Inverse Iteration Technique," *International Journal for Numerical Methods in Engineering*, Vol. 7, pp.17-42
- Gupta, K. K. (1978), "On a Numerical Solution of the Plastic Buckling Problem of Structures," *International Journal for Numerical Methods in Engineering*, Vol. 12, pp. 941-947

- Haaijer, G. (1957), "Plate Buckling in the Strain-Hardening," ASCE, Journal of the Engineering Mechanics Division, Vol. 83, EM2, Proceeding Paper 1212, pp. 1212
- Hancock, G. J., Bradford, M. A., & Trahair, N. S. (1980), "Web Distorsion and Flexural-Torsional Buckling," Journal of the Structural Division, ASCE, Vol. 106, No. ST7, pp. 1557-1571
- Hartmann, A. J. (1967), "Elastic Lateral Buckling of Continuous Beams," ASCE, Journal of Structural Division, Vol. 93, No. ST4, August, pp. 11-26
- Hartmann, A. J. (1971), "Inelastic Flexural-Torsional Buckling," ASCE, Journal of the Engineering Mechanics Division, Vol. 97, No. EM4, August, pp. 1103-1119
- Hrabok, M. M. and Hurdey, T. M. (1984), "A Review and Catalogue of Plate Bending Finite Elements," , International Journal for Numerical Methods in Engineering, Vol. 19, No. 3, pp. 479-495
- Helwig, T. A. (1994), "Lateral Buckling of Bridge Girders bt Metal Deck Forms," Ph. D. Dissertation, The University of Texas at Austin
- Humar, J. L. (1990), "Dynamics of Structures," Prentice Hall, Englewood Cliffs, NJ
- Hunsaker, B. (1973), "An Evaluation of Four Hardening Rules of the Incremental Theory of Plasticity," Master Thesis, Texas A&M University
- Hutchinson, J. W. (1974), "Plastic Buckling," Advances in Applied Mechanics, Vol. 14, pp. 67-144
- Johnson, P. (1972), "Lateral Buckling of Rigid Frames by Finite Element Procedures," CESM Report No. 1, Dept. of Civil Eng., The University of Texas at Austin
- Johnson, P. (1995), Personal Communication

- Johnston, B. G. (1963), "Buckling Behavior above the Tangent Modulus Load," ASCE Transactions, Vol. 128, Part I, pp. 819 - 848
- Johnston, B. G. (1983), "Column Buckling Theory: Historic Highlights," ASCE, Journal of Structural Engineering, Vol. 109, No. 9, pp. 2086-2096
- Kapur, K. K. and Hartz, B. J. (1966), "Stability of Plates Using the Finite Element Method," ASCE, Journal of Engineering Mechanics Division, Vol. 92, No. EM 2, April
- Kitipornchai, S. and Wong-Chong, A. D. (1987), "Inelastic Buckling of Welded Mono-symmetric I-Beams," Journal of Structural Engineering, ASCE, Vol. 113, pp. 740-756
- Kreg, R. D. and Kreg, D. B. (1977), "Accuracies of Numerical Solution Methods for the Elastic-Perfectly Plastic Model," Journal of Pressure Vessel Technology, Transactions of ASME, November, pp. 510-515
- Lay, M. G. (1965), "Flange Local Buckling in Wide-Flange Shape," ASCE, Journal of the Structural Division, Vol. 91, ST 6, Proceeding Paper 4554, pp.95-116
- Lay, M. G. and Galambos, T. V. (1966), "Bracing Requirements for Inelastic Steel Beams," ASCE, Journal of the Structural Division, Vol. 92, No. ST2, April, pp. 207-228
- Levy, A. and Pifko, A. B. (1981), "On Computational Strategies for Problems Involving Plasticity and Creep," International Journal for Numerical Methods in Engineering, Vol. 17, pp. 747-771
- Lubliner, J. (1990), "Plasticity Theory," Macmillan Publishing Co., New York
- Meek, J. L. and Lin, W. J. (1990), "Geometric and Material Nonlinear Analysis of Thin-Walled Beam-Columns," ASCE, Journal of Structural Engineering, Vol. 116, No. 6, June

- Mroz, Z. (1967), "On the Description of Anisotropic Workhardening," *Journal of the Mechanics Physics of Solids*, Vol. 15, pp. 163-175
- Muton, B. R. and Trahair, N. S. (1973), "Stiffness Requirements for Lateral Bracing," *ASCE, Journal of the Structural Division*, Vol. 99, No. ST 10, October, pp. 2167 - 2182
- Nakamura, T. (1988), "Strength and Deformability of H-Shaped Steel Beams and Lateral Bracing Requirements," *Journal of Constructional Steel Research*, Vol. 9, pp. 217 - 228
- Neal, B. G. (1950), "The Lateral Instability of Yielded Mild-Steel Beams of Rectangular Cross Section," *Philosophical Transactions of the Royal Society*, Vol. 242A, London
- Nethercot, D. A. and Trahair, N. S. (1976), "Inelastic Lateral Buckling of Determinate Beams," *Journal of the Structural Division, ASCE*, Vol. 102, No. ST4, Proceeding Paper 12020, pp. 701-717
- Nethercot, D. A. (1983), "Elastic Lateral Buckling of Beams," *Beams and Beam Columns*, Edited by R. Narayanan, Applied Science Publishers, pp. 1-34
- Owen, D. R. J. and Hinton, E. (1980), "Finite Elements in Plasticity: Theory and Practice," Pineridge Press Limited, Swansea, U.K.
- Payne, H. and Czyzak, S. J. (1960), "On the Torsion of of a Thin-wall Cylinder Following a Plastic Extension," *Journal of Mechanical Physics and Solids*, Vol. 88, pp.39-44
- Pifko, A. and Isakson, G. (1969), "A Finite Element Method for the Plastic Buckling Analsis of Plates," *AIAA Journal*, Vol. 7, No. 10, pp. 1950-1956
- Pincus, G. (1964), "On the Laterl Support of Inelastic Columns," *AISC Engineering Journal*, Fourth Quarter, October, pp. 113 - 115

- Plaut, R. (1993), "Requirements for Lateral Bracing of Columns with Two Spans," ASCE, *Journal of Structural Engineering*, Vol. 119, No. 10, pp. 2913-31
- Popov, E. P. and Petersson, H. (1978), "Cyclic Metal Plasticity: Experiments and Theory," ASCE, *Journal of the Engineering Mechanics Division*, Vol. 104, No. EM6, pp. 1371-1388
- Powell, G. M. and Klingner, R. (1970), "Elastic Lateral Buckling of Steel Beams," ASCE, *Journal of the Structural Division*, Vol. 96, No. ST9, pp. 1919-1932
- Pride, R. A. and Heimerl, G. J. (1950), "Plastic Buckling of Simply Supported Compressed Plates," National Advisory Committee for Aeronautics (NACA), Technical Note No. 1817
- Pugh, E. D. L., Hinton, E., and Zienkiewicz, O. C. (1978), "A Study of Quadrilateral Plate Bending Elements with 'Reduced' Integration," *International Journal for Numerical Methods in Engineering*, Vol. 12, pp. 1059-1079
- Schreyer, H. L., Kulak, R. F., and Kramer, J. M. (1979), "Accurate Numerical Solutions for Elastic-Plastic Models," *Journal of Pressure Vessel Technology*, Transactions of ASME, Vol. 101, August, pp. 226-234
- Shammamy, M. R. and Sidebottom, O. M. (1967), "Incremental Versus Total-strain Theories for Proportionate and Non-proportionate Loading of Torsion-Tension Members," *Experimental Mechanics*, December 1967, pp. 497-505
- Shanley, F. R. (1946), "The Column Paradox," *Journal of Aeronautical Science*, Vol. 13, No. 5, pp. 678
- Shanley, F. R. (1947), "Inelastic Column Theory," *Journal of Aeronautical Science*, Vol. 14, No. 5, pp. 261-267

- Stowel, E. Z. (1948), "A United Theory of Plastic Buckling," National Advisory Committee for Aeronautics, Technical Note No. 1556
- Tassoulas, J. L. (1995), "Inelastic Behavior of Materials: Class Note," Dept. of Civil Engineering, The University of Texas at Austin, Spring Semester
- Thürlimann, B. (1962), "New Aspects Concerning Inelastic Instability of Steel Structures," ASCE Transactions, Vol. 127, Paper No. 3381
- Timoshenko, S. P. and Gere, J. M. (1961), "Theory of Elastic Stability," McGraw-Hill Book Company, Inc., New York
- Trahair, N. S. (1969), "Elastic Stability of Continuous Beams," Journal of the Structural Division, ASCE, Vol. 95, No. ST6, pp. 1295-1312
- Trahair, N. S. (1983), "Inelastic Lateral Buckling of Beams," Beams and Beam Columns: Stability and Strength, Edited by R. Narayanan, Applied Science Publishers, London, pp. 35-70
- Trahair, N. S. and Nethercot, D. A. (1984), "Bracing Requirements in Thin-Walled Structures," Developments in Thin-Walled Structures Vol. 2, Elsevier Applied Science Publishers, London
- Wakabayashi, M. and Nakamura, T. (1983), "Buckling of Laterally Braced Beams," Engineering Structure, Vol. 5, April, pp. 108-117
- Wang, Y. C. and Nethercot, D. A. (1989), "Ultimate Strength Analysis of Three-Dimensional Braced I-Beams," Proceedings of Institute of Civil Engineers, Part 2, Vol. 87, March, pp. 87-112
- Wang, Y. C. and Nethercot, D. A. (1990), "Bracing Requirements for Laterally Unrestrained Beams," Journal of Constructional Steel Research, Vol. 17, pp. 305 - 315
- WATCOM FORTRAN 77³² User's Guide 4th Edition (1993), WATCOM International Corporation, Ontario, Canada

- Winter, G. (1958), "Lateral Buckling of Columns and Beams," ASCE, Journal of the Structural Division, Vol. 84, No. ST2, March, pp. 1561
- Wong-Chung, A. D. and Kitipornchai, S. (1987), "Partially Braced Inelastic Beam Buckling Experiments," Journal of Constructional Steel Research, Vol. 7
- Yamada, Y., Yoshimura, N., and Sakurai, T. (1968), "Plastic Stress-Strain Matrix and its Application for the Solution of Elastic-Plastic Problems by the Finite Element Method," International Journal of Mechanical Science, Vol. 10, pp. 343-354
- Zienkiwicz, O. C., Taylor, R. L., and Too, J. M. (1971), "Reduced Integration Technique in General Analysis of Plates and Shells," International Journal for Numerical Methods in Engineering, Vol. 3, pp. 275-290

VITA

Heungbae Gil was born in YeSan, ChoongNam, Korea on April 15, 1966, the last son of Oh, Chang-Geun and late Gil, Byung-Ku. After completing his work at NamTaeJon High School, TaeJon, Korea, in 1984, he entered Korea University in Seoul, Korea. From January 1986 to July 1986, he served in Korea Air Force. He received the degree of Bachelor of Science in Civil Engineering from Korea University in February 1989. In September 1989, he entered the Graduate School of The University of Illinois at Urbana-Champaign. From May 1990 to December 1991, he worked as a Research Assistant at US Army Corps-Civil Engineering Research Laboratory in Champaign. He received the degree of Mater of Science in Civil Engineering from The University of Illinois at Urbana-Champaign in December of 1991. In January 1992, he entered the Graduate School of The University of Texas at Austin.

Permanent Address:TaeJon, Seo-Ku, Kalma-Dong, Kalma Apt.101-1304
KOREA (zip code) 302-171

This dissertation was typed by the author.